Rheological properties of Red Blood Cells

Dissertation

**im Rahmen eines Cotutelle-Verfahrens zur Erlangung des Grades
des Doktors der Naturwissenschaften
der Naturwissenschaftlich-Technischen Fakultät II
-Physik und Mechatronik-
der Universität des Saarlandes
und des Docteur de l'Université de Grenoble**

Thèse

**dans le cadre d'une cotutelle pour obtenir le grade de
Docteur de l'Université de Grenoble
Spécialité: Physique pour les sciences du vivant
et de Doktor der Naturwissenschaften der Universität des Saarlandes**

von/présentée par

Matthias Brust

Saarbrücken

2013

Diese Arbeit wurde von der Deutsch-Französischen Hochschule (DFH) finanziell gefördert.
Cette thèse était subventionné par l'Université franco-allemende (UFA).

Tag des Kolloquiums: 28.06.2013

Dekan: Prof. Dr. Christian Wagner

Mitglieder des Prüfungsausschusses:

Vorsitzender:	Prof. Dr. Albrecht Ott
Gutachter:	Prof. Dr. Christian Wagner
	Dr. Anke Lindner (HDR)
Beisitzer:	Dr. Chaouqi Misbah (directeur de recherche)
	Dr. Manouk Abkarian (HDR)
Akademischer Mitarbeiter:	Dr. Andreas Tschöpe

Eidesstattliche Erklärung

Hiermit versichere ich an Eides statt, dass ich die vorliegende Doktorarbeit selbstständig und nur unter Verwendung der genannten Quellen und Hilfsmittel angefertigt habe.

Par la présente, je certifie que j'ai rédigé cette thèse indépendemment et seulement avec les sources mentionnées.

Saarbrücken, 11.04.2013

Matthias Brust

"The fact that we live at the bottom of a deep gravity well, on the surface of a gas covered planet going around a nuclear fireball 90 million miles away and think this to be normal is obviously some indication of how skewed our perspective tends to be."

Douglas Adams (The Salmon of Doubt: Hitchhiking the galaxy one last time, 2002)

Abstract

In this work, the rheological properties of human blood are investigated by two different approaches. The flow properties of plasma, the liquid component of blood, is analyzed under three different conditions: shear flow, elongational flow and contraction flow. Up to now, the plasma was considered as a Newtonian fluid, while the non-Newtonian properties of blood were only attributed to the red blood cells. The performed experiments reveal a viscoelastic behavior of the plasma which has to be considered in future studies. In addition to the plasma, also diluted polymer solutions are analyzed in order to find a good model solution for plasma.

The second part concerns the red blood cells. Their adhesion to linear aggregates is held responsible for the well-known shear thinning behavior of blood but the reason for the cluster formation is still not clear. The interaction energy between two red blood cells and the distribution of different sized clusters flowing through narrow channels are measured under the influence of the two macromolecules dextran and fibrinogen. As the aggregates are actually broken at high shear rates, the current understanding is that they would not play a role for the properties of blood flow. However, an increased amount of clusters at physiological fibrinogen concentrations can be shown, even at shear rates which are common in the microvascular system, which clarifies that the aggregation cannot be neglected in the description of blood flow through the capillary network.

Abrégé

Dans cette thèse, les propriétés rhéologiques du sang sont étudiées suivant deux approches differentes. Les propriétés de l'écoulement du plasma sont analysées selon trois modes différents : sous cisaillement, en extension et en constriction. Jusqu'à présent, le plasma était considéré comme un fluide newtonien, et le comportement complexe du sang était simplement attribué à la présence des globules rouges. Les expériences menées ont montré un comportement visco-élastique du plasma, que doit désomais être pris en compte dans les études futures.

La deuxième axe traite des globules rouges. Leur assemblage en agrégats rectilignes est à l'origine du comportement rhéofluidifiant, mais les causes de la formation des agrégats restent encore vagues. L'énergie d'interaction entre deux cellules et la distribution des tailles des clusters dans des canaux microfluidiques ont été mesurées en présence de dextran et de fibrinogène. Comme les agrégats sont normalement cassés à des taux de cisaillement élevés, on a cru qu'ils ne jouaient pas de rôle dans l'écoulement du sang. Mais le fait que le nombre de clusters augmente à des concentrations physiologiques de fibrinogène, même pour des taux de cisaillement correspondant à ceux du système microvasculaire, il est clair que l'agrégation ne peut pas être négligée dans la description de l'écoulement du sang en le réseau capillaire.

Kurzzusammenfassung

In dieser Arbeit werden die rheologischen Eigenschaften von menschlichem Blut mit zwei verschiedenen Zugängen untersucht. Im ersten Teil werden die Fließeigenschaften von Plasma unter drei Bedingungen analysiert: Scherfluss, Dehnungsfluss und Kontraktionsfluss. Bis jetzt galt Plasma als Newtonsche Flüssigkeit, während die nicht Newtonschen Eigenschaften von Blut ausschließlich den roten Blutzellen zugeordnet wurden. Die durchgeführten Experimente zeigen ein viskoelastisches Verhalten von Plasma, welches in zukünftigen Studien zu berücksichtigen ist.

Der zweite Teil beschäftigt sich mit den roten Blutzellen. Ihre Adhäsion zu linearen Aggregaten wird für das wohlbekannte scherverdünnende Verhalten von Blut verantwortlich gemacht, aber der Grund für die Entstehung der Cluster ist noch immer unklar. Die Interaktionsenergie zwischen zwei Blutzellen und die Verteilung verschieden großer Cluster, die durch schmale Kanäle fließen, werden unter dem Einfluss der beiden Makromoleküle Dextran und Fibrinogen gemessen. Da die Aggregate bei größeren Scherraten eigentlich aufgebrochen werden, war man bisher der Meinung, sie würden keine Rolle für den Blutfluss spielen, aber ein erhöhter Anteil von Clustern bei physiologischen Fibrinogenkonzentrationen, sogar bei Scherraten die im mikrovaskulären System üblich sind, stellt klar, dass die Aggregation bei der Beschreibung des Blutflusses im kapillaren Netzwerk nicht vernachlässigt werden kann.

Table of Contents

1. Introduction

1.1. Introduction (english)

Blood is the most important fluid in the body of humans and most animals. Its functions are the transport of oxygen, nutrients and hormones to the cells all over the body, the removal of metabolic waste products from the cells and the regulation of the body temperature. Furthermore, blood has the capability to coagulate and close wounds to stop bleeding after a vessel has been ruptured. This self-repair mechanism is crucial for securing the survival of the organism.

Consequently, the above-mentioned characteristics of blood lead to the occurrence of severe problems if the flow of blood through the vascular system of the body is disturbed. The blockage of blood vessels due to thrombosis, occurring in both the arterial and the venous circulatory system, has fatal impact on the body [62]. It can cause myocardial infarctions or apoplectic strokes (arterial thrombosis) and pulmonary embolisms (venous thrombosis), it consequently is responsible for the three main reasons of cardiovascular diseases and finally the most frequent cause of death in the developed world.

Nevertheless, the blood flow and especially the correlations and causes leading to the aggregation of blood components to form thrombi are by far not fully understood. The knowledge about the principles behind those processes is indispensable for the development of effective medical treatment, thus the importance of further investigations in this area. Particularly, the interdisciplinary work of medicine, biology and physics has become more and more important in the past years. Although the investigated system is purely biological on the first view, it is necessary to study physical characteristics. The flow properties of blood are also crucial for the success of medical treatment and the delivery of drugs to the appropriate destination. Although research about blood and blood rheology has increased severely over the last decades, there are still many open questions. In this dissertation, the rheological properties of blood flow are investigated by **two different approaches**. In one part, the **clustering of the main solid component of blood, the red blood cells**, was analyzed under different conditions and in the other part, the focus was set to the **flow properties of the liquid phase of blood, the plasma.** Both parts are important to achieve a better understanding of the blood flow.

As blood is a yield-stress fluid [88] it is necessary to apply a certain stress before it starts to flow. In figure 1.1, one can see that the viscosity of blood decreases if the

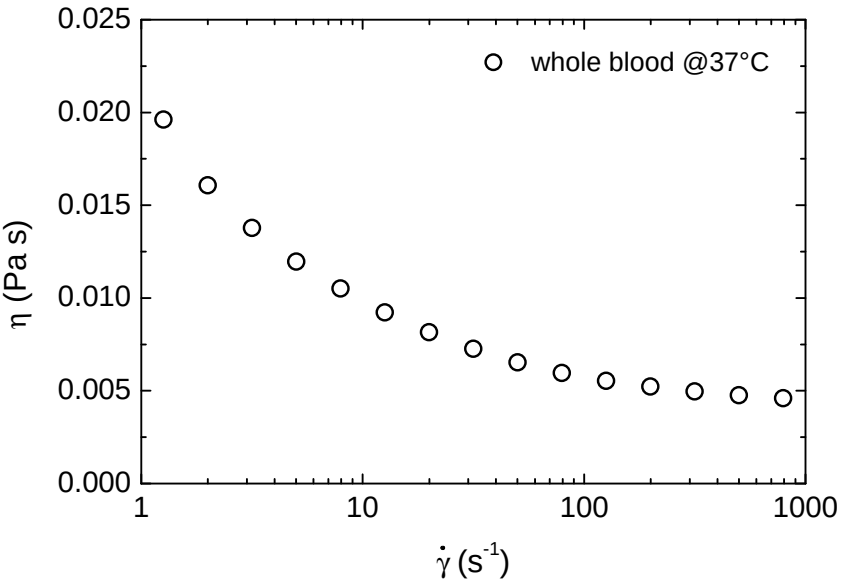

Figure 1.1.: Viscosity η of human blood for different shear rates $\dot{\gamma}$. The shear-thinning behavior is clearly visible.

shear rate to which it is exposed increases. This effect is called shear thinning behavior and was reported for blood almost 100 years ago [51]. During the research leading to the discovery of the reason for this non-Newtonian behavior, a strong connection to the aggregation of red blood cells was revealed.

The reversible adhesion of red blood cells to linear aggregates during the circulation of blood in the vascular system occurs continuously. At low shear rates, the amount of aggregates is increased. This effect is held responsible for the higher viscosity of blood in relation to higher shear rates, where the aggregates are broken again. Hence, the understanding of the adhesion mechanism and the conditions under which it takes place are very important. A deeper knowledge of the process could allow for a decision under which circumstances the normal, unproblematic aggregation changes to a situation where the aggregates become bigger or the adhesion becomes stronger resulting in an obstruction of the blood flow. It has been suggested that a macromolecularly induced depletion interaction could be responsible for the cluster formation.

Therefore, the influence of two different depletion agents on the aggregation of red blood cells was investigated with two different techniques. On the single cell level, the interaction energy between two cells was measured by means of single cell force spectroscopy and on the cluster level the distribution of the cluster size was observed during the flow through narrow microfluidic channels. In contrast to these methods, prior related research measured the adhesion of red blood cells only by using indirect

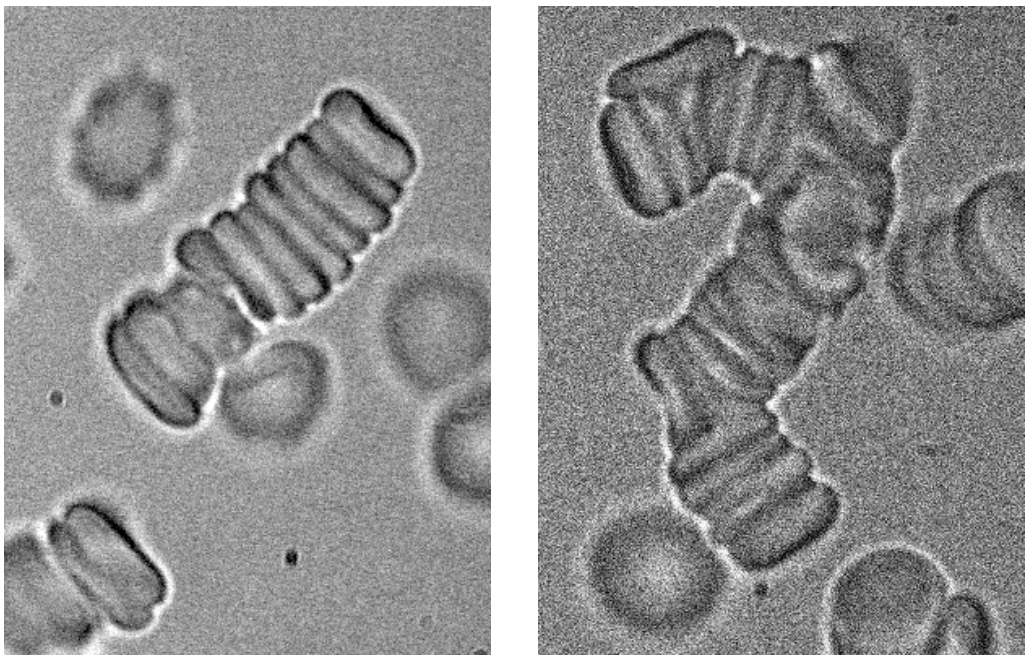

Figure 1.2.: Two images showing aggregates of human red blood cells in a physiological buffer solution containing a long-chain sugar polymer.

measurement techniques. In figure 1.2 one can see examples of aggregates of red blood cells caused by macromolecules. For a small number of cells they have a linear shape, looking like a stack of coins (left picture in figure 1.2), which gave them the name rouleau. If the number of cells forming a cluster is increased, the structure can also be more complicated due to bending or branching (right picture in figure 1.2).

In the measurements regarding the plasma the open question was the flow behavior. The rheological properties of a complex fluid differ significantly from a simple Newtonian fluid like water. As the addition of macromolecules and proteins to a fluid can affect these properties and those substances can be found in the plasma, a closer look seems prudent. For whole blood the non-Newtonian flow behavior is well known as one can see in the image series in figure 1.3, where a droplet of blood was elongated leading to the formation of a filament instead of a spontaneous Newtonian break-up.

It was claimed that this complex flow behavior is only connected to the red blood cells which are suspended in a purely Newtonian medium, but although the plasma has been considered to behave as a Newtonian fluid in the literature, some hints to a non-Newtonian behavior existed. The occurrence of instabilities affecting the flow strongly depends on elastic effects which can be found in complex fluids. As these instabilities become even more important if the channel branches or gets constricted, which happens frequently in the capillary network of the body, the question if plasma is a complex fluid or not is of high relevance. The interplay of inertial and elastic

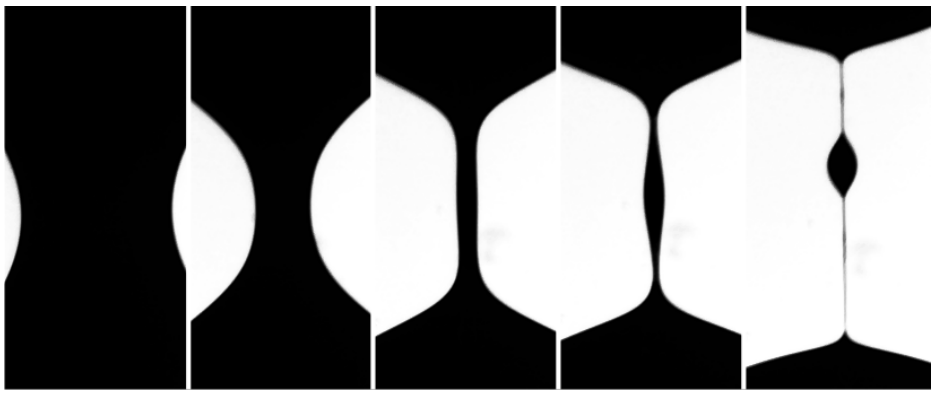

Figure 1.3.: This series of images shows the thinning of a blood filament (in black) over time after the stretching of a droplet.

forces crucially affects the flow of a liquid through a constriction in a channel. While inertial forces lead to vortices downstream of the constriction, elasticity suppresses them and provokes vortices in the region before the narrowing. The characteristics of plasma, blood and different polymer solutions which could act as model fluids were investigated by different rheometer and microfluidics experiments.

Overview

After this **first introductory chapter**, I will give an overview about the literature and the current state of research in **chapter two**. The theoretical background of the investigated phenomena will be explained in **chapter three**. Then I will describe the experimental setup in the **fourth chapter**. Afterwards the results will be presented and discussed. **Chapter five** regards the rheological properties of plasma and some model solutions with the rotational and elongational shear measurements and the flow measurements in a contraction fluidics. The clustering of red blood cells due to depletion induced interactions as a result of the addition of the sugar polymer Dextran70 or the coagulation factor Fibrinogen will be illustrated in **chapter six**. Finally, I will sum up the results in **chapter seven** and give some concluding remarks as well as future prospects.

1.2. Introduction (français)

Le sang est le fluide le plus important du corps humain et aussi celui de la plupart des animaux. Ses fonctions sont le transport de l'oxygène, des nutriments et des hormones dans toutes les cellules du corps, le transport des déchets du métabolisme des cellules et la régularisation de la témperature du corps. De plus, le sang a la capacité de coaguler et peut ainsi obstruer la paroi endommagée d'un vaisseau pour stopper l'hémorragie. Ce mécanisme d'autoguérison est un critère important pour assurer la survie de l'organisme. Ainsi, toute perturbation de l'écoulement sanguin peut conduire à des problèmes plus au moins graves de santé.

L'obstruction des vaisseaux par thrombose, qui se passe tant dans le circuit artériel que dans le circuit veineux, a des conséquences fatales pour le corps [62]. Cela peut provoquer des infarctus du myocarde ou des attaques d'apoplexie (thromboses artérielles) et des embolies pulmonaires (thromboses veineuses), conduisant le plus souvent à des accidents cardio-vasculaires, qui sont considérés à juste titre comme une des plus grandes causes de mortalité dans le monde occidental.

Pourtant une étude détaillée des propriétés de l'écoulement du sang et surtout des causes conduisant à l'agrégation de ses composants en thrombus reste à faire. Une bonne compréhension des propriétés du sang est d'autant plus nécessaire pour développer un traitement médical efficace, ce qui montre toute l'importance de conduire des recherches dans ce domaine. Tout ceci a fini par favoriser une collaboration de plus en plus efficace entre les domaines de la médicine, de la biologie et de la physique. Bien que le système étudié soit seulement biologique au premier coup d'oeil, il est nécessaire d'analyser le problème d'un point de vue physique. Les propriétés de l'écoulement du sang sont aussi très importantes pour le succès des traitements médicaux et pour le transport des médicaments vers leurs zones d'action. Bien que la recherche concernant le sang et sa rhéologie se soit fortement intensifiée pendant ces dernières décennies, plusieurs questions restent ouvertes. Dans cette thèse, les propriétés rhéologiques du sang sont étudiées suivant deux approches differentes. Dans une partie, l'agrégation des principaux éléments solides du sang, les globules rouges, a été analysée sous différentes conditions, et dans l'autre partie les propriétés de l'écoulement de la partie liquide du sang, le plasma, ont été explorées. Les deux parties sont importantes pour obtenir une meilleure compréhension de l'écoulement du sang.

Comme le sang est un fluide à contrainte secie [88], il est nécessaire d'appliquer une certaine contrainte de cisaillement avant que l'écoulement commence. Dans la figure 1.1, on constate que la viscosité du sang diminue quand la vitesse de cisaillement à laquelle il est exposé augmente. Un tel fluide est qualifié de rhéofluidifiant. Ce phénomène a pu être observé depuis presque un siècle [51]. En recherchant les raisons de cette attitude non-newtonienne, une connexion forte avec l'adhésion des globules rouges a été constatée.

L'adhésion réversible des globules rouges en aggrégats linéaires dans les vaisseaux s'effectue continuellement. Pour un taux de cisaillement faible, le nombre d'agrégats est élevé, conduisant à une augmentation de la viscosité. La viscosité effective est inversement proportionelle à la taille des agrégats. Leur taille diminue lorsque le taux de cisaillement augmente. C'est pourquoi, la compréhension du mécanisme d'adhésion et les conditions dans lesquelles l'adhésion se produit sont très importantes. Une meilleure compréhension de ce processus peut permettre de dire sous quelles circonstances le phénomène d'agrégation se transforme en une situation où les agrégats deviennent plus grands ou bien l'adhésion devient plus forte, résultant en une perturbation de l'écoulement du sang.

Deux techniques différentes ont été utilisées pour étudier l'effet de deux agents de déplétion sur l'agrégation des globules rouges. Au niveau unicellulaire, l'énergie d'interaction entre deux cellules a été mesurée avec un microscope à force atomique sur une cellule isolée. Cette méthode a permis de quantifier directement l'énergie d'interaction, contrairement aux méthodes trouvées dans la littérature. Au niveau intercellulaire, la distribution des tailles des clusters dans un écoulement de Poiseuille a été observée dans des canaux microfluidiques. Dans la figure 1.2, on peut observer des exemples d'agrégats de globules rouges induits par la présence de macromolécules. Pour un petit nombre de cellules, ils adoptent une forme rectiligne (image de gauche, figure 1.2) ressemblant à un empilement de pièces de monnaie, ce qui leur a valu le nom de "rouleau". Quand le nombre de cellules qui forment le cluster est grand, la structure peut devenir plus complexe, du fait qu'elle peut se courber ou se ramifier(image de droite, figure 1.2).

L'autre axe de cette thèse est d'étudier le comportement rhéologique du plasma. Les propriétés rhéologiques d'un fluide complexe different de celles d'un fluide newtonien comme l'eau. Comme l'ajout de macromolécules et de protéines dans un fluide peut affecter ses propriétés, et que de pareilles substances existent dans le plasma, une approche plus prudente est à envisager. Pour le sang, les propriétés d'écoulement non-newtonien sont bien connues. C'est-ce qu'on observe dans la figure 1.3, où une goutte de sang a été étirée, conduisent à la formation d'un filament, et non pas à la brisure typique d'un fluide newtonien.

Il était communément admis que le comportement complexe du sang était seulement dû à la présence des globules rouges en suspension dans un milieu purement newtonien. Mais bien que le plasma soit considéré comme un fluide newtonien dans la littérature, quelques expériences indiquent un comportement non-newtonien. L'apparition d'instabilités, pouvant influencer l'écoulement dépend fortement des effets visco-élastiques qui peuvent être observés dans les fluides complexes. Comme ces instabilités deviennent encore plus importantes quand les canaux se ramifient ou se contractent, une chose qui se passe fréquemment dans le réseau capillaire, la question de savoir si le plasma est un fluide complexe ou non est de la plus grande importance. La compétition entre forces inertielles et élastiques influence fortement l'écoulement du fluide dans une constriction. Alors, que les forces inertielles génèrent des tour-

billons en aval de la constriction, les forces élastiques les font disparaître et créent de nouveaux tourbillons en amont de celle-ci. Les propriétés du plasma, du sang et de différentes solutions de polymères jouant le rôle de fluide modèle, ont été étudiées à l'aide d'expériences rhéométriques et microfluidiques.

Aperçu

Après cette introduction (chapitre un), je vais donner dans le deuxième chapitre de cette thèse une vue globale de l'état de l'art. Les principes théoriques des phénomènes étudiés seront expliqués dans le troisième chapitre. Puis je vais décrire le dispositif expérimental dans le quatrième chapitre. Ensuite, les résultats seront présentés et discutés. Le chapitre cinque porte sur les propriétés rhéologiques du plasma et de quelques solutions modèles observées lors des expériences réalisées en cisaillement, en extension et en constriction. L'agrégation des globules rouges causée par la déplétion due à la présence du polymère Dextran70 ou de fibrinogènes - facteur coagulant présent naturellement dans le plasma - est illustrée dans le sixième chapitre. Enfin je récapitulerai les résultats dans le septième chapitre et puis je conclurai en pointent quelques perspectives futures.

1.3. Einleitung (deutsch)

Blut ist die wichtigste Flüssigkeit im Körper des Menschen und der meisten Tiere. Seine Funktionen sind der Transport von Sauerstoff, Nährstoffen und Hormonen zu den Zellen im gesamten Körper, der Abtransport von Stoffwechselendprodukten aus den Zellen sowie die Regulierung der Körpertemperatur. Außerdem besitzt Blut die Fähigkeit zu gerinnen und Wunden zu verschließen, um Blutungen zu stoppen, nachdem ein Gefäß verletzt wurde. Dieser Selbstheilungsmechanismus ist eine wichtige Eigenschaft um das Überleben des Organismus zu sichern.

Daher führen alle diese Eigenschaften zum Auftreten schwerwiegender Probleme, wenn der Blutfluss durch das Gefäßsystem des Körpers durch irgendwelche Faktoren gestört wird. Die Verstopfung von Blutgefäßen durch Thrombose, welche sowohl im arteriellen als auch im venösen Kreislauf vorkommt, hat fatale Folgen für den Körper [62]. Sie verursacht Herzinfarkte oder Schlaganfälle (arterielle Thrombosen) und Lungenembolien (venöse Thrombosen), womit sie für die drei häufigsten Ursachen von Herz-Kreislauferkrankungen verantwortlich ist und schließlich die häufigste Todesursache in der westlichen Welt darstellt.

Dennoch sind der Blutfluss und vor allem die Zusammenhänge und Gründe, die zur Aggregation von Blutkomponenten zu Thromben führen, bei weitem nicht vollständig verstanden. Die Kenntnis über die Grundlagen dieser Prozesse ist wichtig für die Entwicklung effektiver medizinischer Behandlung und somit ist die Bedeutung weiterführender Forschung auf diesem Gebiet offensichtlich. Besonders die interdisziplinäre Arbeit von Medizin, Biologie und Physik ist innerhalb der letzten Jahre immer wichtiger geworden. Obwohl das untersuchte System auf den ersten Blick rein biologisch ist, ist es notwendig physikalische Eigenschaften zu erforschen. Die Fließeigenschaften des Blutes sind auch entscheidend für den Erfolg medizinischer Behandlung und den Transport von Medikamenten zum gewünschten Wirkungsort. Obwohl die Forschung über Blut und Blutrheologie in den letzten Jahrzehnten stark zugenommen hat, gibt es noch viele offene Fragen. In dieser Dissertation werden die rheologischen Eigenschaften des Blutflusses mittels **zweier unterschiedlicher Zugänge** untersucht. Im ersten Teil werden die **Zusammenlagerung des festen Hauptbestandteils des Blutes, der roten Blutzellen,** unter verschiedenen Bedingungen analysiert und in dem anderen Teil lag der Schwerpunkt auf den **Fließeigenschaften des flüssigen Blutanteils, des Plasmas.** Beide Teile sind wichtig, um ein besseres Verständnis über den Blutfluss zu erlangen.

Da es sich bei Blut um eine „yield-stress“-Flüssigkeit handelt [88], ist es notwendig eine bestimmte Belastung aufzubringen, bevor es zu fließen beginnt. In Abbildung 1.1 kann man sehen, dass die Viskosität des Blutes abnimmt, wenn die aufgezwungene Scherrate ansteigt. Dieser Effekt wird als Scherverdünnung bezeichnet und wurde schon vor fast 100 Jahren für Blut berichtet [51]. Während der Forschung nach dem Grund für dieses nicht-Newtonsche Verhalten wurde eine starke Verknüpfung mit der Aggregation roter Blutzellen erkannt.

Die reversible Adhäsion von roten Blutzellen zu geradlinigen Aggregaten während der Blutzirkulation in der Gefäßstruktur erfolgt fortlaufend. Bei kleinen Scherraten ist die Anzahl der Aggregate erhöht, was als Grund für die höhere Viskosität des Blutes im Vergleich zu höheren Scherraten angesehen wird. Bei Letzteren werden die Aggregate wieder aufgebrochen, sodass die Viskosität abnimmt. Daher sind das Verständnis des Adhäsionsmechanismus und der Bedingungen, unter denen sie auftritt, sehr wichtig. Ein tieferes Verständnis des Prozesses könnte eine Entscheidung ermöglichen, unter welchen Bedingungen die normale, unproblematische Aggregation sich zu einer Situation ändert, in der die Aggregate größer oder die Adhäsion stärker werden, was eine Behinderung des Blutflusses nach sich zieht. Es wurde vermutet, dass eine durch Makromoleküle hervorgerufene Depletionsinteraktion für die Cluster-Bildung verantwortlich sein könnte.

Folglich wird der Einfluss zweier unterschiedlicher „Depletions-Erreger“ auf die Aggregation der roten Blutzellen mit zwei verschiedenen Techniken untersucht. Auf dem Einzelzell-Niveau wird die Interaktionsenergie zwischen zwei Zellen mittels Einzelzell-Kraft-Spektroskopie gemessen und auf dem Cluster-Niveau wird die Verteilung der Clustergröße beim Fluss durch schmale Mikrokanäle beobachtet. Im Gegensatz zu diesen Methoden wurden in früheren Untersuchungenen der Adhäsion roter Blutzellen nur indirekte Messtechniken verwendet. In Abbildung 1.2 kann man Beispiele von Aggregaten roter Blutzellen sehen, die durch Makromoleküle verursacht werden. Für eine kleine Anzahl von Zellen haben sie eine geradlinige Form (linkes Bild in Abbildung 1.2), die ihnen den Namen „Rouleau“ gegeben hat. Wenn die Zahl der Zellen, die den Cluster formen, erhöht ist, kann die Struktur durch Krümmungen und Verzweigungen komplizierter werden (rechtes Bild in Abbildung 1.2).

In den Messungen, die sich mit dem Blutplasma beschäftigten, war das Fließverhalten die offene Frage. Die rheologischen Eigenschaften eines komplexen Fluids unterscheiden sich bedeutend von denen eines einfachen, Newtonschen Fluids wie Wasser. Da die Zugabe von Makromolekülen und Proteinen zu einem Fluid diese Eigenschaften beeinflussen kann und solche Substanzen im Plasma vorkommen, scheint eine genauere Betrachtung sinnvoll. Für Vollblut sind nicht-Newtonsche Fließeigenschaften wohlbekannt, wie man in der Bilderserie in Abbildung 1.3 erkennen kann. Die Abbildung zeigt einen Bluttropfen, der gedehnt wird, was zur Ausbildung eines Filaments führt anstatt zu einem spontanen Newtonschen Abriss.

Es wurde behauptet, dass dieses komplexe Fließverhalten nur mit den roten Blutzellen zusammenhängt, die von einem Newtonschen Medium umgeben sind, aber obwohl Plasma in der Literatur als Newtonsches Fluid betrachtet wird, existieren einige Hinweise zu nicht-Newtonschem Verhalten. Das Auftreten von Instabilitäten, welche den Fluss beeinflussen, hängt stark von elastischen Effekten ab, die in komplexen Flüssigkeiten zu beobachten sind. Da diese Instabilitäten sogar noch wichtiger werden, wenn sich die Kanäle verzweigen oder verengen, was im kapillaren Netzwerk des Körpers sehr häufig vorkommt, ist die Frage ob Plasma eine komplexe Flüssigkeit ist oder nicht von hoher Relevanz. Die Wechselwirkung von inertialen und elastischen Kräften be-

einflusst maßgeblich den Fluss einer Flüssigkeit durch eine Verengung in einem Kanal. Während inertiale Kräfte zu Verwirbelungen hinter der Engstelle führen, unterdrückt Elastizität diese und verursacht Verwirbelungen im Bereich vor der Verengung. Die Eigenschaften von Plasma, Blut und unterschiedlichen Polymerlösungen, welche als Modelllösung dienen können, werden mit verschiedenen Rheometer- und Mikrofluidikexperimenten untersucht.

Übersicht

Nach dem **ersten Kapitel** mit dieser Einleitung werde ich einen Literaturüberblick mit dem aktuellen Stand der Forschung im **zweiten Kapitel** geben. Die theoretischen Grundlagen der untersuchten Phänomene werden im **dritten Kapitel** erklärt. Dann werde ich im **vierten Kapitel** den experimentellen Aufbau beschreiben. Danach werden die Ergebnisse präsentiert und diskutiert. **Kapitel fünf** betrachtet die rheologischen Eigenschaften von Plasma und einigen Modelllösungen mit den Rotationsfluss- und Dehnungsflussexperimenten und den Experimenten in einer Kontraktionsfluidik. Die Zusammenlagerung von roten Blutzellen aufgrund des, durch das Zuckerpolymer Dextran70 oder des Koagulationsfaktors Fibrinogen, induzierten Depletionseffekts wird im **sechsten Kapitel** dargestellt. Schließlich werde ich die Ergebnisse in **Kapitel sieben** zusammenfassen und einige abschließende Anmerkungen machen, sowie zukünftige Perspektiven aufzeigen.

2. Literature overview

2.1. Rheology of Plasma

The blood plasma solution consists to approximately 92% of water and is commonly believed to be Newtonian [11, 108, 122]. Some experiments [31, 52] showed that the non-Newtonian behavior of plasma in shear flows can be attributed to a layer of plasma proteins which has built at the liquid-air interface. Hence, these effects can be characterized as surface effects rather than bulk effects. It is possible to suppress these surface effects by the addition of a small amount of surfactant [52] or using a guard-ring in the rheometer experiments [31].

In contrary, whole blood is a complex fluid which exhibits non-Newtonian properties [86, 79]. In the early 1970s some measurements with a Couette geometry [59] and a cylindrical tube [113] showed a non-Newtonian behavior of whole blood. Properties like shear-thinning and viscoelasticity could be observed. The reason for this behavior seems to be the deformability of the red blood cells (RBCs) and their tendency to form aggregates [121]. These structures are formed at low shear rates due to plasma proteins and cause an increase of the blood viscosity [115]. Besides, it could be observed that blood exhibits a yield stress [88], so it is necessary to reach a critical shear stress to start a motion of the fluid. At values lower than the critical shear stress the fluid behaves like a solid (yield stress fluid).

For high shear rates the aforementioned aggregates are broken which leads, together with a following elongation of the individual red blood cells, to a decrease of the viscosity, the shear-thinning [25].

All these effects seem to be of minor importance for the flow in large vessels, where the blood can be considered to behave Newtonian, but may become important in the microcirculation system, where the diameters of the capillaries reach values of only 6 µm and a viscoelastic behavior can be observed [86]. If the flow through a vessel is influenced by geometric features, like contractions, expansions or bifurcations, these non-Newtonian effects can be enhanced as one can see in the case of abnormal narrowing of a vessel due to stenosis [108]. Nevertheless, the shear rates in capillaries are claimed to be sufficiently high to break up the aggregates, so that the latter should in the end have no influence on the microvasculatory blood flow [100].

The most common models to describe the rheology of blood and its shear-thinning behavior are the Carreau model [58] and the Casson model [45], where the behavior of the blood viscosity is characterized with different power laws. The importance of

the comprehensive understanding of the rheological blood properties becomes obvious regarding its influence on cardiovascular diseases, drug transportation or the development of medical implants like stents and heart valves. Therefore, the performance of experiments is crucial. Due to safety reasons and difficulties with the handling of blood, the usage of blood analog solutions has become quite common, because of several advantages like non-toxicity and lower cost [114]. Many different solutions and suspensions were proposed and have proven to useful substitutes, like aqueous solutions of polyacrylamide and xanthan gum [121, 49] or biconcave particles suspended in Dextran70 [60].

The laminar blood flow was studied extensively as well as the appearance of flow instabilities under pathological conditions like in the vicinity of an aneurysm or blockage [105, 5]. It is however necessary to distinguish between two kinds of instabilities: those driven by inertia and those driven by viscoelasticity. The two can be distinguished by observing the flow of a fluid through a contraction in a microfluidic channel, where viscoelasticty leads to upstream vortices, while the vortices due to inertial effects occur downstream of the contraction [96, 95]. The approach with the contraction microfluidics has been used to test the flow of two common blood analog solutions (xanthan gum and polyacrylamide) and the investigations showed a significantly different flow behavior for the two solutions with the same shear viscosity, but different elongational viscosity [108]. Hence, the shear viscosity is not the only important parameter to consider in order to find a model solution for plasma. Some other bio-fluids, e.g. saliva and DNA solutions, showed a viscoelastic behavior in elongational flow too [13, 50].

2.2. Clustering of red blood cells

The aggregation of red blood cells has already been known for a long time. The observation of the phase separation of blood was even used in ancient Greece [42] and the sedimentation rate of erythrocytes, still used as an indicator for diseases, has been observed for more than one century, first described by Biernacki in 1897 [14]. It is therefore one of the oldest diagnostic methods in modern medicine [10].

The first studies with the polyglucose dextran as a plasma substitute started in the 1940s. Since the 1980s, the two general areas which are investigated are the mechanism of aggregation and the role of cellular factors in aggregate formation and the in vivo significance of RBC aggregation and its role as a determinant of blood flow [10]. As mentioned before in the introduction, there exist two different models to explain the polymer induced aggregation of RBCs. The cross-bridging model which was developed by Merrill et al. [74] for the case of plasma proteins and by Brooks [19] and Chien [26] for dextran-induced aggregation. The alternative is the depletion model which was already introduced in 1954 for hard spheres [3], but applied to the RBC aggregation only in 1988 [41, 6].

The principle of the bridging model is a simple adsorption of a macromolecule from the solution to the surface of a RBC followed by the adsorption of the same molecule to a second cell which approaches the first one. The macromolecule consequently builds a bridge between the two cells.

The formation of rouleaux due to depletion interaction has been described in several publications, both theoretically [72, 81] and experimentally [2, 7]. A few examples of measurements about the dextran induced aggregation are: Buxbaum et al. [22] performed pipette measurements to determine the surface affinity of spherical RBC fragments to an intact RBC by the extent of its encapsulation. It could be shown that the encapsulation increases with the polymer concentration (dextran) for neutral cells (neuraminidase treated) and is bell-shaped for untreated cells. Chu et al. [28] also found an increase of the adhesion energy between two cells with the polymer concentration of the surrounding medium in experiments where the two cells were brought into contact with micropipettes. In the experiments of Pribush et al. [90] the aggregation of RBCs was measured via capacitance of the solution under the influence of different shear rates. The results show a strong negative relationship between the aggregation and the shear rates. Thus, the rouleaux can be dissolved if the applied shear forces are sufficient [101].

Several works also claim a positive effect of the plasma protein fibrinogen, which plays the most important role in the coagulation process, on the adhesion of RBCs [106, 61, 64]. Marton et al. [66] investigated the fibrinogen-induced aggregation with various methods. Another suitable plasma protein to enforce the RBC adhesion is the Immunoglobulin G [65]. In the case of Albumin, no effect could be evidenced, although the situation is not completely clear [91].

In a Poiseuille flow, it was also possible to observe an adhesion simply due to hydrodynamical interactions without the presence of macromolecules [116]. A theoretical description for RBC-like vesicles also predicts the formation of clusters due to hydrodynamical interactions because of an increased flow velocity for single vesicles. They become more deformed by the flow and thus can stay closer to the center line of the capillary where the velocity is maximal which leads to an approach of previous vesicles, resulting in the formation of a cluster [70, 71]. Another numerical method, where the influence of artifacts due to non-physical boundary conditions could be excluded, confirmed the hydrodynamical clustering of RBC-like vesicles [46].

The two models can both describe the nonspecific adhesion of the RBC adhesion but none of them can explain the whole aggregation and disaggregation process completely. After the bridging model was favored for over thirty years, the depletion model gets more and more support lately [8].

3. Theory

3.1. Fluid dynamics

In this section I will present the principles of fluid dynamics and give an overview on different instabilities and effects which can occur during flow. I will describe inertially driven instabilities in simple fluids and introduce complex fluids where the occurrence of viscoelastic instabilities as well as shear-thinning behavior could be observed.

3.1.1. Basic principles

The most important relation to describe the fluid dynamics is the Navier-Stokes equation which was derived independently by Navier and Stokes in the first half of the 19th century as an enhancement to the Euler equations. Actually, it is not one equation but a system of four nonlinear partial differential equations. It is valid for viscous and incompressible Newtonian fluids and can be solved exactly in cases with boundary conditions. The flow of a viscous fluid is not homogenous but differs with the distance from the underlying force. The gradient of the velocity perpendicular to the direction of propagation can be written as $\dot{\gamma} = dv_x/dy$ and is called shear rate. For a Newtonian fluid, the relation between the tangential tension τ and the shear rate $\dot{\gamma}$ is linear with the proportional constant η being the viscosity ($\tau = \eta\dot{\gamma}$). The Navier-Stokes equation can then be written as:

$$\rho\left(\frac{\partial\vec{v}}{\partial t} + \left(\vec{v}\cdot\vec{\nabla}\right)\vec{v}\right) = \rho\vec{f} - \vec{\nabla}p + \eta\vec{\nabla}^2\vec{v}, \tag{3.1}$$

$$\text{with: } \vec{\nabla}\cdot\vec{v} = 0, \tag{3.2}$$

in which $\vec{v}$ is the fluid velocity, f the external force per mass unit $f = \frac{dF}{dm}$ (for example gravity), ρ the density of the fluid, p the pressure and η the viscosity of the fluid [12]. The equation is derived with the principles of the conservation of momentum, mass and energy and the assumption that the fluid is incompressible ($\vec{\nabla}\cdot\vec{v} = 0$). With the Navier-Stokes equation, it is possible to solve a lot of important flow problems, like air flow below the speed of sound or the flow of water. It is valid as long as the density of the fluid stays rather constant. A more general version is also valid for the case of compressible fluids but more complicated to deduce and needs also the equation of state for an ideal gas.

The specific (normalized with the mass) forces on the right hand side of the equation are divided into the external force f, the pressure force from the surrounding fluid $\vec{\nabla}p$ and the internal force due to the viscosity $\eta\vec{\nabla}^2\vec{v}$. The non-linear term $\left(\vec{v}\cdot\vec{\nabla}\right)\vec{v}$ on the left hand side comes from the inertia of the fluid and is called convective acceleration. It describes the spatial effect of time independent acceleration of the fluid with respect to space: If a viscous fluid flows through a converging nozzle one can observe this change in velocity over position. At small scales, this inertial effect is damped by the viscous effects which are presented by the last term on the right side $\eta\vec{\nabla}^2\vec{v}$.

The ratio between inertial forces and viscous forces is called Reynolds number which is a very important indicator to decide whether a flow is laminar or turbulent. If v is the velocity of a fluid and l is a typical length scale of the system (e.g. the diameter of a cylindrical channel) the Reynolds number can be calculated as:

$$Re = \frac{\rho v l}{\eta}. \tag{3.3}$$

If the Reynolds number is very small ($Re \ll 1$) the term on the left hand side in 3.1 can be neglected and the equation can be simplified to the Stokes equation:

$$0 = \rho\vec{f} - \vec{\nabla}p + \eta\vec{\nabla}^2\vec{v}, \tag{3.4}$$

which is linear and much easier to solve. The Navier-Stokes equation can be used to derive the law of Hagen-Poiseuille for the pressure drop of a fluid in a long cylindrical pipe:

$$\Delta p = \frac{8\eta l Q}{\pi r^4}, \tag{3.5}$$

in which l is the length of the pipe, r is the radius and $Q = dV/dt$ the volumetric flow rate [38]. The constants for the actual pipe on the right hand side can be put together to the hydrodynamical resistance $R_h = \frac{8\eta l}{\pi r^4}$. With a simple modification, the law is also valid for rectangular channels where the hydrodynamical resistance changes to $R_h = \frac{12\eta l}{wh^3(1-0{,}63h/w)}$ with the width w and the height h of the channel [21]. The calculation of hydrodynamical resistances for more complex assemblies can be done analogous to electrical networks.

Also derivable from the Navier-Stokes equation (3.1), the velocity profile for the flow through a pipe is given by:

$$v = -\frac{1}{4\eta}\frac{\Delta p}{\Delta x}\left(R^2 - r^2\right), \tag{3.6}$$

where Δx is the position along the cylindrical axis of the channel, Δp the pressure drop from the entrance to this point, R the radius of the channel and r the radial position. This flow profile is known as the Poiseuille flow. If the flow is just laminar,

i.e. $Re \ll 1$, it is possible to bring two different fluids via two inlets and a Y-junction into the same channel in which they will just flow side by side and only mix due to diffusion which is rather a slow process compared to convection. The transition from laminar to turbulent flow is a very complicated process which is still not fully understood. Reynolds found in his experiments that the transition from one to the other takes place at a Reynolds number between 2000 and 13000, depending strongly on the smoothness of the channels entrance and the flow geometry [93]. Hence, in most cases, the flow in a microfluidic device can be considered as laminar, as Reynolds number for these devices are typically in the order of 1 or below for reasonable velocities.

The advantages of microfluidic channels with very small dimensions are the little amount of required liquid to perform experiments which allows also the investigation of rather expensive and rare substances and the low Reynolds number, whereby the flow in the microfluidics stays laminar.

3.1.2. Inertial vortex instability

As mentioned before, the Reynolds number is an indicator for the transition of a laminar to a turbulent flow situation. If the ratio between the inertial and the viscous forces is small (Re<1), the flow will stay laminar. With an increase of the flow velocity, the inertial forces increase compared to the viscous forces and the flow becomes unstable [117, 84]. The observation of a Newtonian fluid passing a contraction in a channel reveals vortices downstream of the expansion, when the channel-width has increased again to the initial value (figure 3.1). This behavior also occurs for the flow through an abruptly widening channel. These vortices develop at the exit corner of the expansion and grow symmetrically to the salient corner with increasing flow rates [104]. If the inertial forces are increased further the vortices grow onwards downstream the channel. Before the contraction, the flow stays stable and no vortices are generated upstream of the constriction.

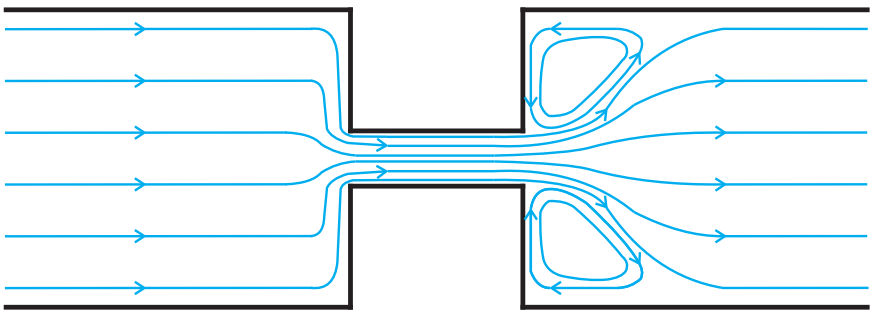

Figure 3.1.: Example of vortices downstream of the expansion due to inertial effects which can be observed for Reynolds numbers in the constricted part in the range of 20 to 100, depending also on the contraction ratio.

3.1.3. Complex fluids

In contrast to Newtonian fluids where the viscosity is constant (figure 3.2, left part), the situation changes significantly for complex fluids where the viscosity can depend on different parameters (figure 3.2, right part), such as shear rate or time.

For these so-called non-Newtonian fluids some very interesting phenomena can be observed, like the die-swell effect [111] or the tubeless siphon [53]. These effects are also of great importance for many commercial applications and consequently they are of great interest for the industry. If the viscosity $\eta(\dot{\gamma})$ depends on the shear rate, the fluid is called shear-thinning (e.g. paint) or shear-thickening (e.g. starch solution), depending on whether the viscosity decreases or increases with the shear rate. For some fluids it can even be necessary to increase the applied stress up to a certain value, the so-called yield point, before the shear sets in (intercept with y-axis in the right part of figure 3.2). These fluids are denominated as yield fluids or Bingham plastic (e.g. mayonnaise).

Another group of complex fluids is built by the thixotropic and viscoelastic fluids, where the flow behavior also depends on the time. For a thixotropic liquid, the viscosity decreases after it has been stressed for some time and returns again to the initial value after the applied stress was stopped (e.g. ketchup). A flow changes the internal energy of a viscoelastic fluid (e.g. dough) due to strains on its structure and is therefore responsible for its different flow behavior. For example, the droplets in a dispersion or the macromolecules in a polymer solution are deformed, resulting in viscoelastic behavior [47]. A polymer is a long-chain molecule which consists of repeating units of a monomer. The polymers can be described as a chain where the single atoms are mimicked by spheres connected to each other through their binding sites. The basic principle for most of the models is the elastic dumbbell model, where the two spheres are connected via an elastic spring following Hook's law.

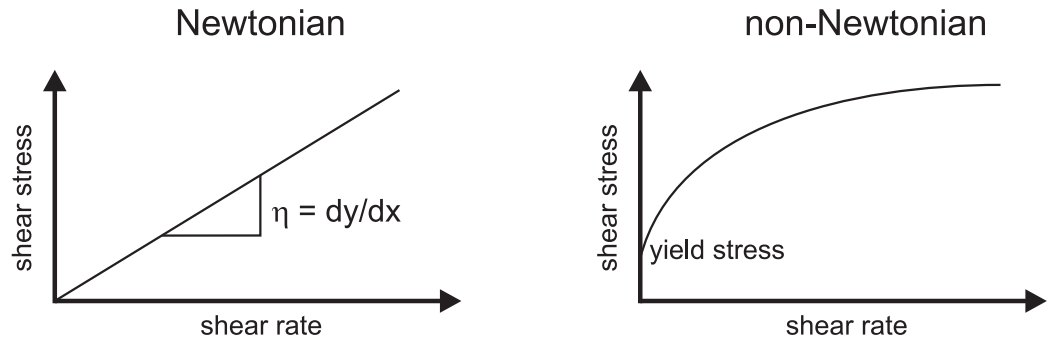

Figure 3.2.: Difference in the relation of shear stress against shear rate for Newtonian (left) and non-Newtonian fluids (right).

3.1.4. Viscoelasticity

The properties of a viscoelastic fluid depend strongly on the timescale of the occurring deformation. For small timescales, a viscoelastic fluid can be described as an elastic solid while it behaves as a viscous liquid for longer timescales. In a Newtonian fluid the normal stresses τ_{xx} and τ_{yy} acting on a fluid element are zero. For a polymer solution the situation is significantly changed due to the capability of the polymers to become stretched. If the shear gradient $\dot{\gamma} = \partial v_x/\partial y$ is large enough, the stretching and the orientation of the polymers lead to a difference in the normal stresses $\tau_{xx} \neq \tau_{yy}$ (see figure 3.3). The fluid thus becomes anisotropic due to the shear [15].

The difference between the normal stress along the flow direction τ_{xx} and the normal stress along the direction of shear τ_{yy} increases quadratically with the shear rate [78]. This effect is driven by the stretching of the polymers which increases with the polymer length. As the increasing polymer length also raises the viscosity of the solution [39, 36], the Reynolds number is decreasing. The inertial effects are however small and hence another dimensionless number is necessary to describe the behavior of polymer solutions. The ratio of the difference of the normal stresses and the shear stress τ_{xy}, called Weissenberg number (Wi) can be used to characterize complex fluids [78]:

$$Wi = \frac{|\tau_{xx} - \tau_{yy}|}{|\tau_{xy}|}. \tag{3.7}$$

If the normal force differences are larger than the shear forces (Wi > 1) the viscoelastic properties change the rheology significantly. The stretching of the polymers in shear flow leads to the storage of elastic energy. After a fluid element was moved to a region

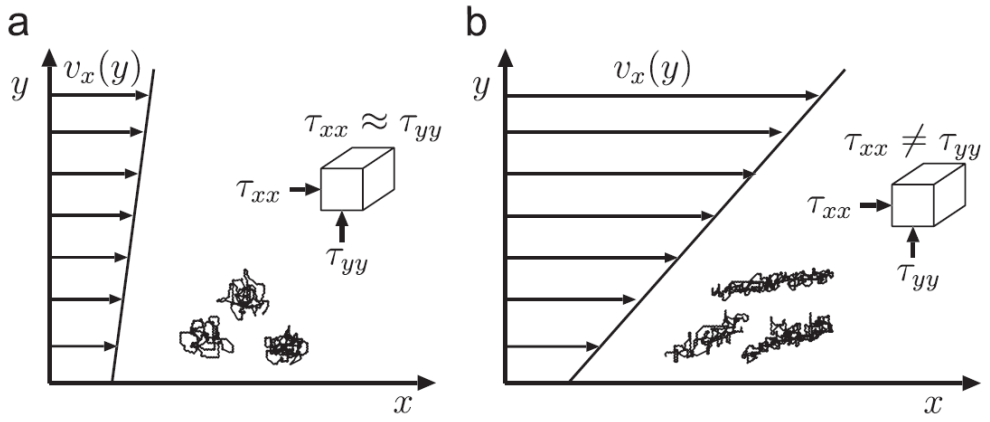

Figure 3.3.: Stretching of the polymers due to an increase of the shear rate leads to an anisotropy of the fluid. a) coiled polymers at low shear rate; b) stretched polymers at higher shear rate. From: Morozov and van Saarloos [78]

with smaller shear forces, this energy can be released. Thus it gives a possibility of elastic energy transfer. The time a polymer requires to adapt to a new situation if the shear rate has been changed is called relaxation time of the polymer. It can be considered as the time a stretched polymer would need to relax to its equilibrium shape after the shear gradient has vanished. For small shear rates, the shear stress τ_{xy} increases linearly with the shear rate, while the normal stress difference increases quadratically with it. This means that Wi also increases linearly with the shear rate ($Wi \sim \dot{\gamma}$) and hence it is possible to write the Weissenberg number as:

$$Wi = \lambda\dot{\gamma}, \tag{3.8}$$

with the parameter λ, which is a characteristic timescale of the polymer. Another widely used dimensionless number, the Deborah number [15] $De \sim \dot{\gamma}$ is also proportional to the shear rate. In the most simple models where the effects of anisotropy, elasticity and relaxation are governed by the same constant, λ, Wi and De are essentially the same, only differing by a numerical factor close to one [78]. The Weissenberg number is usually used to describe the case of a constant shear flow, while the Deborah number mostly describes oscillatory, time-dependent flow situations.

3.1.5. Macroscopic polymer models

There are many different models to describe the behavior of a complex fluid. The simplifications in the derivation of a model lead to an inaccurate description but are nevertheless sufficient to describe most of the observed phenomena.

The easiest model for the viscoelastic polymer solutions which behave like a mixture of an elastic solid and a viscous fluid is the Maxwell model [67]. It is represented by the serial connection of a perfect elastic spring and a pure viscous dashpot (figure 3.4, upper part). Hence, the shear stress is constant $\tau = \tau_e = \tau_v$ and the shear $\gamma = \gamma_e + \gamma_v$ is the sum of the components' shears which is obviously also valid for its time derivative, the shear rate:

$$\dot{\gamma} = \dot{\gamma_e} + \dot{\gamma_v}. \tag{3.9}$$

For a solid the relation between the shear stress and the shear is given by $\tau = G\gamma$, where G is the elastic modulus. The situation in a fluid can be described by $\tau = \eta\dot{\gamma}$ with the viscosity of the fluid η. If the equation for the solid is derived with respect to the time and inserted together with the equation for the fluid into equation 3.9, one gets:

$$\begin{aligned} \dot{\gamma} &= \frac{\dot{\tau}}{G} + \frac{\tau}{\eta} \\ \Leftrightarrow \eta\dot{\gamma} &= \tau + \frac{\eta}{G}\dot{\tau}. \end{aligned} \tag{3.10}$$

The quotient η/G defines a particular time scale, namely the relaxation time of the fluid which is denoted λ. If a shear γ_0 is suddenly imposed at the time $t = 0$ the spring

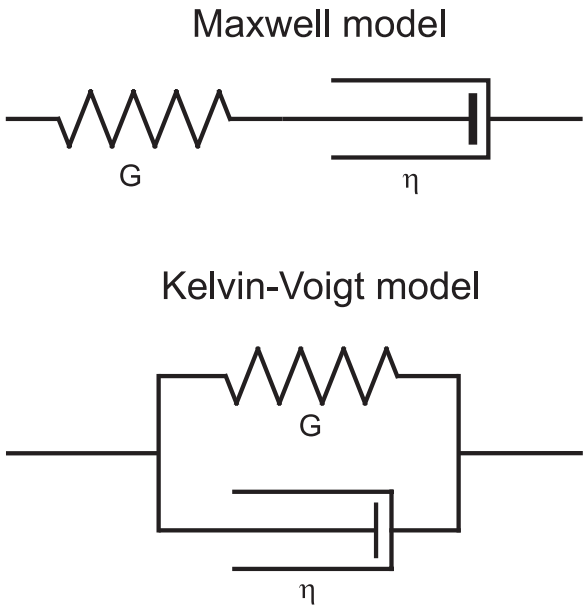

Figure 3.4.: Serial (Maxwell model) and parallel connection (Kelvin-Voigt model) of a spring and a dashpot as models for the behavior of a complex fluid.

is stretched and the applied stress is $\tau_0 = G\gamma_0$. With these boundary conditions, the differential equation 3.10 can be solved and we obtain:

$$\tau(t) = \tau_0 \exp(-t/\lambda). \tag{3.11}$$

The exponential equation describes the stress relaxation. When considering a three-dimensional sample volume, the tensorial form of equation 3.10 is:

$$\eta\underline{\dot{\gamma}} = \underline{\tau} + \frac{\eta}{G}\underline{\dot{\tau}}, \tag{3.12}$$

where the tensorial quantities are the stress tensor:

$$\underline{\tau} = \begin{pmatrix} \tau_{xx} & \tau_{xy} & \tau_{xz} \\ \tau_{yx} & \tau_{yy} & \tau_{yz} \\ \tau_{zx} & \tau_{zy} & \tau_{zz} \end{pmatrix}, \tag{3.13}$$

with τ_{ij} being the force in i-direction acting on the area with the surface normal in j-direction and the shear rate tensor:

$$\underline{\dot{\gamma}} = \vec{\nabla}\,\vec{v}^{\,T} = \begin{pmatrix} \partial v_x/\partial x & \partial v_x/\partial y & \partial v_x/\partial z \\ \partial v_y/\partial x & \partial v_y/\partial y & \partial v_y/\partial z \\ \partial v_z/\partial x & \partial v_z/\partial y & \partial v_z/\partial z \end{pmatrix}. \tag{3.14}$$

For many problems, the shear rate tensor can be simplified because either a velocity component or the derivative of it equals zero.

This linear model needs to be expanded in order to allow the description of nonlinear effects due to large deformations. With the introduction of the upper-convected time derivative, which is the rate of change of a tensor property, the model changes to the upper-convected Maxwell model. The upper-convected time derivative $\underline{\tau}^{\nabla}$ for the stress tensor $\underline{\tau}$ can be written as:

$$\underline{\tau}^{\nabla} = \dot{\underline{\tau}} - (\nabla\vec{v})^T \cdot \underline{\tau} - \underline{\tau} \cdot \nabla\vec{v}. \tag{3.15}$$
$$\text{with the total derivative } \dot{\underline{\tau}} = \frac{\partial}{\partial t}\underline{\tau} + \vec{v} \cdot \nabla\underline{\tau}$$

With this definition, only deformations create stresses in the material, but pure rotations do not. Furthermore, equation 3.12 changes with this time derivative to:

$$\begin{aligned} \eta\dot{\underline{\gamma}} &= \underline{\tau} + \lambda\underline{\tau}^{\nabla} \\ \eta\dot{\underline{\gamma}} &= \underline{\tau} + \lambda \frac{\partial}{\partial t}\underline{\tau} + \lambda\vec{v} \cdot \nabla\underline{\tau} - \lambda (\nabla\vec{v})^T \cdot \underline{\tau} - \lambda\underline{\tau} \cdot \nabla\vec{v}. \end{aligned} \tag{3.16}$$

The upper-convected Maxwell model includes the existence of normal stresses and therefore allows the description of extensional thickening.

The next step in enhancing complex fluid models is the consideration of the solvent which is obviously important for diluted solutions. In this case, the stress tensor is split into one part describing the polymers $\underline{\tau}_p$ and another part for the solvent $\underline{\tau}_s$ [63]:

$$\underline{\tau} = \underline{\tau}_p + \underline{\tau}_s. \tag{3.17}$$

With this relation and $\underline{\tau}_s = \eta_s\dot{\underline{\gamma}}$, equation 3.16 changes to:

$$\begin{aligned} \eta_p\dot{\underline{\gamma}} &= \underline{\tau}_p + \lambda\underline{\tau}_p^{\nabla} \\ &= \underline{\tau} - \eta_s\dot{\underline{\gamma}} + \lambda\underline{\tau}^{\nabla} - \lambda\eta_s\dot{\underline{\gamma}}^{\nabla}. \end{aligned} \tag{3.18}$$

A different sorting of the terms gives the Oldroyd-B model [83]:

$$\underline{\tau} + \lambda\underline{\tau}^{\nabla} = \eta\left(\dot{\underline{\gamma}} + \frac{\eta_s}{\eta}\lambda\dot{\underline{\gamma}}^{\nabla}\right). \tag{3.19}$$

This is the simplest model which captures elasticity, anisotropy and relaxation, the three basic ingredients of polymer rheology [78] and is widely used to describe viscoelastic polymer flow [15, 57]. As the model still lacks the possibility to describe shear-thinning, a further enhancement was necessary. With the consideration of a nonlinear spring connecting the two spheres in a model of an elastic dumbbell, the FENE (finitely extensible nonlinear elastic) model was developed, in which the polymer gets described by beads connected with nonlinear springs. As the mathematical description of this model is very complicated, it will not be illustrated in this work. Instead, the reader is referred to [55] for a detailed introduction to the model.

Another model can be used to describe the creep of a viscoelastic solid. It is called the Kelvin-Voigt model [76] and considers a parallel connection of the spring and the dashpot (figure 3.4, lower part). In this case the shear is constant $\gamma = \gamma_e = \gamma_v$ and the shear stress is the sum of the two components $\tau = \tau_e + \tau_v$. If a sudden stress τ_0 is applied we get $G\frac{d\gamma}{dt} + \eta\frac{d^2\gamma}{dt^2}$ and with the boundary values $\gamma_0 = 0$ and $\gamma(t \to \infty) = \tau_0/G$, the solution of the differential equation is:

$$\gamma(t) = \frac{\tau_0}{G}\left(1 - \exp\left(-t/\lambda\right)\right). \tag{3.20}$$

To describe the creep of a viscoelastic fluid it is necessary to combine the Maxwell model and the Kelvin-Voigt model in a serial connection.

3.1.6. Shear-thinning

A very important effect which can be found in many complex fluids is the shear-thinning behavior. If the shear rate is increased the viscosity does not stay constant but decreases. The reason for this behavior is the alignment of macromolecules in the fluid along the direction of the flow and the break-up of solid objects due to an increase of the flow velocity and thus the shear rate. Consequently, the inner friction becomes lower and the viscosity decreases. In contrast, the opposite effect of shear-thickening can be explained with the sliding of particles in the fluid against each other. At low velocities, the liquid is acting as a lubricant, whereas the increased rubbing against each other at higher velocties increases the viscosity [47].

For a shear-thinning liquid, one can characterize two plateau values: the viscosity at vanishing shear rates η_0, also called zero shear viscosity and the viscosity at huge shear rates η_∞. A simple power-law model used to describe the shear-thinning of a non-Newtonian fluid is the Ostwald-de Waele model [85, 37]:

$$\begin{aligned} \tau &= k\dot{\gamma}^n \\ \eta = \frac{\tau}{\dot{\gamma}} &= k\dot{\gamma}^{n-1}, \end{aligned} \tag{3.21}$$

where k, the consistency and n, the power-law index are constants depending on the properties of a given fluid. If $n = 1$ the liquid is Newtonian, $n < 1$ indicates a shear-thinning behavior and $n > 1$ describes shear-thickening.

As the viscosity of the fluid would need to range from infinity at zero shear rate to zero at infinite shear rates to be in agreement with the model, it does obviously fail to describe the behavior for very small, as well as for very high shear rates and is only useful in the intermediate range. A widely used model which also includes the behavior at low and high shear rates is the Carreau model [23]:

$$\frac{\eta - \eta_\infty}{\eta_0 - \eta_\infty} = \frac{1}{\left(1 + \left(c\dot{\gamma}\right)^2\right)^p} \tag{3.22}$$

The time constant c is called Carreau constant and p is the Carreau exponent. This model allows to fit the behavior of a fluid which behaves almost Newtonian, with plateau values for the viscosity at very small and huge shear rates but shows shear-thinning behavior in between.

3.1.7. Elongational flow and capillary thinning

The expansibility of the polymer chains is a crucial parameter for some interesting non-Newtonian effects. A polymer at rest is normally in a coiled condition but can be influenced and deformed significantly by the motion of the surrounding fluid [82]. A simple shear flow in apolymeric solution is an overlay of an extensional and a rotational movement. The extensional part stretches the polymer along the flow line, while the turning due to the rotational part leads to a shortening which results in a tumbling motion of the polymer [103]. Therefore, the influence of a shear flow on a polymer is less severe than a pure extensional flow.

If a fluid is stretched in one direction, it consequently thins in the perdendicular direction which results in a stretching of the polymer (see figure 3.5). Thus, the contact surface for hydrodynamical forces enlarges and the stretching is further increased. This process is called coil-stretch transition [34].

A pure extensional flow can be realized during the break-up of a droplet or a capillary thinning process which can be created in the CaBER experiment. The responsible effect for the thinning of the capillary bridge is the surface tension. It is necessary to distinguish between three cases for the thinning process of a capillary bridge: low- and high-viscous Newtonian fluids and non-Newtonian fluids. For low-viscous Newtonian fluids the viscosity η does not play a role in the constriction. This inertial capillary thinning is only determined by the surface tension σ and the

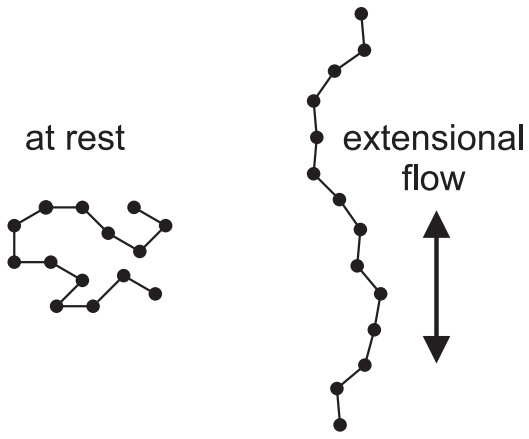

Figure 3.5.: Polymer at rest in a coiled condition (left) and stretched in an elongational flow (right).

inertia of the fluid, represented by its density ρ. The diameter of the capillary bridge follows the equation $h(t) = a\left(\frac{\sigma}{\rho}\right)^{1/3}(t_0 - t)^{2/3}$ with the factor a representing the asymmetrical cutoff [47]. For a wider range of viscous fluids, the viscosity is acting against the surface tension leading to a viscous capillary thinning with the diameter $h(t) = b\frac{2\sigma}{\eta}(t_0 - t)$, with the parameter b depending on the absence of inertia (at the beginning [87, 69]) or the presence of inertial effects (shortly before the cutoff [40, 97]).

For fluids containing polymers, the behavior is changed significantly compared to those without polymers, even if the amount of polymers is rather low. Their behavior is therefore very important in industrial applications, where the elongational part is important in most of the occurring flows. The capillary break-up is suppressed due to the presence of the polymers and a filament between two reservoirs is formed which is thinning exponentially with time. The reason for this behavior is the interplay of the surface tension which is responsible for the thinning and the elastic tensions of the polymers acting against the process and slowing it down [47]. The width of the filament thins with

$$h(t) = h_0 e^{-t/\lambda_C}, \tag{3.23}$$

in which h_0 is the diameter at the beginning of the exponential thinning (at $t = 0$) and λ_C is the CaBER relaxation time of the polymer. After the polymers are stretched completely, the fluid is acting Newtonian again, but with an increased viscosity [47].

The purely elongational flow in the filament during the thinning process can be described with the relation between the strain rate $\dot{\epsilon}$ and the velocities in axial and radial direction:

$$v_z = \dot{\epsilon} z v_r = -\frac{1}{2}\dot{\epsilon} r. \tag{3.24}$$

In the equations v_z and z denote the velocity and the position in axial direction, while v_r and r gives the velocity and the position in radial direction. After the replacement of r by $h(t)$ and the insertion of equation 3.23, the strain can be written as:

$$\dot{\epsilon}(t) = -2\frac{\partial h(t)/\partial t}{h(t)} = \frac{2}{\lambda_C}. \tag{3.25}$$

From this equation, one can see that the strain rate is independent from time and belongs only to the fluid properties. It is consequently constant for a given solution. Therefore, the polymers can get stretched if the strain rate is acting for a sufficient time to absorb the strain. Until the full stretching of the polymers is reached, the exponential thinning continues.

For a Newtonian shear flow, the stress depends linearly on the shear rate and the viscosity is given as $\eta = \tau/\dot{\gamma}$. Despite this shear viscosity, one can also define an extensional viscosity for the situation of purely elongational flow: The elastic stress τ_e depends linearly on the strain rate $\dot{\epsilon}$ and the proportionality constant is the elongational viscosity $\eta_e = \tau_e/\dot{\epsilon}$. According to the law of Trouton [118] the elongational viscosity is three times bigger than the shear viscosity $\eta_e = 3\eta$.

For a non-Newtonian fluid the elastic stress can be written as the difference of the normal stresses $\tau_{zz} - \tau_{rr}$, where τ_{zz} is the stress in axial direction and τ_{rr} is the stress in radial direction. Hence, the elongational viscosity is [102]:

$$\eta_e(t) = \frac{\tau_{zz} - \tau_{rr}}{\dot{\epsilon}(t)}. \tag{3.26}$$

Since the elastic stresses in the filament are compensated by the surface tension, the difference of the normal stresses can be replaced by the Laplace pressure $2\sigma/h(t)$ and one obtains with equations 3.25 and 3.23:

$$\eta_e(t) = \frac{2\sigma}{h(t)\dot{\epsilon}(t)} = \frac{\sigma\lambda_C}{h(t)} = \frac{\sigma\lambda_C}{h_0} e^{t/\lambda_C}. \tag{3.27}$$

3.1.8. Viscoelastic instabilities

For elastic fluids, the flow situation through a contraction-expansion microfluidics is changed significantly in comparison to a Newtonian fluid. For example, the vortices which can be observed downstream of the expansion for Newtonian liquids due to inertial forces are suppressed by the elastic forces. However, the elasticity leads to a development of vortices upstream of the contraction (figure 3.6) which grow in size for increasing shear rates and hence higher flow rates.

The dimensionless parameters used in [96] to describe the dynamics of a flow through micro-scale geometries are the Weissenberg number Wi and the Reynolds number Re introduced in the previous section as well as the elasticity number El and the contraction ratio of the microfluidic device. Here, the Reynolds number is calculated as:

$$Re = \frac{\rho v_c D_h}{\eta_0} = \frac{2\rho Q}{(w_c + h)\,\eta_0}, \tag{3.28}$$

where ρ is the density, η_0 the zero shear viscosity, v_c the mean velocity and $D_h = 2w_c h/(w_c + h)$ the hydraulic diameter of the channel with the contraction width w_c and the height h (characteristic lengthscale). An indicator for the development of elastic effects is the aforementioned Weissenberg number, in this case defined as:

$$Wi = \lambda\dot{\gamma}_c = \frac{\lambda v_c}{w_c/2} = \frac{\lambda Q}{h w_c^2/2}, \tag{3.29}$$

in which λ is the fluid relaxation time and $\dot{\gamma}_c$ is the shear rate in the contraction. The elasticity number is independent from the flow rate and belongs only to the fluid properties and the characteristic length scale of the channel and takes the form:

$$El = \frac{Wi}{Re} = \frac{2\lambda\eta_0}{\rho w_c D_h} = \frac{\lambda\eta_0\,(w_c + h)}{\rho w_c^2 h}. \tag{3.30}$$

As can be seen, this number is simply the ratio of the elastic stresses to inertial effects.

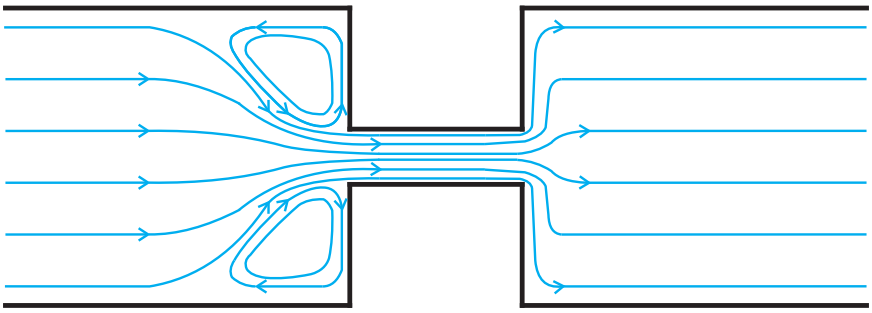

Figure 3.6.: The elasticity of complex fluids provokes vortices upstream of the contraction, while the inertially triggered vortices downstream of the expansion are suppressed.

At very low flow velocities, a viscoelastic fluid flows steadily through an abrupt contraction-expansion channel without any observable differences to a Newtonian fluid. If the flow velocity is increased and hence the shear rate is sufficiently high to induce elastic effects, the streak lines upstream of the contraction will bend, while the appearance of inertial vortices downstream of the expansion is suppressed by the elasticity. The flow upstream will become unsteady and finally, vortices will develop in front of the contraction. For rather small flow rates, the effect of the elasticity is dominating, which means that the upstream vortices will increase in size. A further increase of the flow velocity intensifies the inertial forces and thus the occurrence of vortices downstream of the expansion can be observed. For very large flow rates, the inertial effects can even overcome the elastic effects and reduce the size of the upstream vortices until they are completely suppressed.

While Wi gives information about the onset of an instability upstream of the contraction, El is an indicator for the appearance of the instability [96, 95]. Differences in El at constant Wi gives information if the vortices are starting as lip vortices at the entrance corner of the contraction, which develop to corner vortices in the salient corner of the channel, or as inertio-elastic instabilities followed by corner vortices growing upstream the channel either symmetrically or unsteadily and spatially unstable.

The role of the elasticity and the inertia of the fluid are opposed for a contraction and an expansion flow [16, 117]. A possible explanation for the reduction of downstream vortices due to elastic effects could be the die-swell effect. The elastic energy which was stored in the stretched polymers is released at the contraction exit, pushing the vortices to the border of the channel [9].

3.2. Depletion theory

The depletion theory was first mentioned by Asakura and Oosawa [3, 4] in their work of 1954 where they described the interaction in a solution containing solid spheres with two different sizes. At the walls and around the bigger spheres, one can find forbidden zones where the centers of the smaller spheres can not enter just due to geometrical reasons (figure 3.7). The size of these zones is obviously the radius of the small spheres. If a big sphere approaches the wall or another sphere these zones start to overlap which leads to an increase of the total volume where the small spheres can possibly stay. With this increase of the volume, the entropy increases and therefore the free energy decreases. Hence, it would be necessary to decrease the entropy if the big spheres should be seperated again and as a force is needed for an entropy decrease, the interaction between the big spheres is attractive.

The effect can be understood from a more practical point of view if one imagines the situation of the small molecules which constantly hit the big spheres equally from all sides due to Brownian motion. If the big spheres approach each other the molecules in between get pushed away and therefore, the osmotic pressure from the outer sides is higher than the pressure in between the spheres because the collisions of the molecules which were squeezed away are missing. This also means that the depletion effect amplifies itself, the closer the big spheres come to each other.

To calcalute the depletion force between two solid spheres in a solution of small, solid particles, one has to regard the change of the free energy in dependence of the

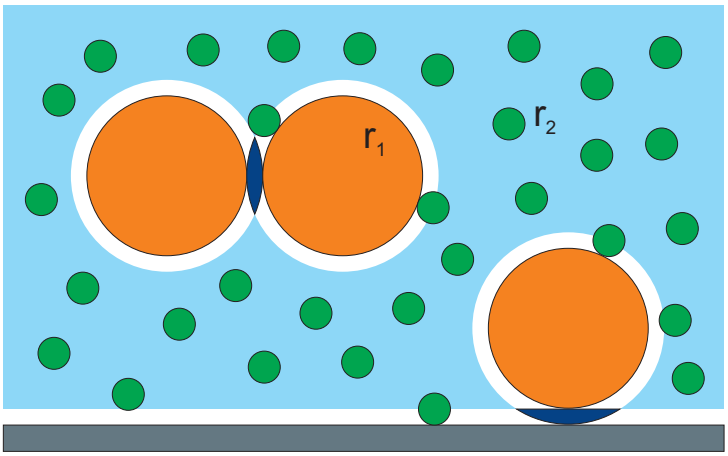

Figure 3.7.: Sketch of a binary solution of solid spheres to demonstrate the depletion effect. If the big orange spheres approach each other or the wall, the white zones which are forbidden for the centers of the small green spheres are overlapping, leading to an increase of the volume (indicated in dark blue) where the centers of the green spheres can stay.

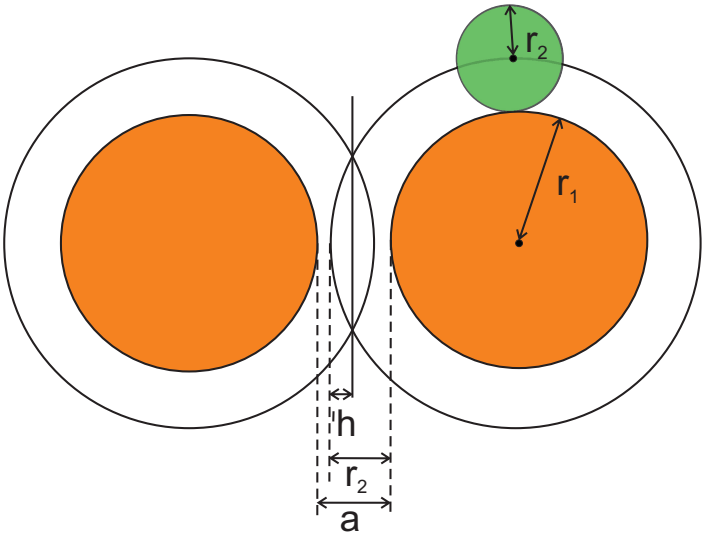

Figure 3.8.: Sketch of two spheres close to each other where the overlapping of the depletion zone is clearly visible. The parameters to calculate the increase of the free volume are the surface-to-surface distance of the big spheres a, the radii of the big and the small spheres r_1 and r_2, respectively and the height of the spherical cap h (representing one half of the overlapping volume).

variation of the volume for the small particles:

$$\Delta F = -Nk_BTln\left(1+\frac{\Delta V}{V}\right), \tag{3.31}$$

with the number of particles N, temperature T, Boltzmann constant k_B and the volume V. As $\Delta V \ll V$ and $\ln(1+x) \approx x$ for $x \ll 1$, it follows for the entropic force f with the surface-to-surface distance of the big spheres a:

$$f = -\frac{\partial \Delta F}{\partial a} = \frac{Nk_BT}{V}\frac{\partial \Delta V}{\partial a}. \tag{3.32}$$

The increase of the volume when the two spheres approach each other is the volume of the overlap of the two spherical caps which constitutes the forbidden zone for the small particles as can be seen in figure 3.8. The height of these spherical caps is $h = r_2 - \frac{a}{2}$ and therefore the volume change is:

$$\Delta V = 2\frac{h^2\pi}{3}\left(3\left(r_1+r_2\right)-h\right). \tag{3.33}$$

with r_1 and r_2 being the radii of the big and the small spheres respectively. Hence, the force f_{kk} between the two spheres can be calculated as:

$$f_{kk} = -\frac{\pi}{4}\frac{Nk_BT}{V}\left[(2r_1 + 2r_2)^2 - (a + 2r_1)^2\right], \tag{3.34}$$

where $0 < a < 2r_2$, otherwise there is no force because the forbidden zones do not overlap. If the concentration is smaller than the overlap concentration which was calculated by de Gennes [35] polymers can also be described as small spheres with the polymers radius of gyration.
When applying this effect to red blood cells, it is necessary to take into account that cells are flexible objects which makes the description much more complicated. In fact, it is possible for the cells to deform and also for the smaller spheres to penetrate into the glycocalyx of the cells. This glycocalyx is a layer of sugar molecules which are attached to the cell membrane and surround the cell. The adaption of the depletion model to a system with flexible cells and polymers was already done by Neu et al. [81] who developed a theoretical model which will be presented in the next subsections. The theoretical descriptions in the following paragraphs are oriented on their work and the book of Baskurt et al. [10].

3.2.1. Depletion interaction energy

It is necessary for a considered object, to make a difference between hard surfaces, where the polymer cannot penetrate into the surface, and soft surfaces where a layer of attached macromolecules surrounds the object. In the second case, it is possible for the polymers to penetrate entirely or partially into the surface. The osmotic pressure can be calculated with a viral equation where the coefficients higher than the second order can be neglected.

$$\Pi = \frac{RT}{M_2}c_2^b + B_2\left(c_2^b\right)^2 = -\frac{\mu_1 - \mu_1^0}{v_1} \tag{3.35}$$

R is the gas constant, T the absolute temperature, v_1 the molecular volume of the solvent, M_2 the molecular weight of the polymer and c_2^b the bulk polymer concentration. The solvent has the chemical potential μ_1^0 in polymer free solution and μ_1 in the polymer solution.

The depletion layer thickness can be calculated with an approach of Vincent [119] based on the equilibrium between the compressional or elastic free energy and the osmotic force experienced by polymer chains at a non-absorbing surface:

$$\Delta = -\frac{1}{2}\frac{\Pi}{D} + \frac{1}{2}\sqrt{\left(\frac{\Pi}{D}\right)^2 + 4\Delta_0^2} \tag{3.36}$$

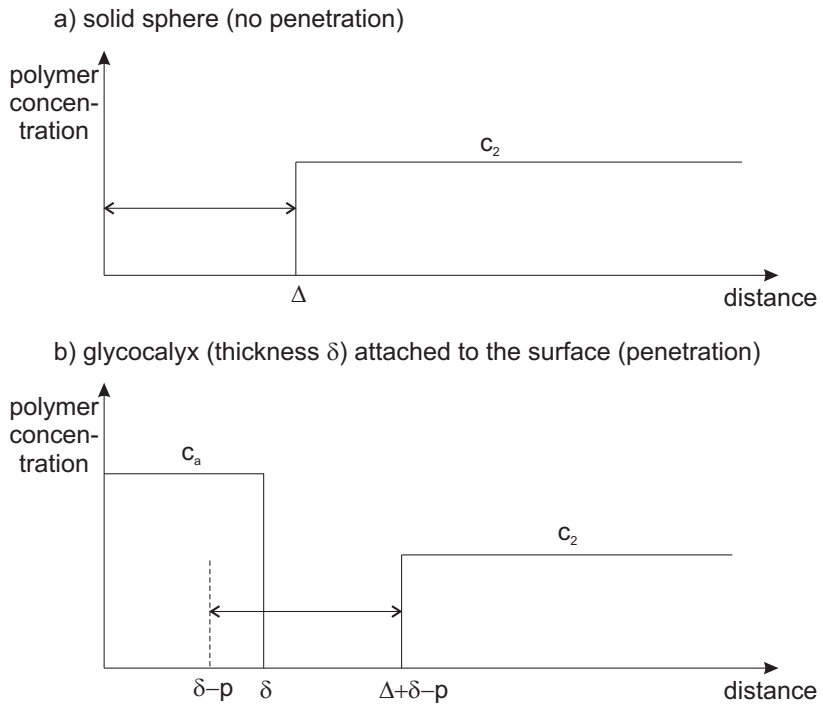

Figure 3.9.: The polymer concentration as a function of the distance from the surface of a cell shows the thickness of the depletion layer for the case of a solid sphere a), where no penetration is possible and the case b) with a layer of molecules attached to the surface, the glycocalyx, in which the polymers can penetrate.

The parameter D depends on the bulk polymer concentration and can be calculated as:

$$D = \frac{2k_BT}{\Delta_0^2}\left(\frac{c_2^b N_a}{M_2}\right)^{2/3} \tag{3.37}$$

in which k_B is the Boltzmann constant, N_a is the Avogadro number and Δ_0 is the depletion thickness for vanishing polymer concentration which equals 1.4 times the radius of gyration R_g [119].

With the osmotic pressure and the depletion layer thickness it is possible to calculate the depletion interaction energy w_D for two cells with the distance d:

$$w_D = -2\Pi\left(\Delta - \frac{d}{2}\right) \tag{3.38}$$

for $d/2 < \Delta$ and $w_D = 0$ for $d/2 > \Delta$. This case describes the situation for a hard surface without the possibility of penetration. As mentioned above, a red blood cell is however surrounded by a polymer layer, the glycocalyx and therefore it is necessary to introduce the possibility of polymer penetration into the surface (see figure 3.9).

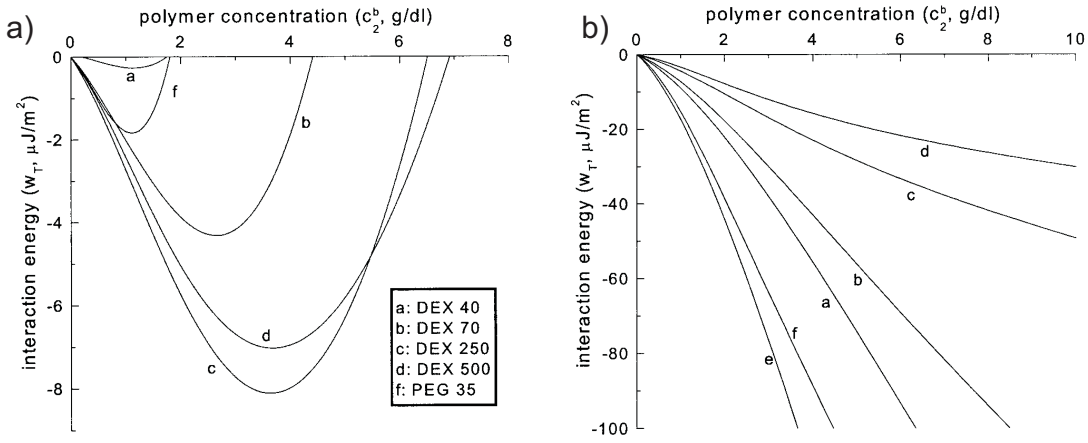

Figure 3.10.: Interaction energy as a function of the polymer concentration for different types of dextran and PEG (poly ethylene glycole). On the left side (a) a penetration of the polymers into the glycocalyx of the cells is possible, on the right side (b) it is not. As can be seen, the possibility of polymer penetration into the glycocalyx leads to a bell-shaped behavior of the interaction energy. From: Neu et al. [81].

With the thickness of the attached polymer layer δ and the penetration depth p the depletion interaction energy can be written as:

$$w_D = -2\Pi\left(\Delta - \frac{d}{2} + \delta - p\right) \tag{3.39}$$

The significantly different behavior of the interaction energy for the two cases with and without the possibility of polymer penetration into the glycocalyx is illustrated in figure 3.10. The penetration depth depends on the concentration, the molecular size and the polymer type. There are two possibilities to calculate p. The first would be to assume that the penetration proceeds until the local osmotic pressure which develops in the attached layer is balanced by the osmotic pressure of the bulk solution [120] and the second is to consider the collapse of the attached polymer under the osmotic pressure of the bulk polymer [56]. It is difficult to apply one of these models to RBCs in polymer solutions, since the interaction between the glycocalyx and different polymers is not well-known. An exponential approximation can nevertheless be used to describe the concentration dependence of the penetration depth:

$$p = \delta\left(1 - e^{-c_2^b/c_2^p}\right) \tag{3.40}$$

with c_2^p indicating the penetration constant of the polymer.

3.2.2. Electrostatic repulsion and total interaction energy

Another important force for the aggregation of red blood cells is the electrostatic interaction. The surface of the red blood cell is negatively charged which leads to repulsion between two cells. The electrostatic free energy can be calculated with an isothermal charging process to be:

$$E = \frac{1}{2}\int_0^d \int_0^\rho \Psi\left(\rho, x\right) d\rho dx \tag{3.41}$$

with the electrostatic potential Ψ between the cells and the charge density ρ. The interaction energy can be calculated by the free energy of the two cells at a separation distance d and the deduction of the free energy of two single cells with $d \to \infty$.

For the electrostatic potential Ψ one first needs to solve the Poisson-Boltzmann equation [44] with the linear approximation usually suitable for the present, moderate electric potentials. It is possible to calculate Ψ for a single cell surface and two cells at a distance d assuming that the charge is evenly distributed within the glycocalyx and the same in both cells. A further simplification is the approximation of the electrostatic potential between two cells by the superposition of the potential of two single cells. The assumption therefore is that the Debye-Hückel length κ^{-1} [98] is small compared with the cell-cell distance d and the thickness of the glycocalyx δ. Hence, the electrostatic interaction energy is:

$$w_E = \frac{\sigma^2}{\delta^2 \epsilon \epsilon_0 \kappa^3} \begin{cases} \sinh\left(\kappa\delta\right)\left(e^{\kappa\delta-\kappa d} - e^{-\kappa d}\right) & d \geq 2\delta \\ \left(2\kappa\delta - \kappa d\right) - \left(e^{-\kappa\delta}+1\right)\sinh\left(\kappa\delta - \kappa d\right) - \sinh\left(\kappa\delta\right)e^{-\kappa d} & d < 2\delta \end{cases} \tag{3.42}$$

with the relative permittivity of the solvent ϵ and the vacuum permittivity ϵ_0. It follows from the preceding part that the total interaction energy w_T per unit area of the cell is

$$w_T = w_D + w_E \tag{3.43}$$

If we consider the electrostatic repulsion and the depletion interaction without the possibility of the polymer to penetrate into the glycocalyx ($p = 0, c_2^p \to \infty$), the total interaction energy increases almost linearly with the polymer concentration. Thereby, the interaction energy has higher values for smaller molecules because the larger depletion layer for the bigger molecules is outweighed by the effect of the greater osmotic pressure difference. In the case of the entire penetration of polymer into the glycocalyx ($p = \delta, c_2^p \to 0$), the realtion between interaction energy and polymer concentration follows a bell-shaped and concave curve with respect to the concentration axis and is also showing an increase of the maximal w_T values with increasing molecular mass.

In earlier measurements Buxbaum et al. [22] tried to determine the cell-cell surface affinities for red blood cells with micropipette techniques. They pushed a membrane

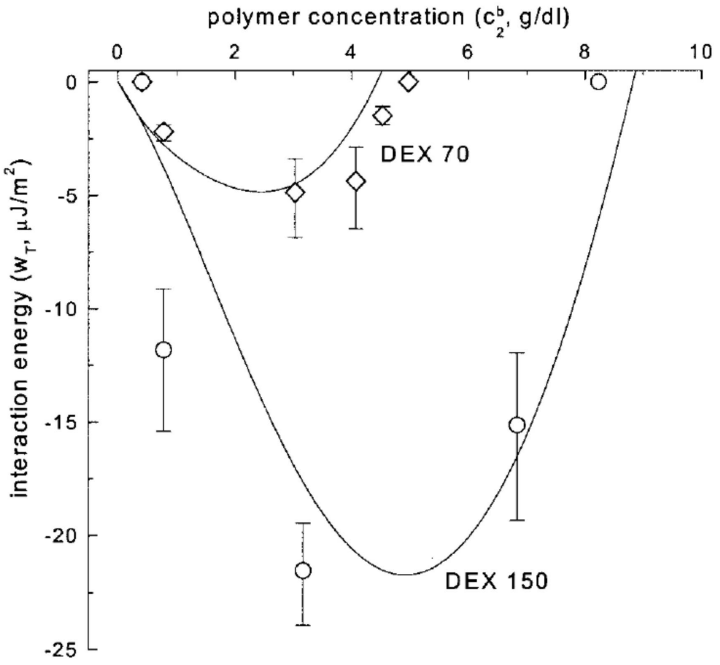

Figure 3.11.: Interaction energy obtained by fitting of the penetration constant to the peak value of the experimental data of Buxbaum et al. [22] and plotted against the polymer concentration for dextran70 and dextran150. From: Neu et al. [81].

sphere against an intact RBC and measured the extent of encapsulation for different dextran concentrations in the surrounding solution. The results showed a biphasic relation between the affinity and the concentration. Neu et al. [81] varied the penetration constant c_2^p in their model until the calculated peak interaction energy was equal to the values of Buxbaum et al. (figure 3.11). With this value for the penetration depth of the polymer the calculated interaction energies are in good agreement with the experimental results. Other experimental investigations with various techniques [80, 17], like light transmission and ultrasound backscattering showed the same concentration dependent behavior as can be seen in figure 3.12.

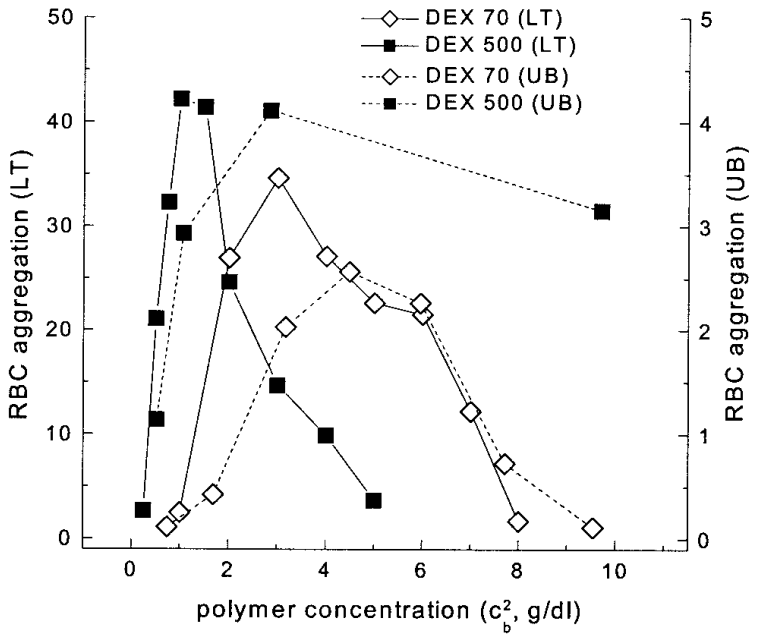

Figure 3.12.: RBC aggregation against the dextran concentration obtained with light transmission measurements (left axis) and ultrasound backscattering experiments (right axis). The bell-shaped behavior is clearly visible. From: Neu et al.[81].

3.2.3. Bridging

The depletion model competes with the bridging model to describe the aggregation of red blood cells. In the depletion model, the reason for the adhesion of the cells are the entropic forces discussed in the previous section caused by the depletion of macromolecules between the cells when they approach each other. In contrast, the bridging model [19, 27] proposes a situation where a macromolecule binds at the cell membranes of two cells which are close to each other and forms a bridge between them (see figure 3.13). In studies on the intercellular distance [26], it was discovered that cells are closer than the diameter of the hydrated macromolecules. Therefore, it was assumed that both end points of the flexible polymers are adsorbed to the surfaces of nearby cells, resulting in an adhesion.

It is difficult to interpret existing data because there exist a lot of potential artifacts influencing the determination of adsorption of macromolecules to red blood cells [54]. Hence, there are still no conclusive data to prove the assumption of the bridging model. However, several studies in the recent years favor the depletion model [2, 81].

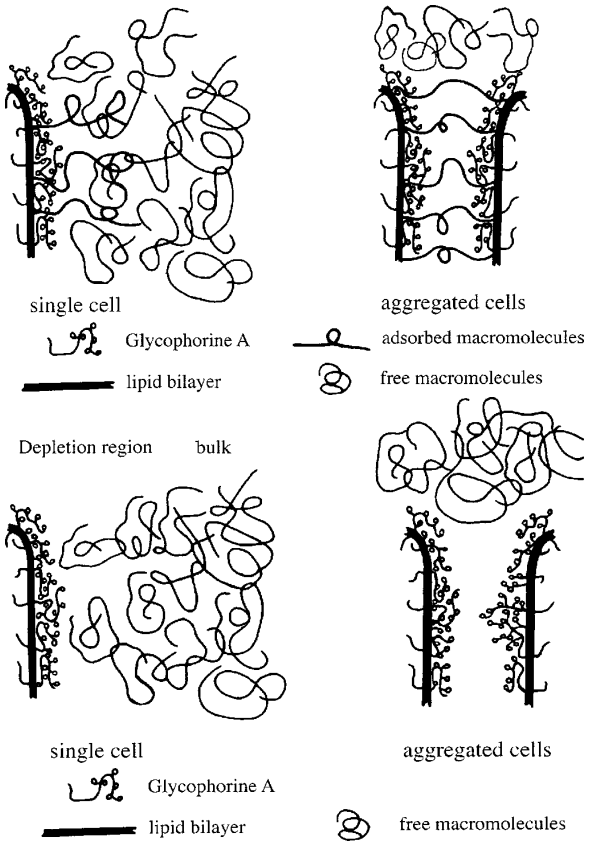

Figure 3.13.: Sketch of the adhesion of two RBCs explained with the bridging model (upper image) and the depletion model (lower image). From: Bäumler et al. [8].

3.3. Red blood cells and blood flow

3.3.1. Composition of blood

The blood (figure 3.14) which is flowing through the body at all times to transport oxygen from the lungs to all our organs and the carbon dioxide back to the lungs consists of two components. The fluid part is called blood plasma and composes 55% of the total volume of the blood in healthy conditions. The blood plasma is an aqueous solution (92% water) of proteins and electrolytes and contains the clotting factors which are necessary to start the process of blood coagulation to close a wound. The amount of salt ions in the solution is about 100 mmol/l for chlorid ions and 140 mmol/l for natrium ions, together with other ions in very small concentrations. The pH value of the fluid is around 7.4 and the density is just slightly above the density of water at 1028 g/l [92].

The residual 45% of the total blood volume are solid components, the blood cells. This percentage is also called hematocrit. The biggest amount of the cellular components are the red blood cells (RBCs) or erythrocytes with 4.5 to 5.5 million per microliter, followed by the platelets or thrombocytes with 300,000 per microliter and finally the white blood cells or leucocytes with 4,000 to 11,000 per microliter. The density of whole blood is 1055 g/l and the blood accounts for 8% of the total weight of the human body, which gives a total blood volume of 5 to 6 litres on average [92].

Under normal conditions, the shape of a red blood cell is a biconcave disc with a diameter of seven to eight micrometers and a thickness of one to two micrometers. The volume of one cell is about 90 fl and the surface has a size of approximately 136 μm^2. It has a life span of about 120 days and older cells are removed continuously from the blood circulation while new cells are produced by the body in the bone marrow at a rate of two million per second. The time a red blood cell needs for one complete circle through the vascular system is about 20 s.

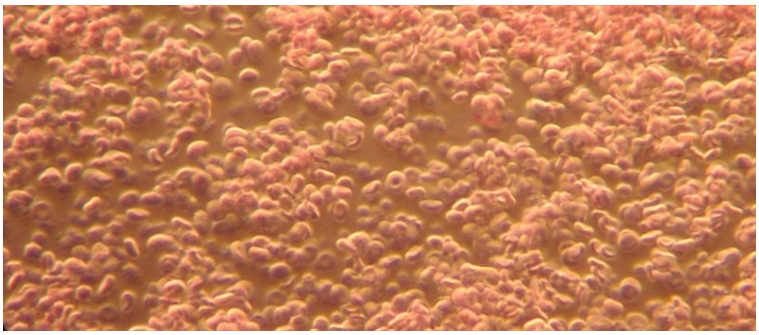

Figure 3.14.: Human blood at a magnification of 1000× in dark field view. The size of the field of view was 200 µm × 100 µm.

A strong increase of the plasma's salt concentration will lead to an efflux of water from the cell and result in cell shrinkage, while decreasing the salt concentrations results in an influx of water (figure 3.15), eventually leading to a disruption of the membrane and therefore the destruction of the cells. This would for example happen if RBCs are stored in pure water.

While the platelets are the central component in the coagulation process and the leucocytes build an important part of the immune system, the main role of the erythrocytes is the transport of oxygen and carbon dioxide. Therefore, the erythrocytes consist to 90% of the protein hemoglobin which binds oxygen very easily and is responsible for the red color of the blood. If the pH value or the salt concentration of the surrounding medium is changed, the erythrocytes undergo a shape transition from a discocyte to another possible shape like stomatocyte, spherocyte or echinocyte.

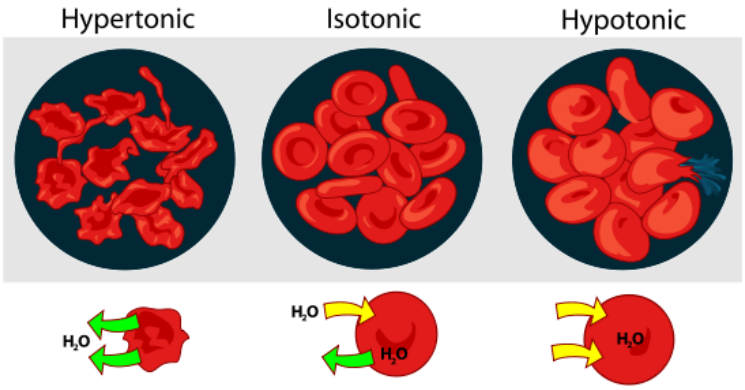

Figure 3.15.: Changes of the RBCs due to osmotic driven variations of the intracellular water amount for different external salt concentrations.

3.3.2. Blood flow

As the surface of the RBCs is much bigger than the size which would be necessary to surround their volume, the cells are very flexible and can manage to squeeze through small capillaries which are thinner than the size of the cells at rest. During the aging process, the cells constantly lose their deformability. Some diseases also influence the flexibility of the cells and thus cause problems because the transport through the narrow capillaries is no longer possible.

Another important attribute of blood flow is the aggregation of red blood cells to each other. The formation of a thrombus in the vascular system can be very dangerous and lead to death. While this adhesion of many red blood cells can cause severe problems like infarction or thrombosis, the reversible adhesion of red blood cells to linear objects, so-called rouleaux, happens constantly during the circulation of the blood [42]. The biggest vessels, connected directly to the heart have diameters

vessel type	diameter [mm]	mean flow velocity [mm/s]	wall shear rate [1/s]
aorta	16-32	600	150-300
artery	2-6	150-500	200-2,000
arteriole	0.04	5	1,000
capillary	0.005-0.01	0.5-1	400-1,600
post-capillary venule	0.02	2	800
venule	0.1	5	400
vein	5-10	150-200	120-320
vena cava	20	100	40-60

Table 3.1.: Diameters of different vessel types, flow velocities through them and wall shear rates calculated as 8v/d [10].

of around 2-3 cm and the velocity of the flow in this part is between 10 cm/s and 60 cm/s. In these vessels, the shear rates are low and the aggregates can form. To cover all areas of the body and have the possibility to deliver oxygen and other important substances to all organs, the system of vessels branches frequently and the smallest capillaries where the exchange of the oxygen and the carbon dioxide takes place are only 5 µm thick. The flow velocity in these narrow channels is in the order of 1 mm/s. Here, the shear rates are higher and it is assumed that the aggregates break again [100]. A tabular overview for the diameters of the different vessel types and the corresponding velocities and shear rates is given in table 3.1.

The rheology of blood has been investigated for a long time. It is known that blood shows a shear-thinning behavior [73] and that a certain yield stress is necessary to start the shear movement [29, 30]. It turned out that the rheological properties of blood at low shear rates up to 20 s^{-1} can be characterized quite sufficiently with the Casson model [24] (see figure 3.16):

$$\tau^{0.5} = b^{0.5} + a^{0.5}\,\dot{\gamma}^{0.5}, \tag{3.44}$$

where a and b are constants. In the case of blood, the constant b equals the yield stress τ_y and the slope a is approximately equal with the viscosity at very high shear rates η_N, when the viscosity does not vary with the shear rate anymore [75, 43]. Therefore, the Casson equation can also be rewritten as:

$$\tau^{0.5} = \tau_y^{0.5} + \eta_N^{0.5}\,\dot{\gamma}^{0.5}. \tag{3.45}$$

At shear rates of 100 s^{-1} and higher, the blood shows Newtonian behavior [75]. The aggregation of red blood cells to rouleaux due to the presence of fibrinogen and other plasma proteins at rest or low shear rates is supposed to be the main reason for the shear-thinning behavior of blood [94]. Studies with red blood cells suspended in

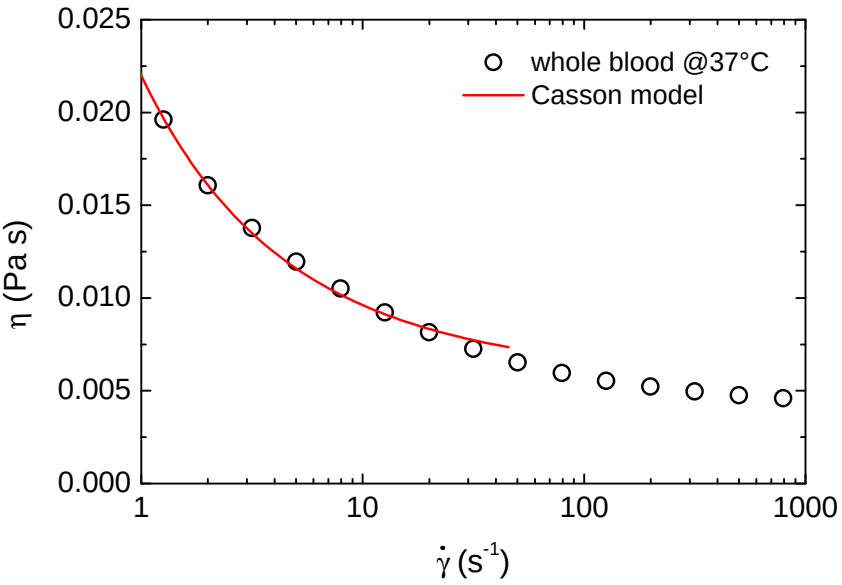

Figure 3.16.: Shear rate-dependent behavior of the blood viscosity fitted with the Casson-model.

physiological buffer solution or serum (plasma without any coagulation factors) show a significant reduction of the effect [94, 48]. Despite the important influence of the aggregation caused by the plasma proteins the rheology of blood also depends on many different factors such as temperature, hematocrit level, cell shape and deformability.

4. Experimental setup

In order to characterize the blood plasma and some complex fluids (different concentrations of poly ethylene oxide in different solvents) in rotational shear movements and elongational stretching movements as well as in the case of the flow through a channel with a varying cross section, three different kinds of measurements were performed. The flow through the contraction-expansion microfluidic device was investigated by myself, while the experiments in the rotational rheometer (Haake MARS) and the capillary break-up extensional rheometer (CaBER) were done by coworkers.

As the data available for the dextran or plasma protein induced adhesion of red blood cells are all obtained by indirect measurement methods the goal was to confirm the data with a direct method in order to get the interaction energy between two cells. We chose to perform single cell force spectroscopy measurements with an AFM (atomic force microscope) for this purpose. The clustering of red blood cells aroused by the influence of dextran and fibrinogen was expected to be also present under flow conditions. Therefore, a microfluidic device was designed which had narrow channels of the size comparable to the red blood cells.

4.1. Rotational shear rheometer

A commercial Haake MARS II rheometer was used to perform the shear-rheometrical measurements. The standard setup is the cone-plate geometry with a round plate at the bottom and a cone with a small angle α above (see figure 4.1). After filling the gap between the cone and the plate with the fluid, it is possible to shear it by rotating the cone and at the same time measure the torque acting on the cone. The relation between the measured torque T and the shear stress $\tau = A\,T$ is given by the geometry factor A of the actual setup, which depends on specific properties of the geometry.

Hence, it is possible to get the apparent viscosity of the fluid $\eta(\dot{\gamma}) = \tau/\dot{\gamma}$ as the quotient of the shear stress and the shear rate ($\dot{\gamma} = \frac{\partial v_x}{\partial y} = \Omega/\alpha$). The advantage of the cone-plate geometry is the small amount of fluid necessary to perform a measurement (1.3 ml are sufficient). However, the liquid-air interface at the edge of the geometry may lead to surface effects which distort the measured values. The double-cone geometry can be used to minimize these surface effects because the liquid-air interface is much smaller and also located at a position where the torque is minimal.

During the measurement, the temperature of the fluid is kept constant ($\Delta T = \pm 1°\mathrm{C}$) with a thermostat. To get the pure viscosity of the polymer η_p, it is obviously

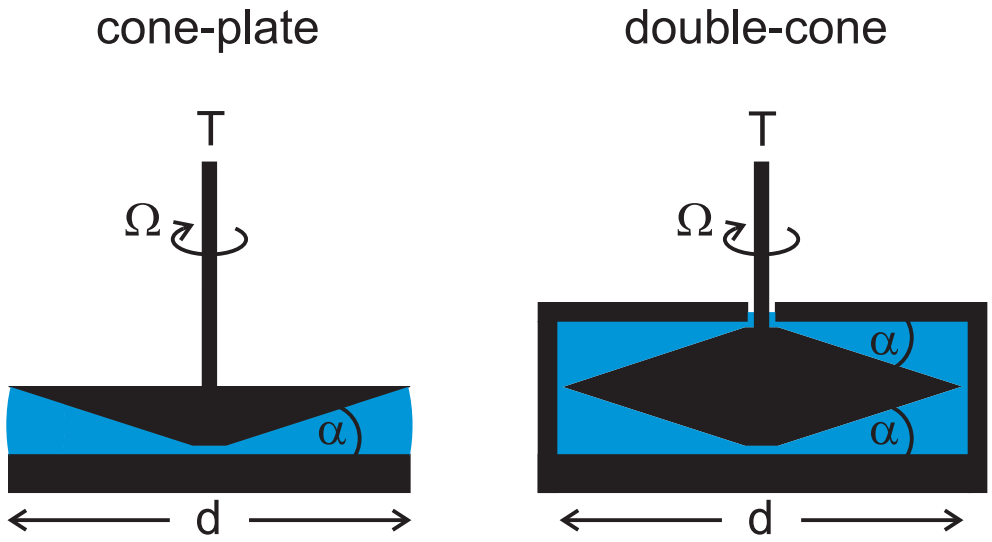

Figure 4.1.: Sketch of the principle of the rheometer measurements and two standard geometries (cone-plate and double-cone with the angle α). The fluid gets sheared with a constant angular velocity Ω, while the torque T can be measured.

necessary to eliminate the viscosity of the solvent η_s by substracting it from the measured value $\eta_p = \eta - \eta_s$. In figure 4.1 one can see the principle of a rheometer measurement. In general, there are two possible modes to run the rheometer. The shear rate can be preset to a fixed value and the torque needed to reach this value is measured (rate-controlled) or the shear rate is measured for a constant torque value (stress-controlled). Our measurements were performed in the rate controlled mode.

4.2. Capillary break-up extensional rheometer

The measurements for investigation of the purely elongational properties of different fluids were done in a self-built CaBER setup. The main parts are two round plates with a diameter of 1 mm oriented coaxially and parallel to each other, whereof the upper one could be moved with a linear motor (see figure 4.2).

A droplet of the fluid is placed on the fixed lower plate with a pipet before the upper plate is approached to the lower one until it is also in full contact with the droplet. Then, the upper plate gets withdrawn again, either linearly or in a step movement. Thus, it was possible to elongate a small amount of a fluid with a defined rate. During the withdrawal process, a capillary bridge is built between the two plates or in more detail between the two fluid reservoirs which are located on the plates and have a hemispherical shape. The capillary bridge is getting thinner over time and breaks

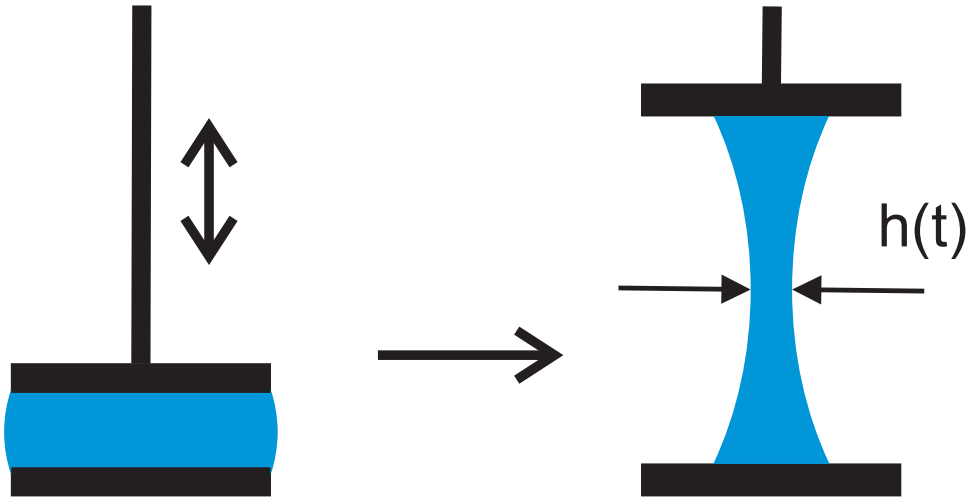

Figure 4.2.: Simplified sketch showing the CaBER experiment. The thinning of the filament $h(t)$ is recorded with a high speed camera.

very fastly for Newtonian fluids, while the thinning for complex fluids is driven by capillary forces and follows an exponential law (see section 3.1.7).

The filament is illuminated with a halogen lamp from behind and a high-speed camera is used to record the thinning process which is observed through a tube lense and a microscope objective (magnification of 2×, 4×, 10×, 20× or 50×). Illumination source, sample, objective, tube lens and camera are aligned in a row, so that the filament is recorded as a shadow image. The frame rate of the camera was about 1,000 Hz, because of the high velocity of the process. A trigger signal is sent to the camera which assures the record of the desired thinning process. The recorded images are processed in a connected computer to determine the diameter of the capillary bridge at its narrowest point in dependance of the time. A fit of the obtained values with equation 3.23 gives rise to the CaBER relaxation time λ_C. According to the Oldroyd-B model, the polymer relaxation time can then be estimated as $\lambda = \lambda_C/3$ [110, 1].

4.3. Contraction microfluidic device

The fluidics for observation of the flow through a contraction-expansion with the ratio 16:1:16 has an initial width of $W = 400$ µm and a length of $L = 30$ mm. In the middle is an abrupt contraction with a width of $w = 25$ µm which is $l = 100$ µm long before the channel expands again abruptly to the initial width. The height is $h = 53$ µm and is constant in the whole device. A drawing of the channel's contraction part is shown in figure 4.3.

At the inlet and the outlet a polyethylen tube with an inner diameter of 0.5 mm and an outer diameter of 0.7 mm is connected. The fluid is filled in a glass syringe,

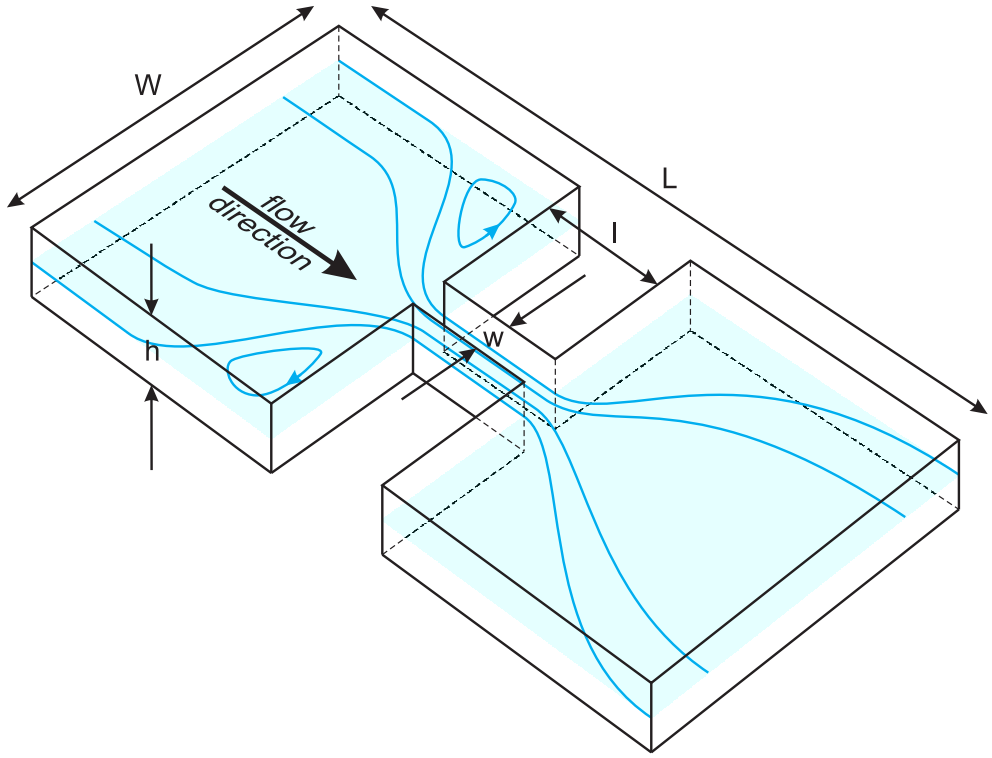

Figure 4.3.: Sketch of the contraction-expansion microfluidics with the description of all dimensions.

which is attached to the tube via a hollow needle, and is pushed with a syringe pump (neMESYS, cetoni) into the microfluidic channel at a defined flow rate. For all fluids lacking red blood cells, it is necessary to add a tracer particle solution containing fluorescent beads with a diameter of 500 nm at a concentration of 2 µl per ml to visualize the streamlines.

The microfluidic device is positioned on an inverted microscope and can be illuminated either with a LED light source or for the fluorescence measurements with a mercury gas lamp. The part of the channel directly upstream of the contraction is observed with a 20× objective, whereby the field of view is just big enough to see the complete width of the channel. A fluorescence-sensitive camera connected to the microscope is used to record movie sequences of the flow for different fluid velocities with a duration of some seconds. A picture of the setup is shown in figure 4.4 for measurements with blood.

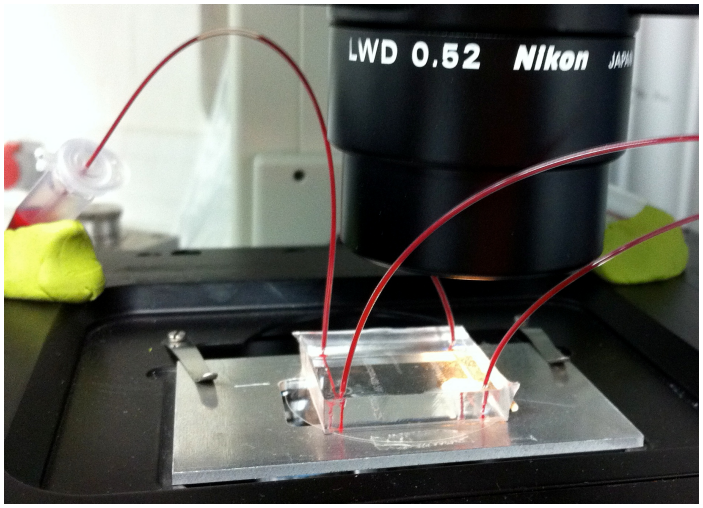

Figure 4.4.: Picture of the contraction microfluidic device on the microscope during measurements with blood as can be seen by the red color of the tubes.

4.4. Atomic force spectroscopy

When using an AFM, the goal usually is to measure the surface profile of a probe. With this method it is possible to reach resolutions in the order of the size of an atom. By using the variation of the single cell force spectroscopy (SCFS), it is possible to measure the force between two objects by attaching one to a tipless cantilever while the other one is stuck at the bottom of a petridish.

The measurements reported on in this thesis are performed with a NanoWizard 2® AFM setup with integrated CellHesion® module by JPK Instruments. The whole system is installed on an inverted microscope allowing to observe the sample which is absolutely essential for the positioning of the cantilever during the measurements. The petri dish with the sample can be moved in the x-y plane to find an object for a measurement, followed by the rough alignment of the cantilever to the same position.

Two piezo elements are then used for the exact adjustment of the cantilever in the x-y plane (range of 100 µm) and a third one to move the cantilever in z-direction (range of 15 µm) and approach the objects until they touch each other. Afterwards, the cantilever is withdrawn again while measuring the deflection of the cantilever during the whole process. For that purpose, a laser beam is aligned to the tip of the cantilever and the reflection of the laser is detected with a four-quadrant photodiode. The change in the position of the reflected laser signal allows to evaluate the position of the cantilever deflection. According to Hook's law the force between the two objects can be calculated from this deflection and the stiffness of the cantilever which is known from a prior calibration. The most common procedure to calibrate cantilevers is the thermal noise method wherein the measured thermal noise in the deflection signal is

related to the spring constant of the cantilever by the equipartition theorem. Thus, the spring constant can be calculated to be $k = \frac{k_B T}{\langle z^2 \rangle}$ with the variation of the movement z giving the thermal noise and the absolute temperature T and the Boltzmann constant k_B.

The adhesion energy between the cells and the maximum adhesion force can be evaluated from the force-distance curve recorded during the measurement process. Figure 4.5 shows the different steps of the procedure: 1) Approach of the two cells, 2) contact of the cells with a preset force and for a defined time, 3) separation of the cells by retracting the cantilever while its bending gets measured, 4) the cells are separated again after the cantilever has been retracted for a sufficient distance to equal the adhesion force and break the connection. Below the illustration of the four steps, the associated force-distance diagram is shown with the different steps being designated by the different colors. Normally, the z-range of the cantilever is 15 µm which is sufficient for most AFM applications, but due to the high flexibility of many cells this range is not enough to separate the cells from each other or from the substrate. The upgrading with the CellHesion® module increases the z-range to 100 µm with the possibility to move the sample towards the cantilever or away from it. This increased pulling range also allows the separation of very flexible cells, like red blood cells.

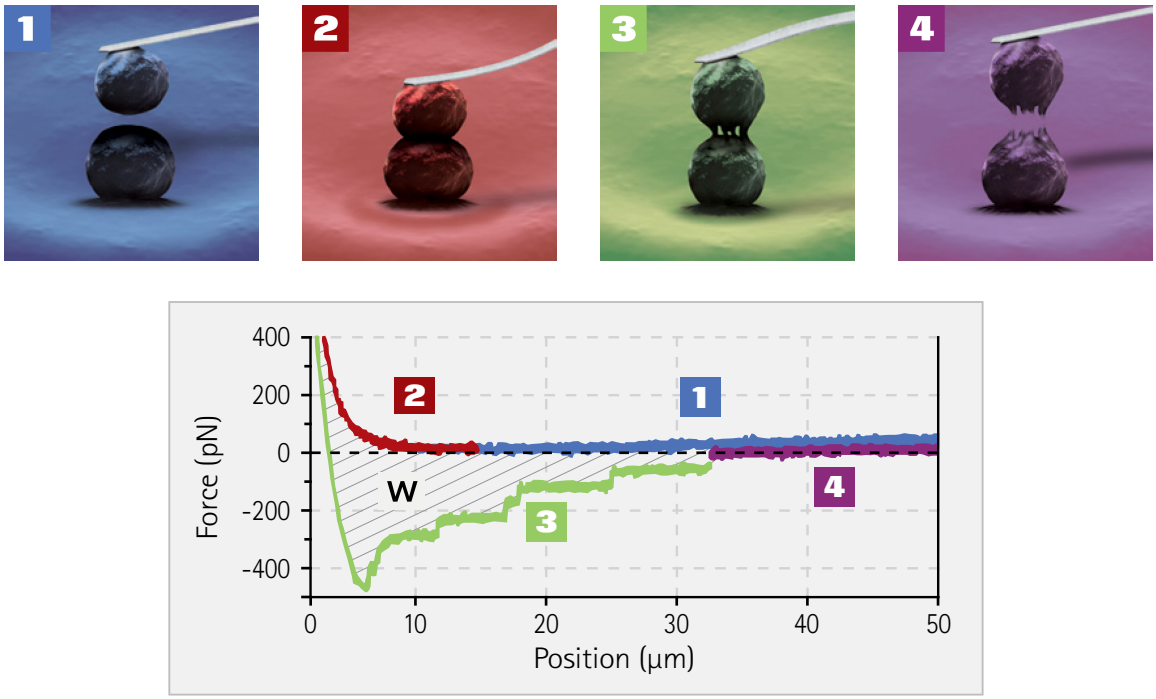

Figure 4.5.: The four steps of an atomic force spectroscopy measurement and an exemplary force-distance curve. From: JPK Instruments, Berlin.

The solution containing the RBCs and the depletion agent is filled in a temperature-controlled fluid chamber where the cells sediment to the bottom. In order to measure the interaction energy between two RBCs, one cell was glued with the substance Cell-Tak® (BD Biosciences, 35240) onto a cantilever. Therefore the cantilever (MLCT-O, Bruker, spring constant around 0,01 N/m) is functionalized with the substance by the application of a small droplet followed by a waiting time of two minutes after which the solution is carefully removed. Another waiting period of three minutes is added to allow the acidic solvent to evaporate before the cantilever is rinsed with ethanol and finally with the buffer solution. Afterwards, the functionalized cantilever is mounted to the scanning unit, followed by the pick-up of a cell by pressing the cantilever on top of it for some seconds and then lifting it again. It is now necessary to passivate the Cell-Tak® again with the addition of BSA to the solution to make sure that the second cell does not stick to the cantilever but only to the attached cell.

After preparing the cantilever, we can now turn to the solution which contains a well-known concentration of the depletion agent we endeavor to investigate. A cell which is stuck on the bottom of the petri dish is searched, the cantilever is positioned above it and approached to the cell. After the cells are pressed together for a fixed time with a certain force, the cantilever is withdrawn again. The force acting on the cantilever is measured during the whole process. In figure 4.5 one can see a typical force-distance curve resulting from this kind of experiment, in which the adhesion force is the maximum of the curve and the interaction energy can be calculated as the area between the curve and the x-axis.

4.5. Clustering measurements in narrow microfluidic channels

4.5.1. Setup

The choice of the fluidics dimensions is governed by two main thoughts. First, the possibility to mimic the flow of the cells through small capillaries and second the simplification of the automatic data evaluation if the cells and hence the clusters do not change their position perpendicular to the flow direction. In order to get higher statistics and also to be able to continue the experiment in the case of a blocked or broken channel, it is reasonable to have many channels in a parallel arrangement. Consequently, a fluidic device containing 30 parallel channels with a rectangular cross-section (width: 10 µm, height 5 µm) and additionnaly some bigger bypass channels for decreasing the flow resistance are created. The total length of the channels is 30 millimeters and they start and end in a big reservoir (height $\approx$ 1 mm).

The inlet is connected via a polyethylen tube (inner diameter 0.5 mm, outer diameter 0.7 mm) and a hollow needle to a one milliliter glass syringe containing the red blood cells in a physiological buffer solution and a certain amount of the deple-

tion agent. The syringe is mounted in a high precision syringe pump (neMESYS, cetoni) for control of the flow rate. The microfluidic channels are observed with an microscope objective at a magnification of 10× in order to have the possibility to observe ten channels at the same time. A sketch of the microfluidic channel and the field of view is shown in figure 4.6. The measurements were recorded with a camera (Imagingsource) at 30 frames per second.

At the beginning of the experiment the solution with the blood cells is mixed with the solution containing the dextran or the fibrinogen. Then, the fluid is charged into the syringe and the inlet of the microfluidic device is filled manually before the syringe pump is switched on. In order to avoid an increase of the red blood cell concentration during the experiment due to sedimentation, the device is held vertically. To make sure that the initial conditions are the same for each measured velocity, the solution in the inlet reservoir of the fluidics is replaced before every sequence of experiments. The fluid of the former measurement goes out via a second tube connected to the inlet reservoir which can be closed afterwards with a clip. A picture of the microfluidics attached to the sample holder can be seen in figure 4.7 where the assignment of the different tubes is noted. Before this step, the syringe is shaken to distribute the cells equally. For each adjusted velocity, the syringe pump is switched on followed by a waiting period of about two minutes for stabilization of the flow. Afterwards, several sequences of 30 seconds each are recorded. The images of these sequences are processed with the program described in the next paragraph.

4.5.2. Image processing and data evaluation

As the quantity of pictures taken for each measurement is too large to be manually evaluated in a convenient timescale, a LabView® routine was programmed to do the evaluation automatically. In a preliminary step, the velocity of the cells in the channels is determined with an IDL® program. Therefore, in each sequence, the difference of the positions of many objects is calculated between two images with a well-known timestep. The mean value of the individual velocities (between ten and fifty) is computed and taken as the velocity of this sequence. The grayscale images have pixel values between 0 and 255.

After the velocity for each sequence is determined, the routine for the evaluation can be started. The number of channels for which the objects are to be detected is chosen and an image is displayed to define the horizontal position of each channel which should be processed by clicking in its center. Then, the program serially processes each sequence of the measurement. It first computes the stepwidth with the velocity of the sequence and the length of the images to know which images need to be analyzed to count every object, but only once.

An enhancement of the pictures to remove everything but the red blood cells is necessary. Hence, a mean of all 900 images is calculated. Afterwards, the real analysis starts and, following the aforementioned stepwidth, the next steps are continously

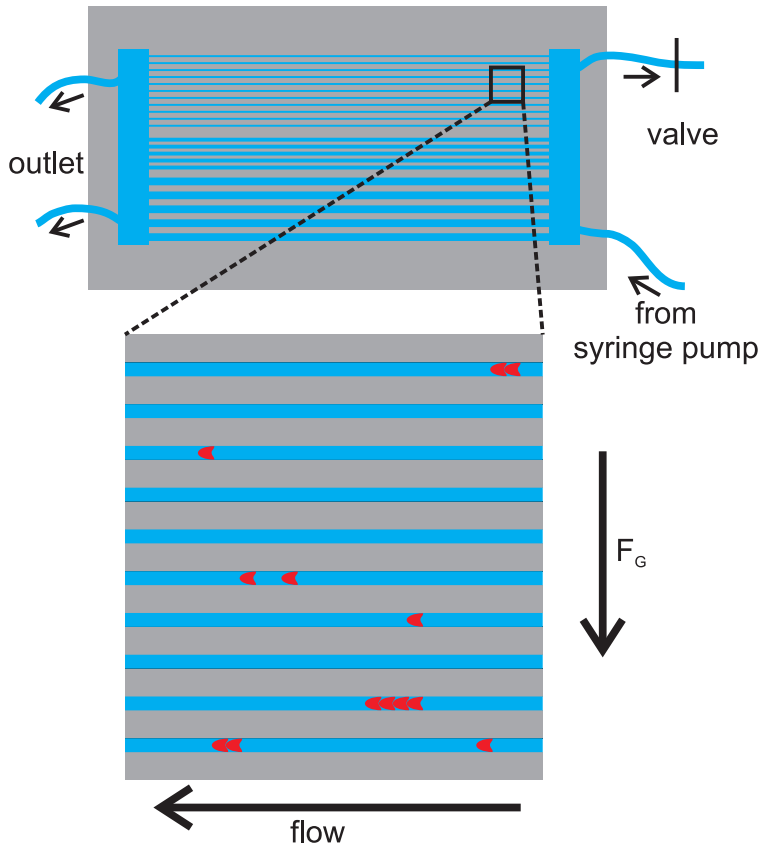

Figure 4.6.: Sketch of the microfluidic device and the field of view which was observed with the camera. The device is held vertically during the experiment. The flow direction and the direction of the gravitational force are indicated with arrows.

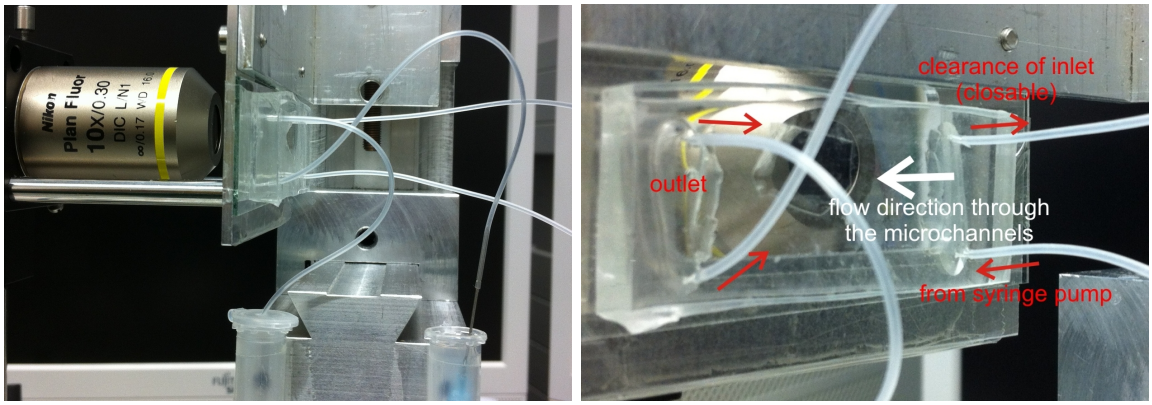

Figure 4.7.: Pictures of the microfluidic device and the objective from two different angles.

repeated. At first, the mean is subtracted from the grayscale picture and the constant 255 is added to shift all values to be positive.

Secondly, the image is binarized at a certain threshold and some corrections are made to clean the pictures of artifacts which are generated during recording due to vibrations.

In the third step, the columns containing the pixel values of each channel are added with the 25 columns to their left and to their right to make sure to get the complete width of the channel even if they are tilted a little bit. This is possible because the channels are separated by 100 pixels. Now, every channel, represented by the sum of 51 columns, is processed one after the other.

The fourth step consists in estimating the positions of all pixels with a value of at least 255, representing the red blood cells. Two red blood cells are considered to form a cluster if the distance between them is smaller then 0.6 $\times$ the length of a cell.

In the fifth step, the program selects with the aforementioned criterion and the preset length of one cell in pixels, how many objects of which size are present in each channel and writes the cluster size together with its vertical position (center of the cluster) into a file. For verification of this automatic evaluation, the detected length of every object is written as a number just next to its position in the channel.

In the final step, the output file is created. Therefore, the amount of the different objects is counted and divided by the total number of objects to obtain the distribution of cluster sizes. The hematocrit is calculated by the total number of cells and the volume of the fluid given by the cross section and number of processed channels and the flow velocity. This value is also written in the output file, together with the velocity, the distribution, the number of clusters and the number of cells.

5. Elastic properties of plasma in rheometer and contraction microfluidic measurements

5.1. Introduction

Plasma is the fluid in which the cellular ingredients of the blood are suspended. The characteristics of blood flow are highly affected by the RBCs, because their fraction is about 45 vol%, but also the properties of the plasma can influence the flow. The liquid phase consists of mainly water with some proteins, mineral ions and glucose.

A Newtonian fluid (e.g. water) is characterized by its viscosity, which is the constant quotient of shear stress and shear rate. The addition of small amounts of polymers to a liquid can significantly change the characteristics of its flow. If the shear stress and the shear rate are no longer proportional, a fluid is called complex or non-Newtonian. For these liquids one can define an apparent viscosity, depending on the shear rate, which is also the quotient of the shear stress and the shear rate, but is not a constant anymore (see figure 3.2 in chapter 3).

Blood is known to show shear-thinning behavior [51] and it is widely believed that the RBCs mostly determine this behavior because they tend to form linear aggregates (rouleaux) at low shear rates which break up again at higher shear rates [11] (see also chapter 3.3.2). The formation of these rouleaux is caused by the plasma proteins and will be discussed in detail in chapter 6 while this chapter will focus on the properties of the liquid medium. As mentioned in the literature survey (chapter 2), up to now, blood plasma was considered a purely Newtonian fluid. In this chapter, I will describe the measurement and present the results which lead to the conclusion that plasma is indeed a visco-elastic fluid. The flow properties are investigated by means of three different methods, each focussing on a different kind of flow. The behavior under shear flow conditions are analyzed with a shear rheometer, the purely elongational flow is surveyed in the CaBER setup and the flow through a suddenly constricted channel is observed in microfluidics measurements (for details on the setup, refer to chapter 4). In further studies, polymer solutions are analyzed to find a good model solution for plasma, not for medical applications, but to accurately mimic its flow behavior to replace it in future experiments by a synthetic liquid.

5.2. Results

We test human blood plasma, whole blood and different polymer solutions with three different measurement techniques. Pure water and a solution of albumin, which is the protein with the highest concentration in plasma ($\approx 60\%$), are also analyzed. In more detail, we use the polymer polyethylene oxide (PEO, Sigma Aldrich) with a molecular mass of $M_w = 4 \cdot 10^6$ g/mol in various concentrations. To increase the viscosity, the polymer is not diluted in pure water but in a mixture of water and glycerol. In solutions containing RBCs, the water is replaced by a physiological buffer solution (PBS, phosphate buffered saline, Invitrogen) to ensure the survival of the cells. It is checked that this buffer solution has the same properties as water with regard to shear viscosity, relaxation time and flow behavior through a contraction. The names and the composition of all solutions are listed in table 5.1. The preparation of the solution is described in more detail in the appendix A.2.2.

solution	solvent *wt%*	PEO *ppm*	RBCs *vol%*
$PEO50_{15/85}$	15/85 glycerol/water	50	-
$PEO500_{15/85}$	15/85 glycerol/water	500	-
$PEO50_{55/45}$	55/45 glycerol/water	50	-
$PBS_{15/85-Hct50}$	15/85 glycerol/PBS	-	50
$PEO50_{15/85-Hct50}$	15/85 glycerol/PBS	50	50

Table 5.1.: Overview about the composition of the investigated solutions.

5.2.1. CaBER and rotational rheometer

The different solutions are tested in the rheometer to obtain their shear viscosity values. A certain amount of fluid is filled in the double-cone geometry and sheared at rates between 1 s^{-1} and 1000 s^{-1} in the rate-controlled mode. The instrumental noise is reduced by following a special protocol: The torque signal for each shear rate was integrated over at least one full revolution of the cone.

In figure 5.1 one can see the shear rate dependent behavior of the viscosity for four of the solutions and water as a reference value. Above the grey shaded area which marks the resolution limit of the rheometer, given by the minimal resolvable torque of $\tau = 2\ \mu$ Nm, the accuracy of the measured values is $\Delta\eta = \pm 0,1$ mPas. The temperature is kept constant at $T = 20 \pm 1°$C. The diagram shows a Newtonian behavior for plasma and the $PEO50_{15/85}$ solution with a constant shear viscosity as can be seen from the almost flat curve. A significant increase of the viscosity and the occurrence of shear-thinning behavior can be observed by the addition of a physiological amount of RBCs to the polymer solution, which is shown in the values belonging to $PEO50_{15/85-Hct50}$.

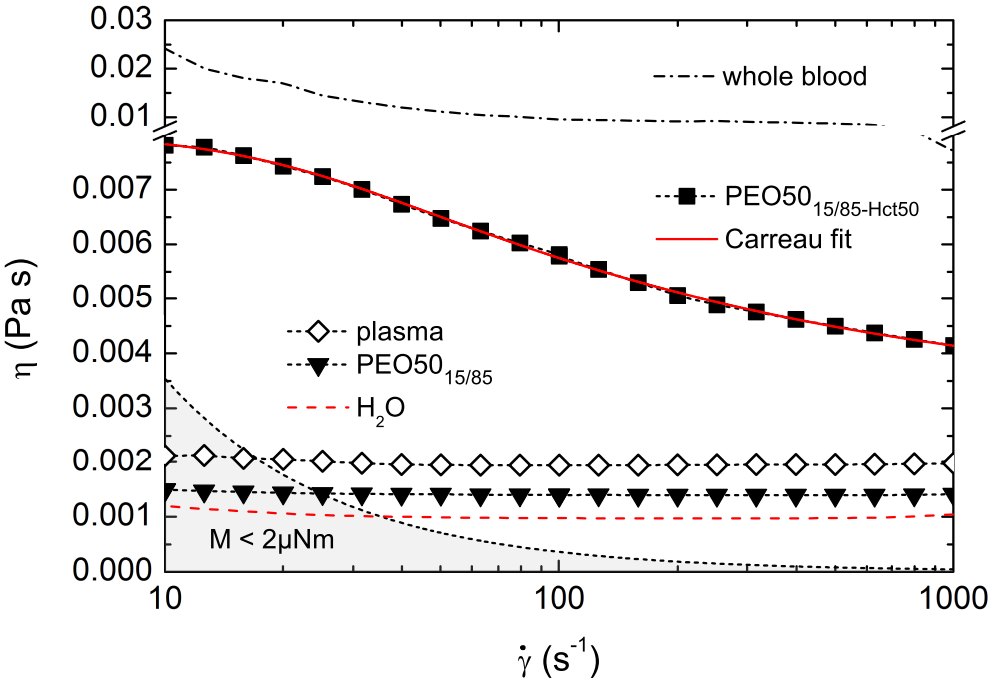

Figure 5.1.: Shear rate dependent viscosity data of two different polymer solutions, plasma, whole blood and water. The grey area at the bottom indicates the regime below the resolution of the rheometer.

The viscosity of whole blood is higher than the viscosity of the $PEO50_{15/85-Hct50}$ solution for all applied values of the torque.

The extensional rheometry is investigated in the CaBER setup to determine the relaxation times λ_C (see section 3.1.7) from the thinning behavior of the solutions. Figure 5.2 gives an overview of the thinning behavior for four different fluids at a magnification of 4×. The break-up of the BSA solution is purely Newtonian, like for water, leaving a well-known satellite droplet. In contrary, the established complex behavior of the blood leads to the formation of a filament which is thinning exponentially over time before breaking up. In the thinning process of the plasma, it is also possible to observe filament formation, a clearly non-Newtonian property. The polymer solution $PEO50_{15/85}$ shows the same characteristics as the plasma. All three solutions without spontaneous break-up also show the typical blistering instability at the very end of the thinning process characterized by the appearance of small beads on the filament [99].

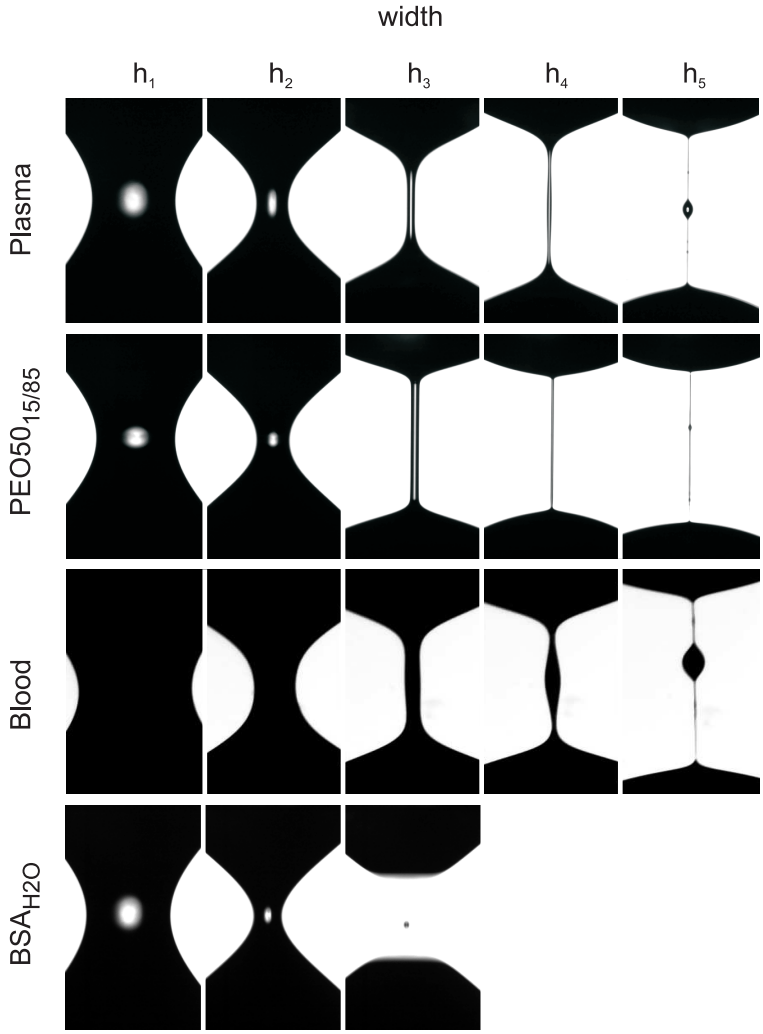

Figure 5.2.: Constriction process of different solutions in the CaBER experiment. The plasma as well as the polymer solution and the whole blood show a capillary bridge which is thinning exponentially over time, while the BSA solution just breaks up spontaneously. The images have a size of 833 µm × 1344 µm.

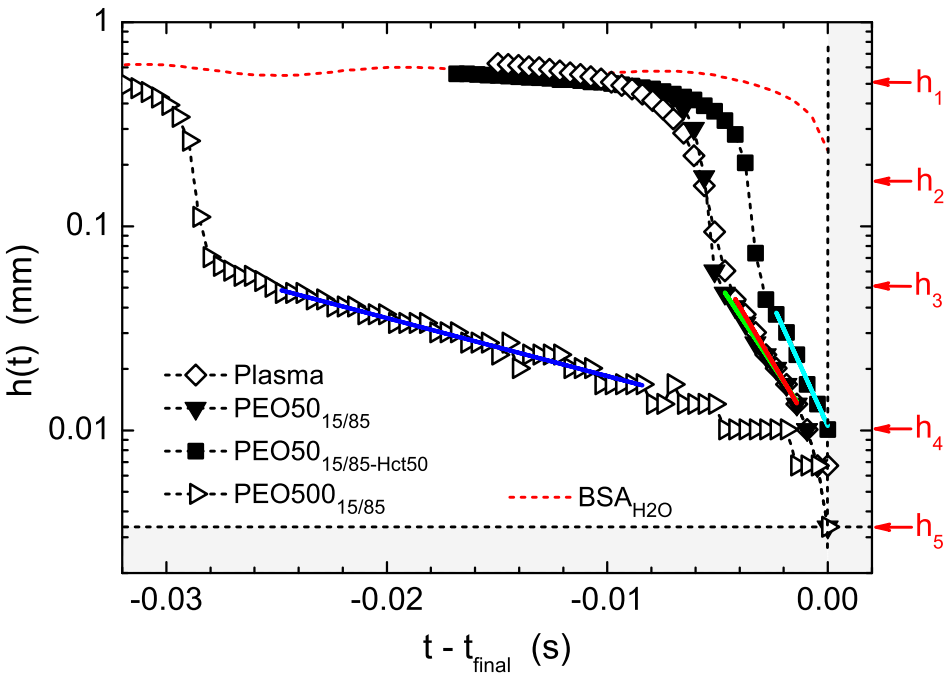

Figure 5.3.: Width of the filament during the thinning process for different solutions in a semilogarithmic plot. The solid lines indicate the fit to obtain the CaBER relaxation time according to equation 3.23.

The minimal width of the filament over time ($t - t_{final}$ to simplify the comparison of the solutions by matching the times of rupture) is shown in figure 5.3 on a semilogarithmic scale. The solid lines indicate the exponential fit during the thinning process and the arrows labeled with h_1 to h_5 on the right side belong to the five pictures in figure 5.2 respectively. The curves start at a width of approximately $h_1 \approx 0,5$ mm and initially describe a uniform thinning down to $h_2 \approx 1,7$ mm. Up to this point, the polymers do not yet affect the flow, so there is no difference between the solutions. During the further thinning of the filament, the Newtonian sample (BSA_{H_2O}) breaks up very rapidly (shortly after width h_2) while the other samples are thinning exponentially over characteristic time scales λ_C.

The values for all solutions are summarized in table 5.2, where the value of η_0 for whole blood is of limited use, because blood is a yield stress fluid with a yield point at approximately 5 mPa, which means that it behaves as a solid until the applied stress reaches this value.

solution	temperature $T[^\circ C]$	shear viscosity $\eta_0[mPa\,s]$	relaxation time $\lambda_C(ms)$
Whole Blood	37	16.9	7.8 ± 0.6
Plasma	20	1.95	2.6 ± 0.2
Plasma	37	1.34	1.5 ± 0.2
$PEO500_{15/85}$	20	2.47*	15.7 ± 0.2
$PEO50_{15/85}$	20	1.40	2.6 ± 0.1
$PEO50_{55/45}$	20	7.88	7.9 ± 0.2
$PEO50_{15/85-Hct50}$	20	8.03*	1.84 ± 0.04
BSA_{H_2O}	20	1.24	Newt.
$PBS_{15/85-Hct50}$	37	7.6*	Newt.
H_2O	20	0.97	Newt.

Table 5.2.: (Zero) shear viscosities η_0 and CaBER relaxation times λ_C of the sample solutions. Values marked with * are obtained by a fit based upon the Carreau model [112].

5.2.2. Contraction-expansion microfluidics

The next step is to investigate the flow through a contraction-expansion channel. This geometry has a significant elongational flow component and resembles the flow at a branching from a larger to a smaller vessel or through a flow restricted vessel. After switching on the syringe pump, the flow is allowed to develop to a steady state before it is recorded for a few seconds with the connected camera. All pictures of the microfluidic flow in this chapter are taken at the position directly above the constriction and have a width of 512 pixels, representing approximately 410 µm, so the complete width of the channel is visible. The contraction ratio of the microfluidics used in this experiments is 16:1.

Figure 5.4 shows the recorded pictures for plasma in the microfluidic channel. It is observed that even for high shear rates up to $800 \cdot 10^3$ s^{-1}, the flow stays Newtonian and no instabilities can be observed. The same behavior is found for $PEO50_{15/85}$, as one can see in figure 5.5. Consequently, so this solution has again the same properties as human plasma.

If either the concentration of the polymer ($PEO500_{15/85}$, figure 5.6) or the viscosity of the solvent ($PEO50_{55/45}$, figure 5.7) is increased, the flow situation is changes. In both cases one can observe an elastic instability, leading to vortices upstream of the contraction. Unfortunately, the quality of the pictures is very low and it is hard to recognize the streamlines, but the automated photosensivity of the camera made it impossible to improve the signal-to-noise ratio of the images. The camera automatically reduces its sensitivity to be able to display the most pronounced signal as the upper border of the spectrum which leads to the loss of signals at the lower border. The particles added to the solution to visualize the streamlines tend to stick

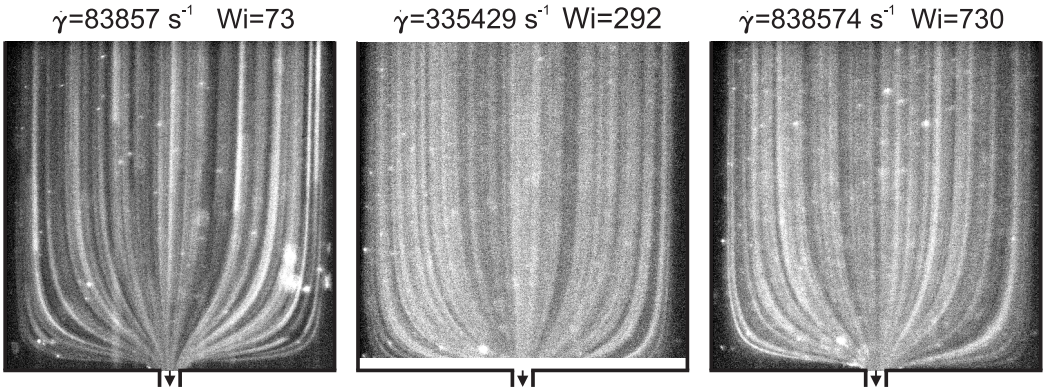

Figure 5.4.: Picture series of plasma immediately upstream of the contraction for different flow rates. The corresponding shear rates and Weissenberg numbers are given above each picture. Even at high shear rates, no instabilities are observable.

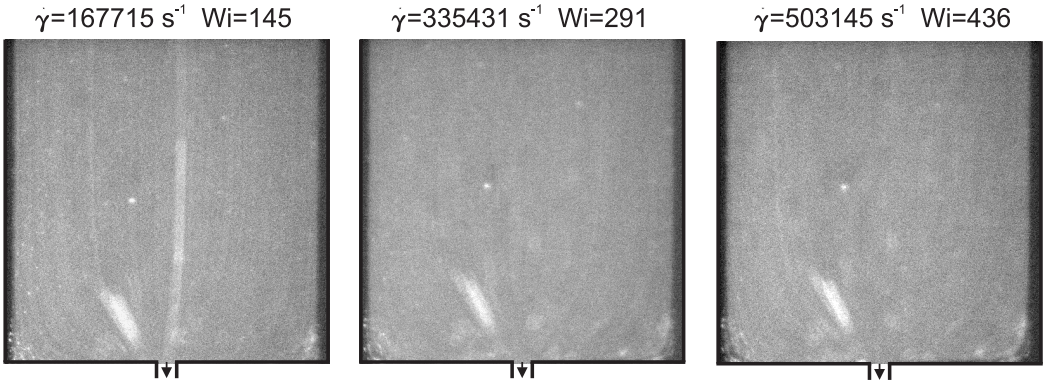

Figure 5.5.: Picture series of the polymer solution $PEO50_{15/85}$ immediately upstream of the contraction for different flow rates. The corresponding shear rates and Weissenberg numbers are given above each picture. The flow shows no instabilities.

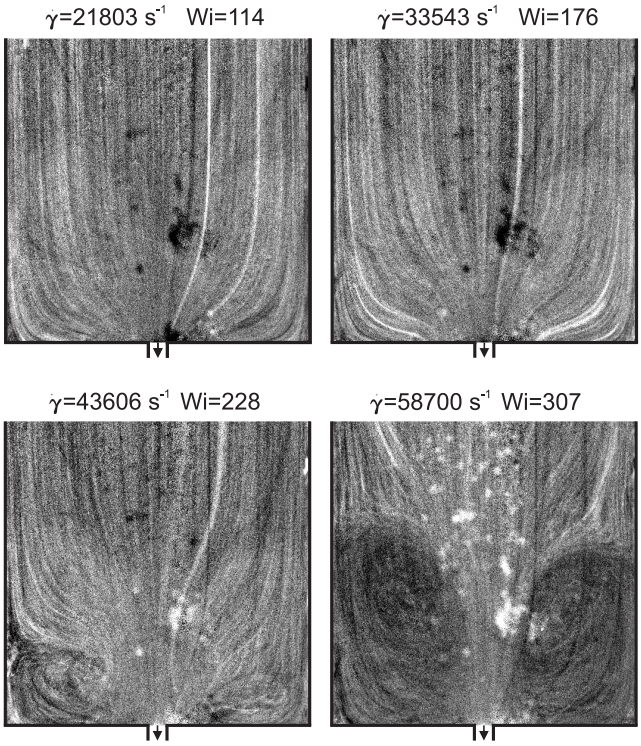

Figure 5.6.: Picture series of $PEO500_{15/85}$ immediately upstream of the contraction for different flow rates. The corresponding shear rates and Weissenberg numbers are given above each picture. The vortices upstream of the constriction are clearly visible in the lower pictures.

at the bottom or the top of the channel and produce a lot of disturbing, scattered light. Due to this unwanted light, signals which are even more pronounced for the $PEO50_{55/45}$ solution, because of the higher viscosity, it is only possible to observe one half of the channel in the images of figure 5.7. In the other half of the channels, so many particles are stuck together at the top or bottom of the channel, that everything else simply appears black. It is consequently necessary to move the field of view in order to avoid this region. Nevertheless, it is possible to observe vortices which show the viscoelastic behavior of these solutions in the contraction flow as can be seen in figure 5.6 and figure 5.7.

The suspension of the RBCs at their physiological concentration in the buffer solution shows, as expected, a purely Newtonian behavior without any instabilities (figure 5.8). On the other hand, the addition of the RBCs to the plasma-like polymer solution is sufficient to induce a clear viscoelastic behavior. The solution shows upstream vortices which increase in size for higher Weissenberg numbers (figure 5.9). They start as small lip vortices at the border of the contraction, grow in two dimensions (x and y) until they extend to the salient corners, ranging the complete width

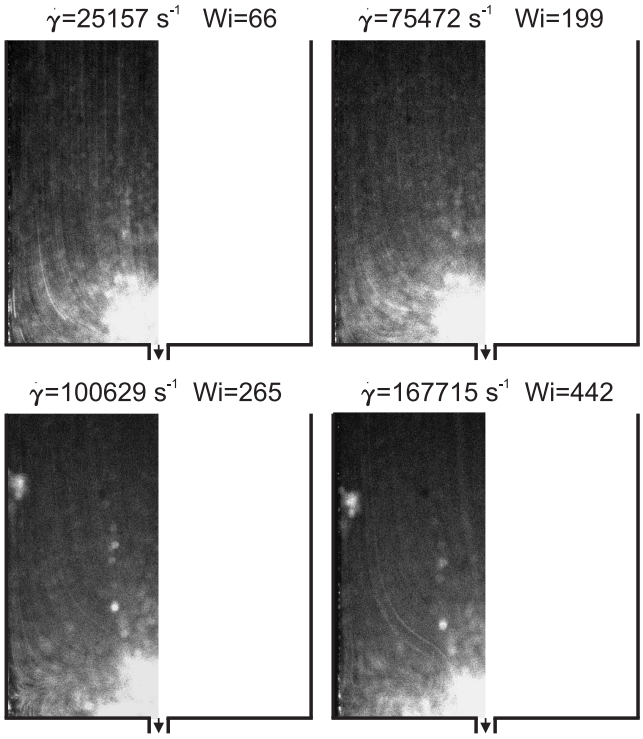

Figure 5.7.: Picture series of $PEO50_{55/45}$ immediately upstream of the contraction for different flow rates. The corresponding shear rates and Weissenberg numbers are given above each picture. As described in the text, the other half of the channel could not be recorded, due to experimental problems. In the lower pictures, it is again possible to observe vortices upstream of the constriction.

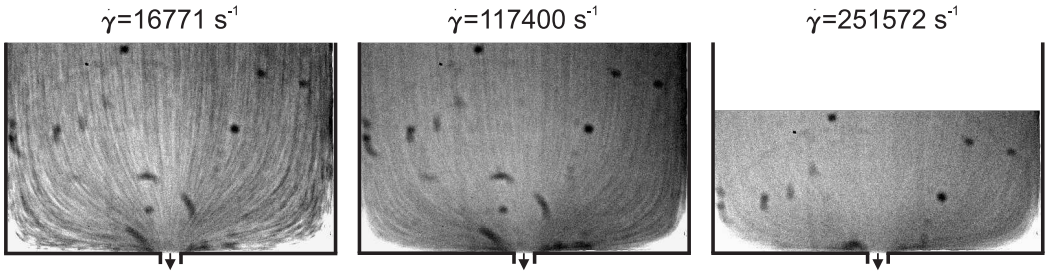

Figure 5.8.: Picture series of $PBS_{15/85-Hct50}$ immediately upstream of the contraction for different flow rates. The corresponding shear rates are given above each picture. For this polymer-free solution with RBCs no instabilities are observed.

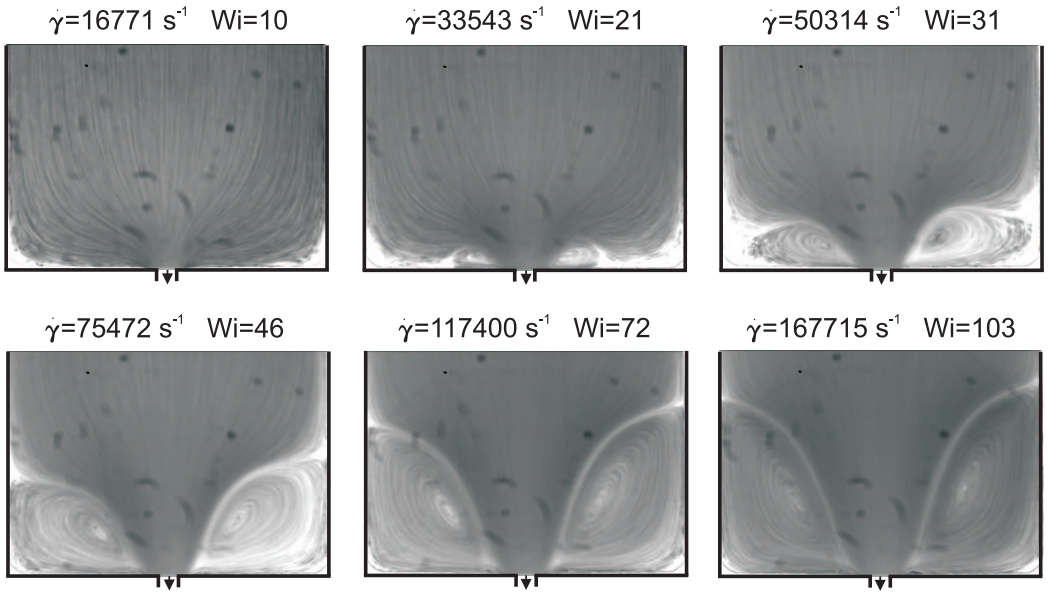

Figure 5.9.: Picture series of $PEO50_{15/85-Hct50}$ immediately upstream of the contraction for different flow rates. The corresponding shear rates and Weissenberg numbers are given above each picture. The vortices start at the contraction and grow in two directions (x and y) with increasing Wi.

of the channel and continue to grow in x-direction further upstream of the channel.

Unfortunately, the flow of whole blood does not show an instability (figure 5.10), as one would expect from the previous results, but as the blood contains many other ingredients, the situation is much more complex and there can be many reasons for the lack of the expected instability. The behavior of all fluids tested in the contraction microfluidics is listed in table 5.3.

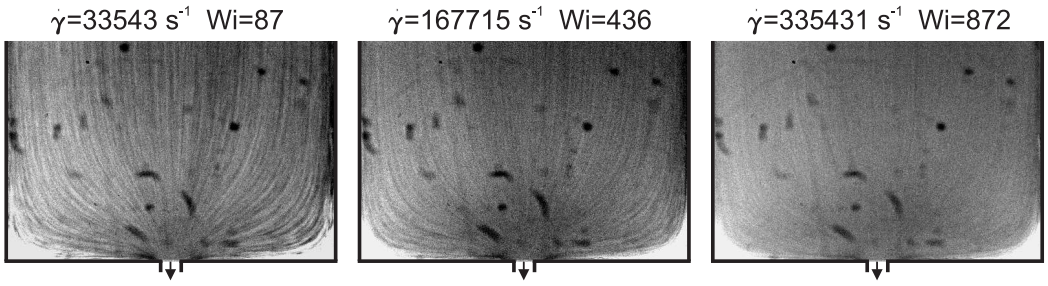

Figure 5.10.: Picture series of blood immediately upstream of the contraction for different flow rates. The corresponding shear rates and Weissenberg numbers are given above each picture. No vortices could be observed for blood.

solution	behavior	shear rate [s^{-1}]
H_2O*	Newtonian	-
BSA_{H_2O}*	Newtonian	-
Plasma	Newtonian	-
$PEO50_{15/85}$	Newtonian	-
$PEO500_{15/85}$	bending of the flowlines vortices (complete channel width)	33,500 43,600
$PEO50_{55/45}$	bending of the flowlines vortices (complete channel width)	75,500 100,600
$PBS_{15/85-Hct50}$	Newtonian	-
$PEO50_{15/85-Hct50}$	growing corner vortices vortices (complete channel width)	33,500 75,500
Whole Blood	Newtonian	-

Table 5.3.: Overview of the results obtained in the contraction microfluidics. If a non-Newtonian behavior was observable, the last column gives the value of the shear rate at which it occured. Pictures for fluids indicated with * are not shown.

5.3. Discussion

In the shear rheometer measurements, the plasma as well as the low concentrated polymer solution both showed a Newtonian behavior. The shear flow does not stretch the polymers sufficiently to create a measurable effect. The addition of a physiological concentration of RBCs to the polymer solution results in a shear-thinning behavior which can be fitted with the Carreau model [23]. As the RBCs suspended in the Newtonian buffer solution do not show any non-Newtonian effects, the origin for the shear-thinning is to be attributed to the polymers, although the effect is not visible without the RBCs. The reason for the different viscosities of the polymeric RBC solution and whole blood could be the depletion-induced adhesion of RBCs due to the plasma proteins [11].

5.3.1. Viscoelasticity of plasma

For the first time, it was possible to demonstrate viscoelastic behavior of plasma in the CaBER experiment and further investigations allowed to exclude the influence of surface effects which were responsible for previous suggestions of non-Newtonian plasma properties. Those surface effects are observed in shear rheometer measurements with a cone-plate geometry due to the liquid-air interface but vanish if a small amount of surfactant (0,01wt% of Tween 20, a soluble nonionic surfactant with the critical micellar concentration of $cmc = 0,07\text{wt}\%$) is added to the plasma. The apparent

shear-thinning is suppressed [52] in this case and the plasma behaves Newtonian in rotational shear measurements. If the cone-plate setup is upgraded with a guard ring to suppress the surface layer or if one switches to the double-cone geometry where the surface area is smaller and without a significant contribution to the total torque, the results with the surfactant are confirmed. In principle, it is possible that the surfactant itself leads to a viscoelastic filament, but the solution of the actual surfactant in water does not show any filament [32, 33, 68].

The addition of the surfactant did not alter the thinning process in the CaBER experiments presented here which again shows that the filament is not caused by a protein surface layer. In additional thinning experiments with the plasma where the surrounding air is replaced by a silicon oil [20], one can as well observe a pronounced filament of the plasma, although there is obviously no liquid-air interface. Despite albumin being the highest concentrated protein in the plasma, the BSA solution does not show any non-Newtonian behavior, so a significant effect of this component can be excluded, yet it is still not clear which proteins are responsible for the viscoelasticity.

5.3.2. Behavior under flow conditions

The investigation of the flow through a constriction of a channel does not reveal the complex behavior of plasma, but the elongational part of the flow seems to be less pronounced because the polymer solution at low concentrations ($PEO50_{15/85}$) does also not reveal complex characteristics in the microfluidics. The addition of the physiological RBC concentration again induces a non-Newtonian behavior and therefore indicates the relevance of the plasma's complex elongational characteristics for the blood flow through branching and narrowing microcapillaries. Since the solution of RBCs without the polymer behaves Newtonian in the contraction flow and particularly in the elongational flow, the polymer generates the viscoelastic behavior of the $PEO50_{15/85-Hct50}$ solution. Even if this concentration of polymers is not high enough to create observable non-Newtonian effects by itself, the addition of the RBCs and hence the increase of viscosity is sufficient for the onset of an instability.

5.3.3. Model solution

If we compare the different polymer solutions that should serve as model systems for the plasma, we see that the $PEO50_{15/85}$ is a good plasma replacement because it fairly matches the shear as well as the elongational properties. A simple increase of the solvent viscosity leads to a solution ($PEO50_{55/45}$) that matches the elongational properties of full blood, but not its shear rheology. Thus, the two solutions with 50vol% hematocrit (with and without polymer) are examined and their values compared with blood. The polymeric hematocrit solution $PEO50_{15/85-Hct50}$ reflects the elongational properties of blood only to some extent but as the $PBS_{15/85-Hct50}$ solution

simply breaks up like a Newtonian liquid, it is clear that the non-Newtonian elongational viscosity (elastic properties of the macromolecules) of plasma contributes to the non-Newtonian elongational viscosity of blood. As mentioned before, the aggregation of the RBCs in the full blood might be responsible for the remaining discrepancies.

5.4. Summary

The measurements and results described in this chapter establish a non-Newtonian behavior of human blood plasma under elongational flow. It was possible to clearly show a viscoelastic thinning behavior of a plasma droplet with the CaBER setup. The effect is not triggered by surface effects, because the solution of albumin, considered to be responsible for the protein surface layer, breaks up in purely Newtonian manner. Additional measurements with a surfactant to prevent the formation of a surface layer by the proteins confirms the results, while a creation of the filament due to the surfactant can also be discarded in a test with the surfactant diluted in pure water. The thinning experiments with the plasma surrounded by a silicon oil also show a pronounced filament of the plasma, although a liquid-air interface of the plasma is obviously missing.

In agreement with the behavior of the dilute polymer solution, a steady shear flow does not indicate any elasticity of the plasma because the polymers are stretched less efficiently in this case. All reports on viscoelasticity of plasma in shear flow can thus be attributed to the formation of a protein surface layer. The results also indicate that the elongational properties of blood are to a large extend determined by the elongational properties of the plasma proteins because the suspension of RBCs at physiological concentration in a buffer solution just breaks up in a Newtonian way in the elongational experiments.

In order to find a good model solution which can mimic the characteristics of plasma in future studies, it turns out that it is necessary to take into account different kinds of flow types. The $PEO50_{15/85}$ solution matches the properties of plasma in the case of shear and elongational flow, as well as in the case of the flow through a constricted channel and can therefore be considered a proper plasma replacement for further investigations. The change in the flow behavior of this polymer solution at low concentration with the occurrence of vortices upstream of the contraction after the addition of RBCs at physiological hematocrit intensifies the relevance of the plasma's viscoelasticity for the flow properties in the microvascular system. In recent numerical results [89], the slight viscoelasticity of the solvent leads to a pronounced cell depletion layer close to the vessel boundaries. In view of these findings, the viscoelasticity of the plasma should be taken into account in future studies.

6. Clustering of red blood cells in narrow channels due to depletion interaction

6.1. Introduction

During the flow of red blood cells through the vascular network inside the human body, the smallest capillaries through which the cells have to pass through are smaller than the diameter of a cell at rest. Due to their high deformability the cells succeed to overcome this constriction.

Also, the adhesion of red blood cells can influence their flow through the small capillaries and is therefore very important for the understanding of blood related diseases. It is known since the 1980s that the formation of linear aggregates, called rouleaux (shaped like a stack of coins) happens all the time during the flow of blood through the human body. They develop in the bigger vessels and are claimed to break-up again in smaller capillaries where the shear rates are higher. The previous studies of the blood rheology with rheometer measurements revealed a shear-thinning behavior of blood which was attributed to the existence of aggregates at small shear rates and their disaggregation with increasing shear rates. As the viscosity reaches a constant level for pronounced shear rates [75] that exist widely in the vascular system [11], it was claimed that the rouleaux are broken up again and hence do not play a role in the physiological blood flow.

This reversible process is described by two different models, the bridging and the depletion model and as mentioned before, it is still not completely clear which one fits the situation better. In the experiments presented in this chapter, the interaction energy between two RBCs is measured by means of single-cell force spectroscopy for the two macromolecules dextran and fibrinogen known to induce an adhesion of the cells. The data of these measurements are the first results of cell-cell adhesion measurements obtained with a direct technique for erythrocytes in discocytic, i.e. natural shape.

In order to mimic the flow through the microvasculature, a microfluidic device with narrow channels of the same size as the smallest capillaries is designed and the distribution of all objects flowing through the channels is counted. The goal of these experiments is to investigate the influence of the flow velocity and thus the shear rate on the clustering under flow conditions as well as the effect of the polymer concentration. This will then allow to gain a better understanding of the situation in small capillaries. In order to be able to compare the results with the single cell measurements, the two tested polymers are again the sugar polymer dextran, which is widely used as a depletion agent in experimental studies, and the protein fibrinogen which is found in the human plasma at concentrations of 2-4 mg/ml [94].

6.2. Results

The interaction energy between two RBCs is measured with the method of cell force spectroscopy for confirmation of previous results. Furthermore, the influence of various interaction energies on the clustering of RBCs in narrow channels is checked. The channels are comparable in size with the smallest capillaries in the vascular system.

6.2.1. Single-cell force spectroscopy

After a cell has been attached to the canilever as described in section 4.4, it is aligned above a cell which is stuck on the bottom of the petri dish. The cantilever is then lowered and the cells are pressed together with a force of 300 pN, before the cantilever is withdrawn again. Obviously, some parameters can play an important role in this protocol, like the force which is used to press the cells together initially, the contact time of the cells and the velocity of the cantilever movement during the withdrawal process. To make sure that reasonable values for these parameters are used, additional measurements were performed in which they were varied to determine the most appropriate ones. The influence of the setpoint force was negligible as the RBCs are very flexible and already a small force is enough to produce a contact area which is sufficient.

In order to avoid additional forces due to bridging effects between the cells which are known to form in the order of seconds [18], the contact time is set to 0 s. After the setpoint force is reached, the withdrawal of the cantilever starts without any delay, resulting in an effective contact time of the cells in the order of 0.2 s because of their flexibility and the velocity of the cantilever movement. This velocity only influences the results if the viscosity of the surrounding medium is significantly increased. To minimize this effect but simultaneously be fast enough to avoid bridging events it is set to 5 μm/s.

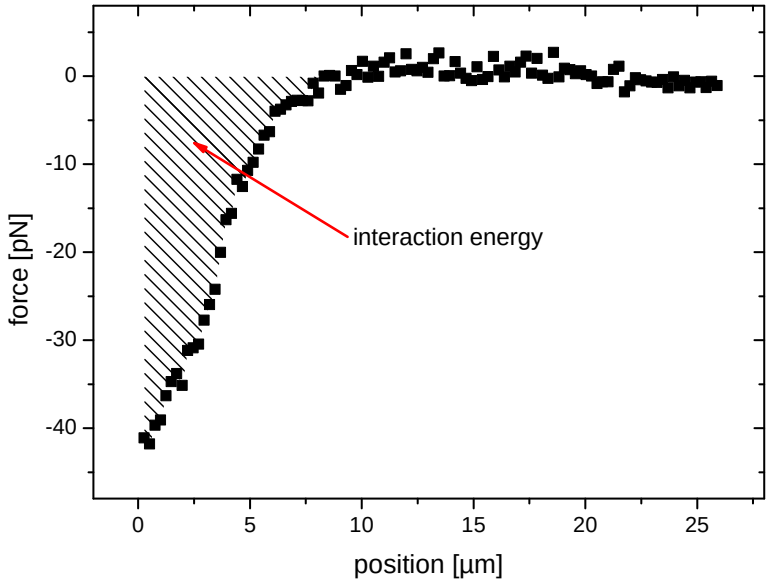

Figure 6.1.: Force between two red blood cells in dependency of the cantilever's position which is connected to the distance between the cells. The interaction energy corresponds to the area between the curve and the x-axis.

In figure 6.1 one can see the separation phase of two cells with the according force for the different positions of the cantilever which correspond to the distance between the cells. The area between the curve and the x-axis gives the intercellular interaction energy. For each datapoint at least ten cells are measured ten times and the interaction energies from all these measurement steps are averaged. All diagrams in this chapter show interaction energy densities which are obtained by the division of the interaction energy by the contact area of two red blood cells. This contact area was derived to be approximately 50 μm^2, corresponding to a circle with the mean radius of a red blood cell.

The results of the measurements with the plasma protein fibrinogen are shown in figure 6.2. An increase of the interaction energy with the concentration is clearly visible. The physiological concentration of fibrinogen in the human body is between 2 and 4 mg/ml [94].

In figure 6.3, one can see these results together with the data for two dextran solutions (which were measured by Steffen et al. [109] with the same method). As shown in the diagram, the curves belonging to the dextran are in excellent agreement with the theory of Neu et al. [81].

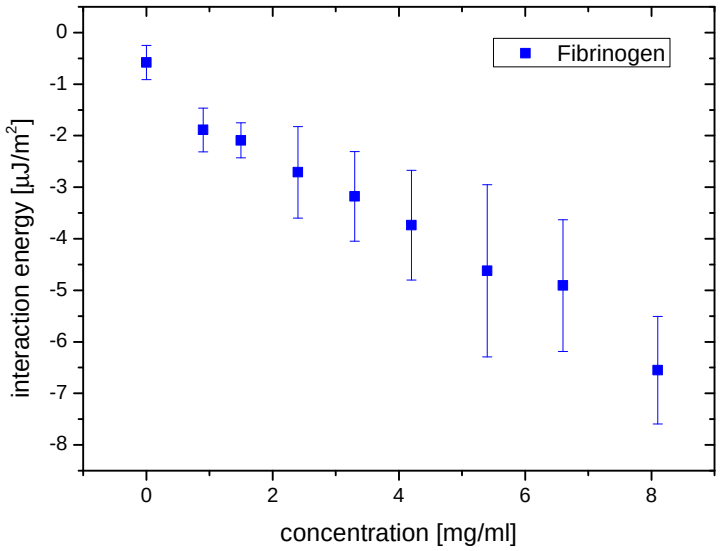

Figure 6.2.: Interaction energies for different concentrations of the coagulation factor fibrinogen obtained with the single-cell force spectroscopy measurements. The physiological amount of fibrinogen is between 2 and 4 mg/ml.

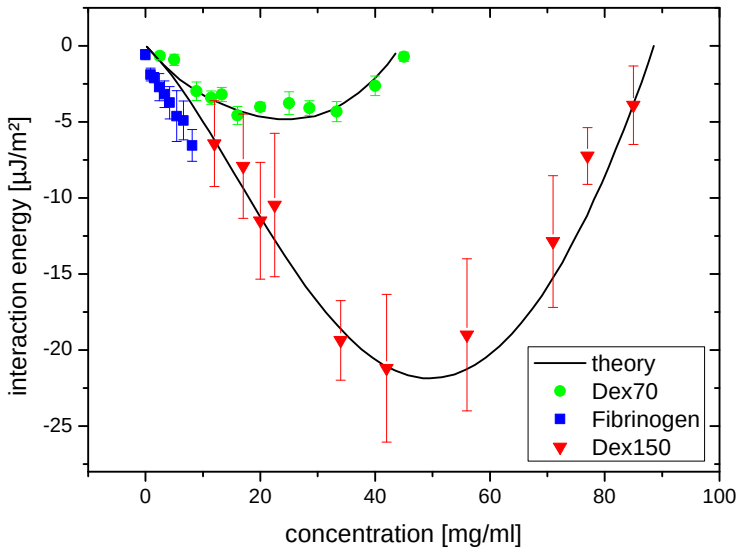

Figure 6.3.: Single-cell force spectroscopy measurements for two types of dextran (M_W = 70 kDa and M_W = 150 kDa) and fibrinogen. The dextran data are from Steffen et al. [109]. The theoretical predictions of Neu et al. [81] are included as a black line.

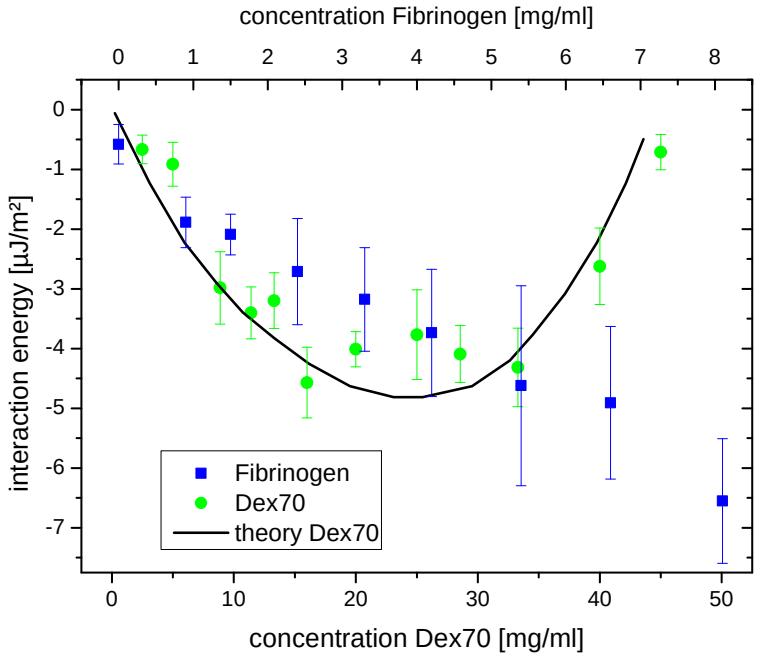

Figure 6.4.: Single cell force spectroscopy measurements for dextran (70 kDa) and fibrinogen. The axes for the concentrations are different in the two cases.

These results are the first direct measurements of the force between two cells under the influence of depletion-inducing macromolecules. The interaction energy for fibrinogen (M_W = 340 kDa) can only be measured for rather small concentrations because it is not possible to dilute it for high concentrations (over 35 mg/ml) and because of experimental problems caused by impurities which adhere to the cantilever at intermediate concentrations (between 8 and 35 mg/ml). The values of the measurable concentrations are comparable to the values of the dextran type with the higher molecular weight (150 kDa). However, when evaluating the interaction energy, the same maximum values can be obtained with the measurable fibrinogen concentrations as for the dextran type with the smaller molecular weight (70 kDa). In figure 6.4, the values for these two substances can be compared with each other.

6.2.2. Microfluidics measurements

In the measurements with the microfluidic channels, the distribution of single cells and clusters of different sizes are investigated. As an example, figure 6.5 shows a series of pictures with different objects flowing through the narrow channels. These exemplary pictures are recorded with a magnification of 20× to illustrate the clusters and to allow an easy recognition, while the actual images in the experiment are recorded with a magnification of only 10× to be able to observe ten parallel channels at the same time (see section 4.5). Although the magnification is obviously not high enough to investigate exact distances between the cells in one cluster, it is possible to detect the number of cells per object and create good statistics. The results obtained in the microfluidic channels show an evident coherence of the number of clusters and the concentration of the depletion agent.

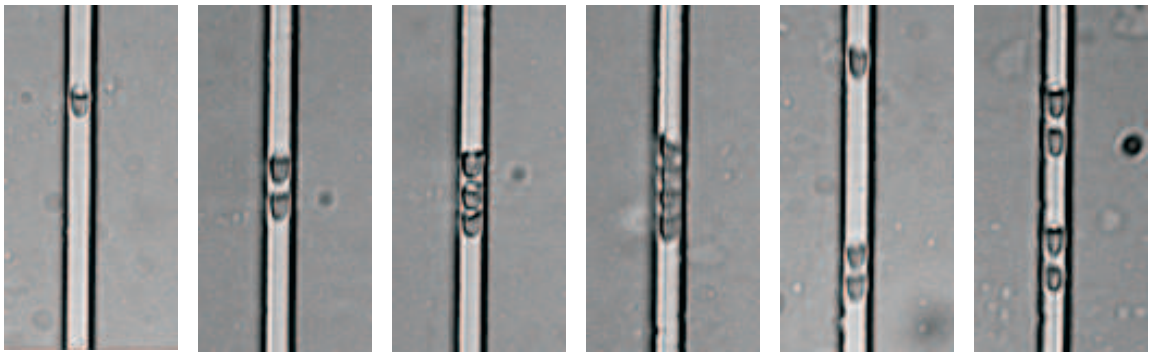

Figure 6.5.: Pictures of red blood cells flowing through the microfluidic channel. From left to right there is a single cell, a cluster of two, three and four cells and a combination of a cluster of two and a single cell as well as two clusters of two cells.

In figure 6.6, one can see the viscosity η of dextran solutions with different concentration. The viscosity values are measured in order to compare them with the results obtained for the relative occurrence of the clusters and exclude an influence of the surrounding medium's viscosity on the RBC aggregation: The viscosity is increasing linearly with the concentration, while the relative occurrence of clusters is bell-shaped.

The first depletion agent to be measured is the long-chain sugar polymer dextran with a molecular weight of 70 kDa. After the analysis of a series of velocities for the same concentration of dextran, it turns out that the velocity has almost no influence on the amount of clusters. Only for two concentrations, one could observe small variations of the amount of single cells with the velocity (figure 6.7, upper part). Since no clear connection between the clustering and the velocity can be found, the results for all velocities are averaged to get a mean value of the distribution for each dextran concentration. The relative occurrence of the cluster sizes of red blood cells for different polymer concentrations is shown in figure 6.8.

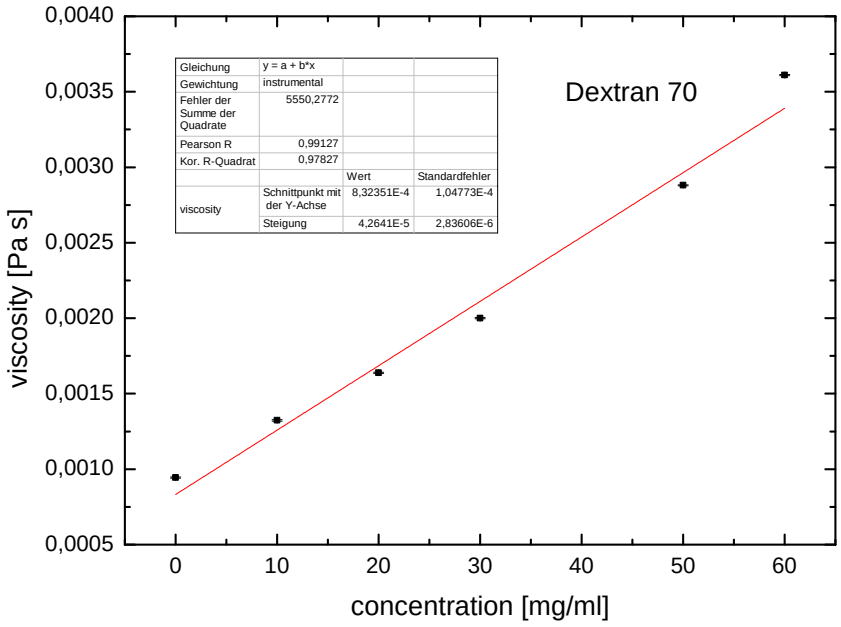

Figure 6.6.: Viscosity for dextran solutions with different concentrations as measured in the shear rheometer.

One can see in the diagram that the curve has the same bell-shape which was already proposed in the model of Neu et al. [81]. The error bars seem to be rather large because of the plurality of parameters which can influence the measurements in a biological system: Red blood cells are not completely identical to each other. They can vary in size (about 10%) and also in shape due to their high flexibility.

At the concentration of 30 mg/ml a data point is missing. This concentration can not be investigated with the current microfluidics setup, because it is not possible to apply the solution into the channel. Already in the syringe, a phase separation occured and the RBCs accumulate to big aggregates, easily visible by the eye. An image of the syringe (figure 6.9) illustrates these difficulties. As the interaction energy is at the maximum level for this concentration, the aggregation of the cells is intense and the bigger objects sediment very quickly. This behavior may also be the reason for the small variations of the distribution in dependence of the flow velocity for dextran as well as for fibrinogen. In figure 6.7, it is clearly visible that fluctuations belonging to the velocity only occur for high values of the interaction energy, close to concentrations which are no longer measurable (dextran: 20 and 40 mg/ml, fibrinogen: 4.2 and 5.4 mg/ml).

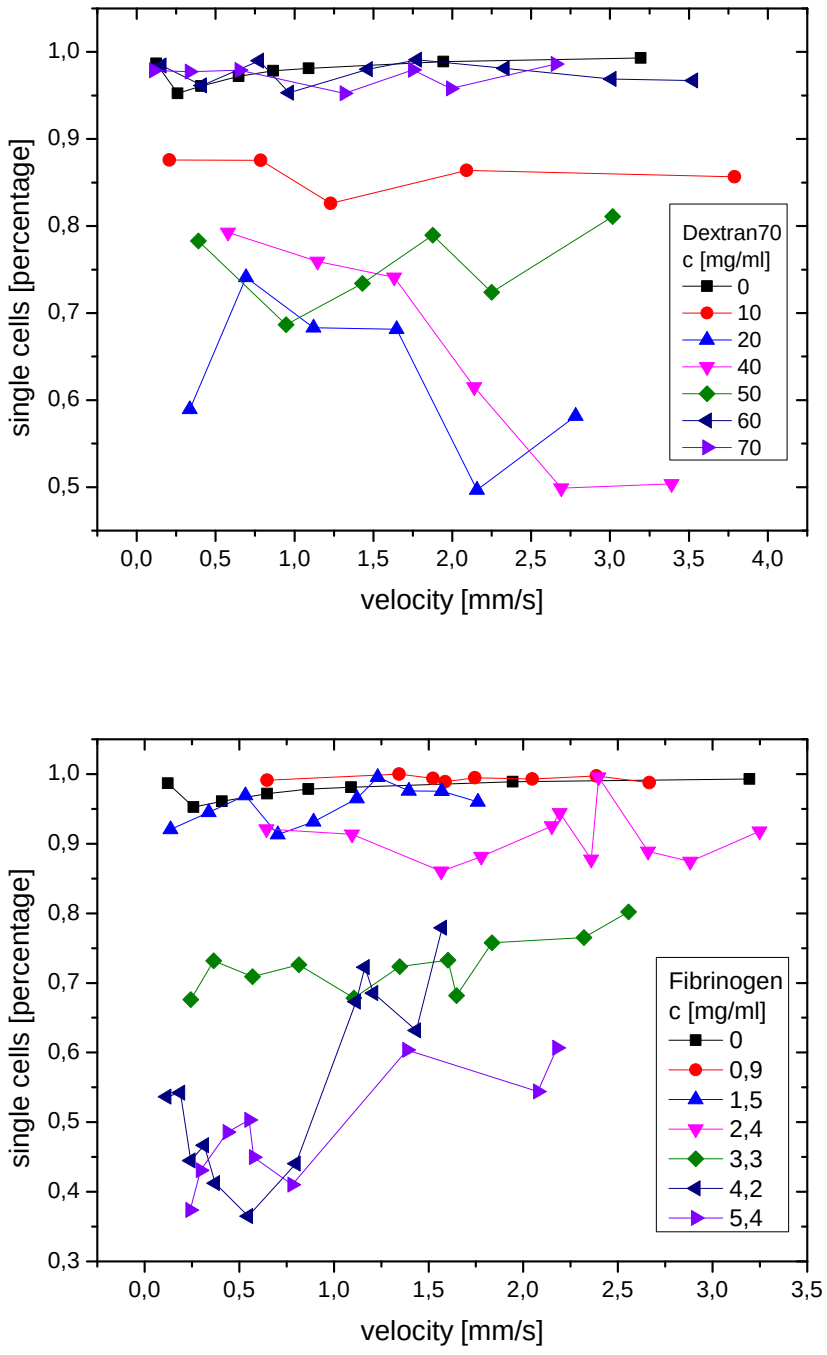

Figure 6.7.: Amount of single cells for different concentrations of dextran (upper part) and fibrinogen (lower part) plotted against the flow velocity. The clustering is almost completely independent from the velocity.

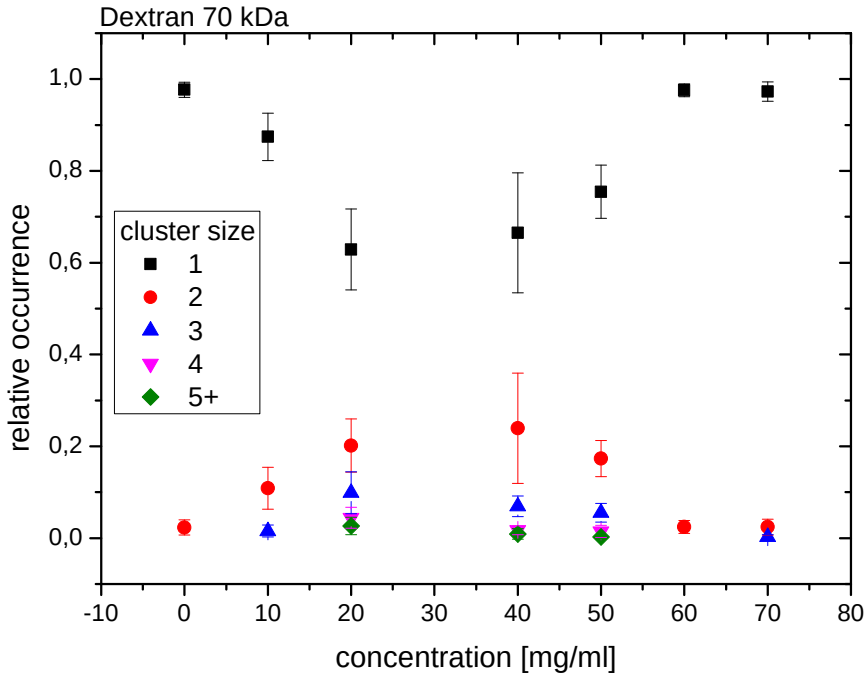

Figure 6.8.: Relative occurrence of all objects (single cells and different sized clusters) for different dextran concentrations. The values are averaged over all velocities. The same bell-shaped behavior as already observed in the SCFS measurements is visible.

Another parameter to be checked is the amount of RBCs in the solution, the hematocrit value. In the experiments, it varies between 0.02% and 0.5% which means that the RBCs are in a very diluted environment. To make sure the variations in the amount of cells does not influence the results, figure 6.10 shows the distribution of clusters in dependence of the hematocrit at a dextran concentration of 20 mg/ml. As can be seen, no significant relation can be found.

In order to make an approach closer to the physiological situation, the influence of the plasma protein fibrinogen is also measured. This protein is naturally responsible for the coagulation of blood to close a wound. After the activation with thrombin, it builds fibrin which creates a network and acts as a glue to form a thrombus. However, in our case, where we do not have this activation, it is assumed that only physical effects play a role.

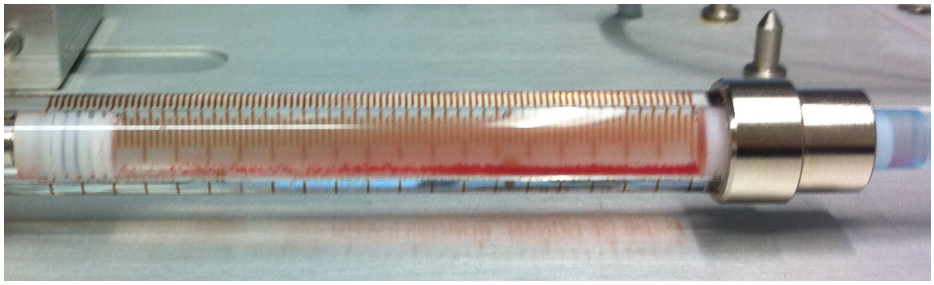

Figure 6.9.: Picture of the glass syringe with big aggregates of RBCs at the bottom, as they occur at concentrations of 30 mg/ml Dex70 or 6.6 and 12 mg/ml Fibrinogen. Due to this aggregation, it is not possible to inject the solution into the microfluidics for high interaction energies.

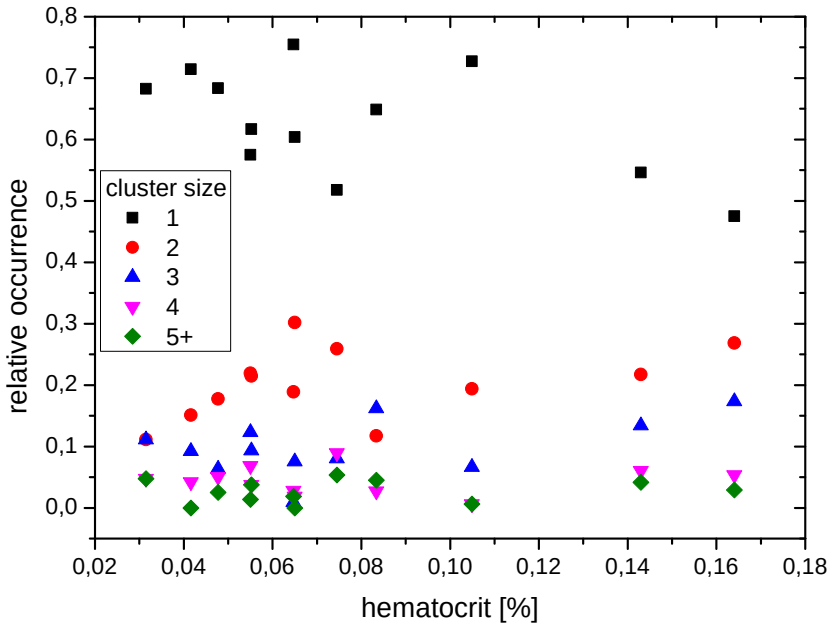

Figure 6.10.: Relative occurrence of all objects against the hematocrit value for a dextran concentration of 20 mg/ml. No connection between the amount of clusters and the hematocrit value could be detected.

In figure 6.7 (lower part), one can also see the dependence of the amount of single cells on the velocity in the case of fibrinogen and again no strong connection can be observed. Therefore, the values for the distribution of one concentration are again obtained by calculating the average over all measured velocities. The results are

shown in figure 6.11 and reveal a different behavior than for the dextran solution. The amount of clusters increases for an increasing concentration but does not decrease again for the highest concentrations.

It is not possible to continue the measurements for concentrations higher than 5.4 mg/ml, because at 6.6 mg/ml, the same sedimentation problems occur as already described above for the dextran at 30 mg/ml. To make sure that 6.6 mg/ml is not the concentration with the maximum interaction energy from where the decreasing starts, a solution with a concentration of 12 mg/ml is prepared but the phase separation which precludes the measurements still occurs. This means that the interaction energy for the case of fibrinogen does not show the bell-shaped behavior which can be observed for the dextran.

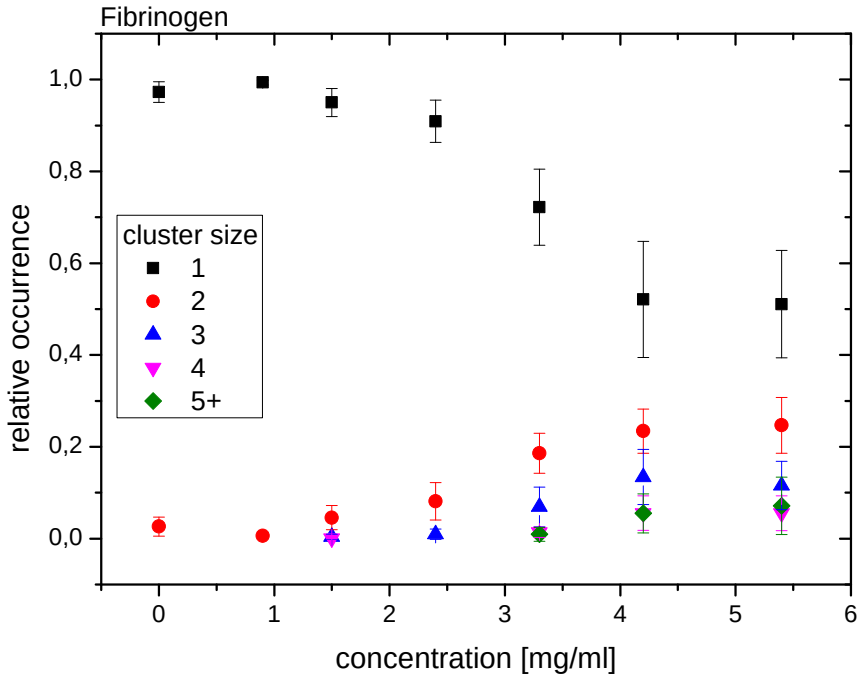

Figure 6.11.: Distribution of all objects (single cells and different sized clusters) for different fibrinogen concentrations. The values are averaged over all velocities.

6.3. Discussion

In the direct measurements of the cell-cell interaction, the results for the dextran solutions show a bell shape of the interaction energy values which after reaching a maximum decreases again. In contrast, the results with the fibrinogen show only an increase of the interaction energy with the concentration and no following decrease. The reason for this is most probably the difference of the two polymers regarding their possibility to penetrate into the glycocalyx as described in section 3.2. For dextran this penetration is possible and hence the bell-shaped behavior of the interaction energy in dependence of the polymer solution was predicted in the theoretical model [81]. Since the interaction energy and the amount of aggregates should be linked, the distribution of the clusters is in good agreement with this prediction and the single cell measurements.

Consequently, as the viscosity is increasing with the dextran concentration, the clustering of the cells cannot be triggered by the viscosity of the surrounding medium, because the amount of clusters decreases again and reaches the same level for the highest concentrations as in the case without dextran although the viscosities differ strongly. For the glycoprotein fibrinogen which is a bigger molecule ($M_W = 340$ kDa) than dextran ($M_W = 70$ kDa or 150 kDa) and in contrast to it not neutral but negatively charged, it can be inferred that it is not possible to penetrate significantly into the glycocalyx of the RBC.

As the theory predicted for this case, the interaction energy just increases with the fibrinogen concentration in the SCFS measurements. The distribution of the clusters in the microfluidics experiments are therefore again in good agreement with the measurements of the interaction energy. The measurable range of concentrations is unfortunately limited due to a pronounced aggregation, resulting in a phase separation of the fluid which occurs consistently at the same value of the interaction energy for both substances. Because of the experimental data's conformity with the theoretical model, the depletion effect becomes more likely to be the reason of the RBC adhesion at the expense of the bridging model.

The physiological concentration of fibrinogen is between 2 and 4 mg/ml under normal conditions but can rise up to 6 mg/ml in case of pregnancy, a big wound or pathological conditions [94]. Therefore, the formation of clusters due to the presence of fibrinogen is highly relevant for the blood flow in the body. In contrast to the majority opinion, the aggregates are not broken up in the small channels mimicking microcapillaries, because the spatial constriction prevents the shear forces from splitting the aggregates.

6.4. Summary

In this chapter the aggregation of red blood cells due to macromolecules was presented. The question whether the adhesion occurs due to the bridging or the depletion theory could still not be answered, but the results deliver a further argument in favor of the depletion model. A theoretical description of the bridging model does still not exist while the model for the depletion-induced cell adhesion was further developed over the last two decades. Some indirect measurement methods gave results which favored the RBC aggregation but could not answer the question of the underlying model.

The single cell force spectroscopy measurements are the first direct measurements of the interaction energy between two cells under the influence of macromolecules. The results are in excellent agreement with the predictions of the depletion model. Additionally, the results obtained with the microfluidics measurements involving a huge number of cells show an increase of the amount of clusters for higher interaction energies and the curves are qualitatively in good agreement with the single-cell measurements. The different behavior of the two depletion agents due to their diverging possibility of penetration into the glycocalyx is clearly visible in the measurements of the interaction energy as well as in the clustering experiments. Because of the independency of the cluster distributions from the flow rate, the claim that the adhesion of RBCs induced by physiological fibrinogen concentrations does not play a role in the blood flow has to be reconsidered.

7. Summary

7.1. Summary (english)

The results of the conducted measurements give new insights on two important aspects of the flow behavior of blood. In the experiments concerning the properties of blood plasma it was possible to find a clearly viscoelastic behavior in the case of purely elongational flow. Contrary to the common opinion in the literature, plasma can consequently be considered to be a non-Newtonian fluid. The viscoelastic properties were not measurable in shear flow or in contractional flow experiments, but in the CaBER experiment where the elongational component of the flow is predominant. The stretching of the polymeric components is highly pronounced and therefore a difference to the other experiments could be observed. It was possible to exclude the influence of surface effects responsible for viscoelastic effects of blood plasma found in earlier measurements [31, 52]. In additional measurements with the addition of a surfactant to prevent the polymers from building a surface layer, the results of our experiments could be confirmed. Furthermore, the rerun of the experiment with silicon oil surrounding the capillary bridge of the plasma provided the same results as well, although an air-liquid interface of the plasma filament obviously did not exist. A solution consisting of 50 ppm PEO in water containing 15 wt% glycerol showed the same behavior as plasma with the three different measurement techniques whereby it can be considered as a model solution for plasma. After the addition of a physiological amount of red blood cells (50 vol%) to this model solution it was possible to observe vortices upstream of the contraction in the microfluidics measurements starting at shear rates of $30 \cdot 10^3$ s^{-1}. This significant change of the flow behavior due to the presence of red blood cells shows that the viscoelastic properties can also play a role in the blood flow through the capillary system even if the occurrence of the instability takes place at shear rates above the common values in capillaries. The expected instability of blood in the contraction channel could however not be confirmed but since blood contains many other ingredients, it is possible that other effects suppress a flow instability. In summary, it can be said that it was possible to clearly show the **viscoelastic behavior of blood plasma** and that this property should be taken into account in future investigations about blood rheology. The results have been published in "Physical Review Letters" [20] and highlighted in "APS physics" and "Physics today" [77, 107].

In the measurements related to the adhesion of red blood cells due to macromolecules, the results for the interaction energy between two cells are in excellent agreement with theoretical predictions of a depletion-based model by Neu et al. [81] and earlier experimental data [22] for the sugar polymer dextran. The agreement of these first direct cell-cell measurements with the predicted theory is an indicator in favor of the depletion model. For the plasma protein fibrinogen, it was possible to measure interaction energies in the same range of concentrations which are present in the human body under normal or pathological conditions. From a macroscopic point of view, the **distribution of all objects flowing through microfluidic channels** with the size of a small capillary into single cells or clusters of different lengths were also in **good qualitative agreement with the single cell measurements**. Hence, the relation between the depletion interaction and the rouleaux formation during the blood circulation through the human body becomes more likely. At the physiological concentration of fibrinogen, the amount of clusters is already increased which may lead to significant effects during flow. Another interesting fact is the independence of the distribution from the flow velocity which means that an increased shear rate due to a higher velocity seems to be insufficient to break the rouleaux again. If the channels are of the same size as the cells, the velocity gradient due to the Poiseuille profile of the flow therefore cannot separate the cells from each other due to the spatial constriction. With these results, it is necessary to reassess the majority opinion that the adhesion of red blood cells due to physiological fibrinogen concentrations is negligible in the flow through the capillary system because of the increased shear rate. Although the blood viscosity has reached a plateau level at these shear rates in rheometer experiments, the break-up of the aggregates is not assured on the microcapillary level. These results will be presented in another publication currently in progress.

The formation of clusters in the presence of a physiological fibrinogen concentration as well as the viscoelastic behavior of blood plasma are two important results in order to gain a deeper understanding of blood flow.

Outlook

The results of this dissertation, with the new insights in two particular details change the point of view about blood flow. In this very complex subject, many areas still exist in which further research is meaningful and necessary. Some examples will be given in the following: In future studies, it could be interesting to follow a cluster on its way through the channel to learn more about the dynamics of the process. A further step to approach the in vivo situation could be to repeat the measurements with a solution containing fibrinogen as well as other plasma macromolecules known to be capable to induce a depletion interaction, like for example some immunoglobulins. Also, the design of a new microfluidic device with branching channels to mimic the microvascular system and observe the behavior of a cluster at a junction might be

interesting. Another challenge of future experiments is to find a possibility to better control the initial conditions of the clustering measurements in the microfluidics. It would be interesting to measure the distribution of the clusters under well-defined and controllable conditions, such as only groups of four cells with a constant distance to each other entering the narrow channels. On the bulk level, a rheometer-driven study of the shear rate-dependent viscosity for the same dextran and fibrinogen concentration which have been investigated in the microfluidics and the single-cell force measurements may also be supportive to the results of this work.

Furthermore, the flow behavior of plasma could be tested in different channel geometries, in order to try visualizing the complex flow behavior also in microfluidics experiments.

7.2. Resumé (français)

Les résultats des mesures effectuées ont mis en lumière de nouveaux aspects importants concernant l'écoulement du sang. Dans les expériences menées sur le plasma, il a été possible d'observer clairement un comportement visco-élastique dans le cas d'écoulements purement élongationnels. Contrairement à ce qui était communément admis dans la littérature, le plasma peut être considéré comme un fluide non-newtonien. Les propriétés visco-élastiques n'ont pas pu être mesurées dans les expériences en écoulement de cisaillement ou en écoulement dans une constriction, mais on a pu les mesurer dans l'expérience CaBER dans laquelle la composante élongationnelle de l'écoulement est dominante. L'étirement des polymères est très prononcé et c'est pourquoi une différence avec les autres expériences a pu être observée. Il a été possible de s'affranchir des effets de surface responsables des effets visco-élastiques trouvés dans le plasma, effets observés dans des travaux antérieurs [31, 52]. En ajoutant une substance tensio-active pour empêcher les polymères de former une couche superficielle, les résultats ont pu être confirmés. De plus, l'expérience a été refaite avec de l'huile silicone entourant le pont capillaire formé par le plasma et a fourni le même résultat, bien qu'aucune interface liquide-gaz n'existe avec le filament de plasma. Une solution de 50 ppm de PEO dans l'eau avec 15 %m de glycérine a montré le même comportement que le plasma avec les trois méthodes différentes pour lesquelles cette solution peut être considérée comme un fluide modèle pour le plasma. Si l'on ajoute à ce fluide modèle des globules rouges à une concentration physiologique (50 %vol), il est possible d'observer des tourbillons en amont de la constriction, pour des taux de cisaillement supérieurs à $30 \cdot 10^3$ s^{-1}. Ce changement crucial de comportement de l'écoulement par la présence des globules rouges montre que les propriétés visco-élastiques peuvent jouer un rôle dans l'écoulement par le système capillaire, même si l'apparition de l'instabilité se passe à un taux de cisaillement plus grand que les valeurs habituelles dans les capillaires. L'instabilité prévue pour le sang dans le microcanal en constriction n'a pas pu être observée, mais comme le sang contient beaucoup d'autres substances, il est possible que d'autres effets aient annihilé l'instabilité. En conclusion, on peut dire qu' il était possible de montrer clairement le comportement visco-élastique du plasma et que cette propriété doit être considéré dans de futures études sur la rhéologie du sang. Les resultats ont été publié dans "Physical Review Letters" [20] et ont été accentués dans "APS physics" et "Physics today" [77, 107].

L'énergie d'interaction entre deux globules rouges a été quantifiée. Les résultats sont en très bon accord avec les prédictions théoriques issues du modèle de déplétion de Neu et al. [81], mais aussi avec des mesures expérimentales antérieures [22] pour le polymère Dextran. L'accord entre les mesures de l'énergie d'interaction entre deux cellules et les prédictions théoriques est un point de plus en faveur du modèle de déplétion. Pour le fibrinogène, protéine du plasma sanguin, il est possible de mesurer des énergies d'interaction du même ordre de grandeur que pour les concentrations présentes dans le corps dans des conditions normales ou pathologique. Du point de vue macroscopique,

la distribution des globules rouges, seuls ou en clusters de différentes tailles, dans des microcanaux de la taille d'un capillaire est en très bon accord avec l'énergie d'interaction mesurée. Ainsi la relation entre la force de déplétion et la formation de rouleaux dans la circulation du sang dans le corps humain est à envisager. A une concentration physiologique de fibrinogène, le nombre de clusters est déjà élevé, ce qui peut avoir des effets significatifs sur l'écoulement. Un autre fait intéressant est l'indépendance de la distribution de clusters par rapport à la vitesse d'écoulement, ce qui veut dire qu'une augmentation du taux de cisaillement dûe à de plus grandes vitesses semblent être insuffisante pour dissocier les rouleaux à nouveau. Si les canaux ont la même taille que les cellules, le gradient de vitesse dû au profile parabolique du Poiseuille ne peut pas séparer les cellules les unes des autres à cause des contraintes spatiales. À la lumière de ces résultats, il est nécessaire de reconsidérer le rôle de la concentration de fibrinogène sur l'adhésion des globules rouges, qui a été souvent négligé sous prétexte que le taux de cisaillement est très élevé dans les capillaires. Bien que la viscosité du sang est arrivée à un niveau constant à ces taux de cisaillement dans les expériences de rhéométrie, la dissociation des agrégats n'est pas assurée en niveau microcapillaire. Ces résultats vont être presentés dans une autre publication, qui est en préparation pour le moment.

La formation des clusters en présence d'une concentration physiologique de fibrinogène aussi bien que le caractère visco-élastique du plasma sanguin sont deux résultats importants dans la perspective de mieux comprendre l'écoulement du sang.

Perspective

Les resultats de cette thèse, avec les nouvelles connaissances dans deux détails particuliers, modifient la façon de considérer l'écoulement du sang. Dans ce sujet complexe, plusieurs domaines dans lesquels une recherche consécutive est raisonnable et nécessaire sont existantes. Quelques exemples sont spécifiés dans ce qui suit. Comme perspective, il serait intéressant de suivre l'évolution d'un cluster dans un microcanal. Une autre étape à franchir vers la situation in vivo est de répéter les mesures précédemments faites avec une solution de fibrinogène, en plus d'autres macromolécules présentes dans le plasma et qui sont connues pour leur abilité à induire une adhésion cellulaire comme les immunoglobulines. En plus, la création des nouveaux canaux microfluidiques avec des branchements pour observer l'attitude d'un cluster à une bifurcation peut être intéressante. Un autre défi pour des expériences futures est de trouver une possibilité pour mieux contrôler les conditions initiales des mesures dans la microfluidique. Il serait intéressant de mesurer la distribution des clusters dans des conditions prédéfinies, comme un groupe de quatre cellules séparées par une constante distance entrant dans un canal étroit. Au niveau global, une étude rhéométrique concernant la viscosité en fonction du taux de cisaillement pour les mêmes concentrations de dextrane et de fibrinogène, comme dans les mesures microfluidiques et les mesures de l'énergie d'interaction, peut renforcer les résultats de ce travail. Le

comportement de l'écoulement du plasma peut être verifié dans des canaux avec des géométries variables, pour essayer de visualiser aussi le comportement complexe dans les expériences microfluidiques.

7.3. Zusammenfassung (deutsch)

Die Ergebnisse der durchgeführten Messungen haben neue Einblicke in zwei wichtige Aspekte des Fließverhaltens von Blut gewährt. In den die Eigenschaften des Blutplasmas betreffenden Experimenten war es möglich, ein viskoelastisches Verhalten im Falle einer reinen Dehnugsströmung klar zu erkennen. Entgegen der allgemeinen Auffassung in der Literatur kann Plasma daher als nicht-Newtonsches Fluid betrachtet werden. Die viskoelastischen Eigenschaften waren in Scherfluss- oder Kontraktionsflussexperimenten nicht messbar, aber sehr wohl im CaBER Experiment, in dem die Dehnungskomponente des Flusses dominierend ist. Die Streckung der Polymer-Bestandteile ist stark ausgeprägt und deswegen konnte ein Unterschied zu den anderen Experimenten beobachtet werden. Es war möglich, den Einfluss von Oberflächeneffekten auszuschließen, die für viskoelastische Effekte des Blutplasmas in früheren Messungen [31, 52] verantwortlich waren. Durch die Zugabe eines oberflächenaktiven Stoffs, um die Polymere an der Bildung einer Oberflächenschicht zu hindern, konnten die Ergebnisse bestätigt werden. Außerdem lieferte eine Wiederholung des Experiments mit einer, die kapillare Brücke umgebenden, Silikonölatmosphäre ebenso das gleiche Ergebnis, obwohl offensichtlich keine flüssig-gasförmige Grenzfläche des Plasmafilaments vorhanden war. Eine Lösung bestehend aus 50 ppm PEO in Wasser mit 15 Gew.-% Glycerin zeigte das gleiche Verhalten wie Plasma in den drei unterschiedlichen Messmethoden, wodurch sie als Modellflüssigkeit für Plasma betrachtet werden kann. Durch die Zugabe roter Blutzellen in einer physiologischen Menge (50 Vol.-%) zu dieser Modellflüssigkeit, war es möglich, Verwirbelungen oberhalb der Verengung in den Messungen mit der Kontraktionsfluidik zu beobachten, die bei Scherraten von $30 \cdot 10^3$ s^{-1} begannen. Diese wesentliche Veränderung des Fließverhaltens durch die Anwesenheit roter Blutzellen zeigt, dass die viskoelastischen Eigenschaften auch eine Rolle im Blutfluss durch das Kapillarsystem spielen können, wenngleich das Auftreten der Instabilitäten bei Scherraten über den üblichen Werten in Kapillaren geschah. Die erwartete Instabilität von Blut in der Kontraktionsfluidik konnte nicht bestätigt werden, aber da im Blut noch viele andere Stoffe enthalten sind, ist es möglich, dass andere Effekte eine Instabilität unterdrückt haben. Zusammenfassend kann gesagt werden, dass es möglich war das **viskoelastische Verhalten des Blutplasmas klar zu zeigen**, und dass diese Eigenschaft in zukünftigen Studien zur Blutrheologie beachtet werden sollte. Die Ergebnisse wurden in „Physical Review Letters“ [20] veröffentlicht und in „APS physics“ und „Physics today“ [77, 107] hervorgehoben.

In den Messungen bezüglich der Adhäsion von roten Blutzellen durch Makromoleküle, waren die Ergebnisse für die Interaktionsenergie zwischen zwei Zellen in hervorragender Übereinstimmung mit theoretischen Vorhersagen eines depletionsbasierten Modells von Neu et. al [81] und früheren experimentellen Daten [22] für das Zuckerpolymer Dextran. Die Übereinstimmung dieser ersten direkten Zell-Zell Messungen mit der vorhergesagten Theorie ist ein Argument für die Validität des Depletionsmodells. Für das Plasmaprotein Fibrinogen war es möglich, für Konzentrationen, die im Kör-

per unter normalen bzw. krankhaften Bedingungen vorkommen, Interaktionsenergien in der gleichen Größenordnung zu messen. Vom makroskopischen Standpunkt her ist die Verteilung aller Objekte in einzelne Zellen oder Cluster verschiedener Größe, die durch kleine Kanäle von der Größe eines Kapillargefäßes fließen, ebenso **in guter Übereinstimmung mit den Einzelzell-Messungen**. Daher wird der Zusammenhang zwischen der Depletions-Wechselwirkung und der Rouleaux-Bildung während der Blutzirkulation durch den menschlichen Körper immer wahrscheinlicher. Bei physiologischen Konzentrationen von Fibrinogen ist der Anteil von Clustern bereits erhöht, was zu bedeutenden Effekten während des Flusses führen könnte. Eine weitere interessante Tatsache ist die Unabhängigkeit der Verteilung von der Fließgeschwindigkeit, was bedeutet, dass eine erhöhte Scherrate aufgrund einer größeren Geschwindigkeit nicht auszureichen scheint, um die Rouleaux wieder aufzubrechen. Wenn die Kanäle dieselbe Größe wie die Zellen haben, kann der Geschwindigkeitsgradient durch das Poiseuille-Profil des Flusses die Zellen durch die räumliche Beschränkung also nicht voneinander trennen. Mit diesen Ergebnissen ist es notwendig, die Mehrheitsmeinung zu überdenken, dass die Adhäsion von roten Blutzellen durch physiologische Fibrinogenkonzentrationen beim Fluß durch das Kapillarsystem wegen der erhöhten Scherrate vernachlässigt werden kann. Obwohl die Blutviskosität bei diesen Scherraten im Rheometer einen konstanten Wert erreicht hat, ist das Aufbrechen der Aggregate in den Mikrokapillaren nicht klar erwiesen. Diese Ergebnisse werden in einer weiteren Veröffentlichung präsentiert werden, an der momentan gearbeitet wird.

Sowohl die Bildung von Clustern in Anwesenheit von physiologischen Fibrinogenkonzentrationen als auch das viskoelastische Verhalten des Blutplasmas sind zwei wichtige Ergebnisse um ein tieferes Verständnis des Blutflusses zu erlangen.

Ausblick

Die Ergebnisse dieser Dissertation mit den neuen Erkenntnissen in zwei speziellen Bereichen verändern die Betrachtungsweise des Blutflusses. In diesem sehr komplexen Gebiet gibt es noch viele Bereiche in denen weiterführende Forschung sinnvoll und notwendig ist. Einige Beispiele werden im folgenden aufgeführt. In zukünftigen Untersuchungen könnte es interessant sein, einen Cluster auf seinem Weg durch den Kanal zu verfolgen, um mehr über die Dynamik des Prozesses zu lernen. Ein weiterer Schritt zum Verständnis der Situation im lebenden Organismus könnte die Wiederholung der Messungen mit einer Lösung sein, die außer Fibrinogen noch andere Plasmamakromoleküle enthält, welche fähig sind, eine Depletionsinteraktion zu induzieren, wie zum Beispiel einige Immunoglobuline. Auch die Erstellung einer neuen Mikrofluidik mit verzweigten Kanälen könnte interessant sein, um das Verhalten eines Clusters an einer Abzweigung zu beobachten. Eine weitere Herausforderung für zukünftige Experimente ist, eine Möglichkeit zu finden, die Anfangsbedingungen der Cluster-Messungen in der Mikrofluidik besser einzustellen. Es wäre interessant, die Verteilung der Cluster unter wohldefinierten Anfangsbedingungen zu messen, wie zum Beispiel, dass ausschließlich

Gruppen von vier Zellen mit jeweils konstantem Abstand zueinander in den schmalen Kanal gelangen. Im Kontinuum vermag eine Rheometer-gestützte Studie der scherratenabhängigen Viskosität für dieselben Dextran- und Fibrinogenkonzentrationen, die in den Mikrofluidik- und Einzelzell-Kraftmessungen untersucht wurden, die Ergebnisse dieser Arbeit unterstützen. Die Fließeigenschaften von Plasma könnten in anderen Kanalgeometrien getestet werden, um die komplexen Eigenschaften auch in Mikrofluidikexperimenten veranschaulichen zu können.

A. Materials and Methods

A.1. Materials

Notation	Name	Size	Company
BSA	Bovine serum albumin	10 g	Polysciences Inc.
Dextran70	Dextran from Leuconostoc mesenteroides $M_W = 64 - 76 \cdot 10^3$	50 g	Sigma Aldrich
Dextran150	Dextran from Leuconostoc mesenteroides $M_W = 150 \cdot 10^3$	100 g	Sigma Aldrich
Fibrinogen	Fibrinogen from human plasma 50-70% protein	250 mg	Sigma Aldrich
PBS	Phosphate buffered saline	500 ml	Invitrogen
Cell-Tak	Cell-Tak	1 ml	BD
Fluorescent beads	Latex beads, carboxylate-modified polystyrene, fluorescent red	1 ml	Sigma Aldrich
PEO	Poly (ethylene oxide) $M_W = 4 \cdot 10^6$	250 g	Sigma Aldrich
Glycerol	Glycerol	1 l	Sigma Aldrich
Surfactant	Tween20	25 ml	Sigma Aldrich
PDMS	Sylgard 184	1 kg	Dow and Cornings
Tubing	Polyethylene tubing	100 m	Laborshop24 GmbH
Glass syringe	H, TLL PTFE Luer Lock	1 ml	ILS
Cantilever	MLCT-O	10	Bruker

Table A.1.: Tabular overview of substances and materials used in the experiments.

A.2. Methods

A.2.1. Microfluidics fabrication

For the production of a microfluidic device by photolithography, it is necessary to create a mask with the required network of channels. It is usually fabricated from fused silica with a thin structured chrome layer on top, but for rather simple geometries without very tiny structures (> 5 µm), printed masks can also be sufficient. With such a mask, it is possible to fabricate the negative of the desired structure on a silica wafer.

A thin layer of a photo-resistant is applied on top of the wafer by spin-coating (figure A.1 a). After the pre-baking for drying of the resistant, the mask is accurately aligned on top of the coated wafer and illuminated with an intense ultraviolet light source (figure A.1 b). There are a lot of different possibilities for this step like for example the contact mode in which the mask is placed directly on top of the wafer, or alternatively the proximity mode with a small distance between wafer and mask or the usage of lens systems to image the mask to the wafer with or without magnification. As the combination of the structure dimensions on the mask, the properties of the photo-resistant and the illumination mode is responsible for the shape of the final topology, the different possibilities for all steps in the fabrication protocol have to be chosen at the beginning of the process and cannot be changed afterwards. In this step the structure of the mask is copied on the resistant layer.

The exposure of the resistant under the transparent parts of the mask causes a change in its chemical structure when illuminated with ultraviolet light while the areas under the opaque parts of the mask remain unchanged (figure A.1 c). In the subsequent developing step, depending on the chosen resistant either the illuminated (positive) or the non-illuminated (negative) part of the resistant is chemically removed by dipping the wafer into a special developing solution (figure A.1 d, negative resistant). To harden the structure, the wafer is baked in an oven.

At this point in the fabrication of the wafer, one can stop and use the structure formed by the resistant for the following production of the actual fluidics what can be sufficient for a lot of applications. If the resistant is however not hard or robust enough for the subsequent steps it is also possible to transfer the structure directly into the silica wafer. The execution of an etching process (figure A.1 e) where the part of the wafer which is covered by the resistant remains intact and the following removal of the resistant (figure A.1 f) results in the same designated surface structure of the silica wafer as present before due to the resistant.

The size of the structures in x and y direction is obviously defined by the mask, while their size in z direction is given by the thickness of the applied photo-resistant and the properties of the etching process. With a single lithography step it is only possible to produce structures where the size in z direction is constant, but several lithography steps can be conducted serially if a variation of the structures in z direction

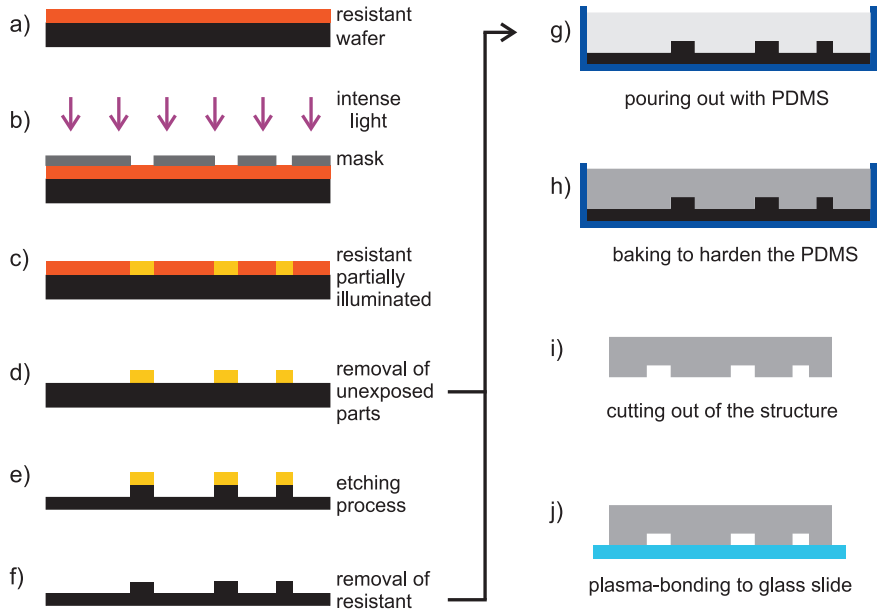

Figure A.1.: Production of a microfluidic channel. Detailed overview of the wafer fabrication and the mold with the PDMS. The steps are described in detail in the text.

is necessary. When the fabrication of the wafer is finished, the actual production of the microfluidic channels can be started. This is the fastest part in the whole process and can be repeated many times with only one wafer. A fluid elastomer called Polydimethylsiloxane (PDMS) is used to make a mold of the structure. This elastomer (Sylgard 184, Dow and Cornings) is stored in two components which need to be mixed in a ratio of one to ten. Subsequently the fluid is degassed by applying a negative pressure difference to remove all the bubbles which have been formed in the mixing process. Then the fluid is filled in a petri dish where the wafer is placed at the bottom (figure A.1 g) and baked in an oven at 60°C for about one hour for hardening (figure A.1 h). Afterwards, the hardened object can be cut from the petri dish, peeled carefully from the wafer (figure A.1 i) and the holes for connecting the tubing must be stamped.

Finally, the PDMS mold and a coverslip are exposed to an oxygen plasma for 30 s to prepare the binding. The mold is pressed on the coverslip immediately after removal from the plasma cleaner (figure A.1 j), followed by a final baking process at 60°C for two hours to stabilize the connection between the PDMS and the glass surface. Now, it is necessary to connect the tubing with the holes in the reservoirs. Therefore, the ends of the tubes are dipped in isopropanol and pushed into the holes. After the connection of the tubing the measurements can be started.

A.2.2. Sample preparation

Contraction measurements

If the solution to observe in the contraction microfluidics contains a polymer, it is added at the day before the measurement and diluted by a gentle shaking process during 24 hours. If the solvent is not pure water but a mixture of water and glycerol, this compound is also prepared one day in advance.

For these measurements, the required amount of blood is much higher than just a droplet. Therefore, the blood samples are obtained by venous blood withdrawal at the medical department and stored in standard tubes with the anticoagulant EDTA. The plasma is gained by double centrifugation of the whole blood at the day of the withdrawal and measured at the same day or the day afterwards. The RBCs are prepared in the same way with the only difference of the choice which part of the separated blood components is used and which one is dumped.

In all solutions without RBCs, it is necessary to add 2 mg/ml of fluorescent beads to visualize the stream lines of the flow in the microfluidics. The beads have a diameter of 500 nm and are coated with a fluorescent dye. They are excited with a mercury vapor lamp (λ_{ex} = 575 nm) and emit light with a different wavelength (λ_{em} = 610 nm), whereby it is possible to filter the light of the mercury lamp and detect just the signal of the fluorescent beads.

After the mixing of the solution, it is drawn up into the 1 ml glass syringe for the contraction microfluidics measurements or filled into the rheometer or the CaBER respectively.

Clustering measurements

For the clustering measurements, one droplet of blood is taken from a fingertip needle prick and diluted in one milliliter of PBS. It is centrifuged at 3000 rpm for three minutes followed by the suction of the complete liquid fraction, leaving only the red blood cells which have sedimented on the bottom. They are then rediluted in 1 ml PBS and the procedure is repeated once with the only difference of the redilution in 1 ml of PBS containing 2 mg of BSA.

The blood withdrawal takes place no longer than three hours before the start of the measurements. A certain concentration of the powdery depletion agent is diluted without severe shaking to avoid the destruction of the polymers in 1 ml of PBS whereas the solution is heated to body temperature to simplify the dissolving of the substance. After the preparation of the experimental setup, the solution with the RBCs and the solution with the depletion agent are mixed and also drawn up into a glass syringe with a volume of 1 ml.

List of Figures

List of Tables

Bibliography

[1] S.L. Anna and G.H. McKinley. Elasto-capillary thinning and breakup of model elastic liquids. *Journal of Rheology*, 45:115–138, 2001.

[2] J. Armstrong, R. Wenby, H. Meiselman, and T. Fisher. The hydrodynamic radii of macromolecules and their effect on red blood cell aggregation. *Biophysical Journal*, 87:4256–4270, 2004.

[3] S. Asakura and F. Oosawa. On interaction between two bodies immersed in a solution of macromolecules. *Journal of Chemical Physics*, 22:1255–1256, 1954.

[4] S. Asakura and F. Oosawa. Interaction between particles suspended in solutions of macromolecules. *Journal of Polymer Science*, 33:183–192, 1958.

[5] H. Baek, M.V. Jayaraman, P.D. Richardson, and G.E. Karniadakis. Flow instability and wall shear stress variation in intracranial aneurysms. *Journal of the Royal Society Interface*, 7:967–988, 2010.

[6] H. Baeumler and E. Donath. Does dextran really significantly increase the surface potential of human red blood cells? *Studia Biophysica*, 120:113–122, 1987.

[7] H. Baeumler, E. Donath, A. Krabi, W. Knippel, A. Budde, and H. Kiesewetter. Electrophoresis of human red blood cells and platelets. Evidence for depletion of dextran. *Biorheology*, 33:333–351, 1996.

[8] H. Baeumler, B. Neu, E. Donath, and H. Kiesewetter. Basic phenomena of red blood cell rouleaux formation. *Biorheology*, 36:439–442, 1999.

[9] A. Baloch, P. Townsend, and M.F. Webster. On vortex development in viscoelastic expansion and contraction flows. *Journal of Non-Newtonian Fluid Mechanics*, 65:133–149, 1996.

[10] O. Baskurt, B. Neu, and H. Meiselman. *Red Blood cell aggregation.* CRC Press, 2011.

[11] O.K. Baskurt and H.J. Meiselman. Blood rheology and hemodynamics. *Seminars in Thrombosis and Hemostasis*, 29(5):435–450, 2003.

[12] G.K. Batchelor. *An Introduction to Fluid Dynamics*. Cambridge University Press, Cambridge, 1967.

[13] P.P. Bhat, S. Appathurai, M.T. Harris, M. Pasquali, G.H. McKinley, and O.A. Basaran. Formation of beads-on-a-string structures during break-up of viscoelastic filaments. *Nature Physics*, 6:625–631, 2010.

[14] E. Biernacki. Samoistna sedymentacja krwi jako naukowa, praktyczno-kliniczna metoda badania. *Gazeta Lekarska*, 17:962–996, 1897.

[15] R.B. Bird, R.C. Armstrong, and O. Hassager. *Dynamics of Polymeric Liquids: Fluid Mechanics*. Wiley, New York, 1987.

[16] D.V. Boger and K. Walters. *Rheological Phenomena in Focus, Rheology Series, Vol. 4*. Elsevier, New York, 1993.

[17] M. Boynard and J.C. Lelievre. Size determination of red blood cell aggregates induced by dextran using ultrasound backscattering phenomenon. *Biorheology*, 27(1):39–46, 1990.

[18] P.J.H. Bronkhorst, J. Grimbergen, G.J. Brakenhoff, R.M. Heethaar, and J.J. Sixma. The mechanism of red blood cell (dis)aggregation investigated by means of direct cell manipulation using multiple optical traping. *British Journal of Haematology*, 96:256–258, 1997.

[19] D. Brooks. Electrostatic effects in dextran mediated cellular interaction. *Journal of Colloid and Interface Science*, 43:714–726, 1973.

[20] M. Brust, C. Schäfer, R. Dörr, L. Pan, M. Garcia, P.E. Arratia, and C. Wagner. Rheology of human blood plasma: Viscoelastic versus Newtonian behavior. *Physical Review Letters*, 110:078305, 2013.

[21] H. Bruus. *Theoretical Microfluidics*. Oxford University Press, Oxford, 2008.

[22] K. Buxbaum, E. Evans, and D. Brooks. Quantitation of surface affinities of red blood cells in dextran. *Biochemistry*, 21:3235–3239, 1982.

[23] J.C. Carreau. Rheological equations from molecular network theories. *Journal of Rheology*, 16:99–127, 1972.

[24] N. Casson. *Rheology of Disperse Systems*. Pergamon Press, London, 1959.

[25] S. Chien. Shear dependence of effective cell volume as a determinant of blood viscosity. *Science*, 168:977–979, 1970.

[26] S. Chien and K. Jan. Red cell aggregation by macromolecules: Roles of surface adsorption and electrostatic repulsion. *Journal of Supramolecular Structure*, 1:385–409, 1973.

[27] S. Chien and L.A. Lang. Physiochemical basis and clinical implications of red cell aggregation. *Clinical Hemorheology*, 7:71–91, 1987.

[28] Y. Chu, S. Dufour, J. Thiery, E. Perez, and F. Pincet. Johnson-Kendall-Roberts theory applied to living cells. *Physical Review Letters*, 94:28102, 2005.

[29] G.R. Cokelet, E.W. Merrill, E.R. Gilliland, H. Shin, A. Britten, and R.E. Wells. The rheology of human blood - measurement near and at zero shear rate. *Transactions of the Society of Rheology*, 7:303–317, 1963.

[30] A.L. Copley, C.R. Huang, and R.G. King. Rheogoniometric studies of whole human blood at shear rates from 1000 to 0.0009 1/s. I. Experimental findings. *Biorheology*, 10:17–22, 1973.

[31] A.L. Copley and R.G. King. Viscous resistance of thromboid (thrombus-like) surface layers in systems of plasma proteins including fibrinogen. *Thrombosis Research*, 1:1–18, 1972.

[32] R.V. Craster, O.K. Matar, and D.T. Papageorgiou. On compound liquid threads with large viscosity contrasts. *Journal of Fluid Mechanics*, 533:95–124, 2005.

[33] R.V. Craster, O.K. Matar, and D.T. Papageorgiou. Breakup of surfactant-laden jets above the critical micelle concentration. *Journal of Fluid Mechanics*, 629:195–219, 2009.

[34] P.G. de Gennes. Coil-stretch transition of dilute flexible polymers under ultra-high velocity gradients. *Journal of Chemical Physics*, 60:5030–5042, 1974.

[35] P.G. de Gennes. *Scaling concepts in polymer physics*. Cornell University Press, 1979.

[36] P.G. de Gennes. *Introduction to Polymer Dynamics*. Cambridge University Press, Cambridge, 1990.

[37] A. de Waele. Viscometry and plastometry. *Journal of the Oil & Colour Chemists' Association*, 6:33–69, 1923.

[38] W. Demtröder. *Experimentalphysik 1, Mechanik und Wärmelehre*. Springer, Berlin, 2006.

[39] M. Doi and S.F. Edwards. *The Theory of Polymer Dynamics*. Clarendon Press, Oxford, 1986.

[40] J. Eggers. Universal pinching of 3d asymmetric free-surface flow. *Physical Review Letters*, 71:3458–3460, 1993.

[41] E. Evans and D. Needham. Attraction between lipid bilayer membranes - comparison of mean field theory and measurements of adhesion energy. *Macromolecules*, 21:1822–1831, 1988.

[42] R. Fahraeus. The suspension stability of the blood. *Physiological Reviews*, 9:241–275, 1929.

[43] D.A. Fedosov, W. Pan, B. Caswell, G. Gompper, and G.E. Karniadakis. Predicting human blood viscosity in silico. *Proceedings of the National Academy of Sciences of the United States of America*, 108:11772–11777, 2011.

[44] F. Fogolari, A. Brigo, and H. Molinari. The poisson-boltzmann equation for biomolecular electrostatics: a tool for structural biology. *Journal of Molecular Recognition*, 15:377–392, 2002.

[45] Y.C. Fung. *Biomechanics: Mechanical Properties of Living Tissues*. Springer, 1993.

[46] G. Ghigliotti, H. Selmi, L. El Asmi, and C. Misbah. Why and how does collective red blood cells motion occur in the blood microcirculation? *Physics of Fluids*, 24:101901, 2012.

[47] S.E. Gier. *Untersuchung der Bildung, des Wachstums und der Bewegung von Tropfen aus komplexen Fluessigkeiten*. PhD thesis, Saarland university, 2010.

[48] J. Goldstone, H. Schmid-Schönbein, and R.E. Wells. The rheology of red blood cell aggregates. *Microvascular Research*, 2:273–286, 1970.

[49] J.D. Gray, I. Owen, and M.P. Escudier. Dynamic scaling of unsteady shear-thinning non-Newtonian fluid flows in a large-scale model of a distal anastomosis. *Experiments in Fluids*, 43:535–546, 2007.

[50] S.J. Haward, V. Sharma, and J.A. Odell. Extensional opto-rheometry with biofluids and ultra-dilute polymer solutions. *Soft Matter*, 7:9908–9921, 2011.

[51] W.R. Hess. Gehorcht das Blut dem allgemeinen Strömungsgesetz der Flüssigkeiten? *Pflügers Archiv für die gesamte Physiologie des Menschen und der Tiere*, 162:187–224, 1915.

[52] A. Jaishankar, V. Sharma, and G.H. McKinley. Interfacial viscoelasticity, yielding and creep ringing of globular protein-surfactant mixtures. *Soft Matter*, 7:7623–7634, 2011.

[53] D.F. James. Open channel siphon with viscoelastic fluids. *Nature*, 212:754–756, 1966.

[54] J. Janzen and D.E. Brooks. Do plasma proteins adsorb to red cells? *Clinical Hemorheology*, 9:695–714, 1989.

[55] S. Jin and L.R. Collins. Dynamics of dissolved polymer chains in isotropic turbulence. *New Journal of Physics*, 9:360, 2007.

[56] A. Jones and B. Vincent. Depletion flocculation in dispersions of sterically-stabilised particles 2: Modifications to theory and further studies. *Colloids and Surfaces*, 42:113–138, 1989.

[57] R.G. Larson. *The Structure and Rheology of Complex Fluids*. Oxford University Press, 1999.

[58] S.W. Lee and D.A. Steinman. On the relative importance of rheology for image-based CFD models of the carotid bifurcation. *Journal of Biomechanical Engineering*, 129:273–278, 2007.

[59] A. Lessner, F. Zahavi, A. Silberberg, E.H. Frei, and F. Dreyfus. *Theoretical and Clinical Hemorheology*. Springer, 1971.

[60] D. Liepsch, G. Thurston, and M. Lee. Studies of fluids simulating blood-like rheological properties and applications in models of arterial branches. *Biorheology*, 28:39–52, 1991.

[61] G. Lowe. *Clinical blood rheology*. CRC Press, 1988.

[62] N. Mackman. Triggers, targets and treatments for thrombosis. *Nature*, 451:914–918, 2008.

[63] C.W. Macosko. *Rheology: Principles, Measurements and Applications*. Wiley, New York, 1994.

[64] N. Maeda, M. Seike, T. Nakajima, Y. Izumida, M. Sekiya, and T. Shiga. Contribution of glycoproteins to fibrinogen-induced aggregation of erythrocytes. *Biochemica et Biophysica Acta*, 1022:72–78, 1990.

[65] N. Maeda and T. Shiga. Opposite effect of albumin on the erythrocyte aggregation induced by immunoglobulin G and fibrinogen. *Biochemica et Biophysica Acta*, 855:127–135, 1986.

[66] Z. Marton, G. Kesmarky, J. Vekasi, A. Cser, R. Russai, B. Horvath, and K. Toth. Red blood cell aggregation measurements in whole blood and in fibrinogen solutions by different methods. *Clinical hemorheology and microcirculation*, 24(2):75–83, 2001.

[67] J.C. Maxwell. On the dynamical theory of gases. *Philosophical Transactions of the Royal Society*, 157:49–88, 1867.

[68] P.T. McGough and O.A. Basaran. Repeated formation of fluid threads in breakup of a surfactant-covered jet. *Physical Review Letters*, 96:054502, 2006.

[69] G.H. McKinley and A. Tripathi. How to extract the newtonian viscosity from capillary break-up measurements in a filament rheometer. *Journal of Rheology*, 44:653–670, 2000.

[70] J.L. McWhirter, H. Noguchi, and G. Gompper. Flow-induced clustering and alignment of vesicles and red blood cells in microcapillaries. *Proceedings of the National Academy of Sciences of the United States of America*, 106:6039–6043, 2009.

[71] J.L. McWhirter, H. Noguchi, and G. Gompper. Deformation and clustering of red blood cells in microcapillary flows. *Soft Matter*, 7:10967–10977, 2011.

[72] H. Meiselman. Red blood cell aggregation: 45 years being curious. *Biorheology*, 46:1–19, 2009.

[73] E.W. Merrill. Rheology of blood. *Physiological Reviews*, 49(4):863–888, 1969.

[74] E.W. Merrill, E.R. Gilliland, T.. Lee, and E. Salzmann. Blood rheology: Effect of fibrinogen deduced by addition. *Circulation Research*, 18:437–446, 1966.

[75] E.W. Merrill and G.A. Pelletier. Viscosity of human blood: transition from newtonian to non-newtonian. *Journal of Applied Physiology*, 23:178–182, 1967.

[76] O.E. Meyer. Theorie der elastischen Nachwirkung. *Annalen der Physik*, 227:108–119, 1874.

[77] D. Monroe. *APS physics, Focus: Blood Plasma is Not So Normal*, February 2013. `http://physics.aps.org/articles/v6/18`.

[78] A.N. Morozov and W. van Saarloos. An introductory essay on subcritical instabilities and the transition to turbulence in visco-elastic parallel shear flows. *Physics Reports*, 447:112–143, 2007.

[79] M. Moyers-Gonzalez, R.G. Owens, and J.F. Fang. A non-homogeneous constitutive model for human blood: Part 1. model derivation and steady flow. *Journal of Fluid Mechanics*, 617:327–354, 2008.

[80] G.B. Nash, R.B. Wenby, S.O. Sowemimo-Coker, and H.J. Meiselman. Influence of cellular properties on red cell aggregation. *Clinical Hemorheology*, 7:93–108, 1987.

[81] B. Neu and H.J. Meiselman. Depletion-mediated red blood cell aggregation in polymer solutions. *Biophysical Journal*, 83:2482–2490, 2002.

[82] T.Q. Nguyen and H.-H. Kausch, editors. *Flexible Polymer Chain Dynamics in Elongational Flow*. Springer, Berlin, 1999.

[83] J.G. Oldroyd. On the formulation of rheological equations of state. *Proceedings of the Royal Society of London A*, 200:523–541, 1950.

[84] D.J. Olson and G.G. Fuller. Contraction and expansion flows of Langmuir monolayers. *Journal of Non-Newtonian Fluid Mechanics*, 89:187–207, 2000.

[85] W. Ostwald. Über die Geschwindigkeitsfunktion der Viskosität disperser Systeme. *Kolloid-Zeitschrift*, 36:99–117, 1925.

[86] R.G. Owens. A new microstructure-based constitutive model for human blood. *Journal of Non-Newtonian Fluid Mechanics*, 140:57–70, 2006.

[87] D.T. Papageorgiou. On the breakup of viscous liquid threads. *Physics of Fluids*, 7:1529–1544, 1995.

[88] C. Picart, J.-M. Piau, H. Galliard, and P. Carpentier. Human blood shear yield stress and its hematocrit dependence. *Journal of Rheology*, 42:1–12, 1998.

[89] P. Pranay. *Dynamics of Suspensions of Elastic Capsules in Polymer Solution*. PhD thesis, University of Wisconsin, 2011.

[90] A. Pribush, D. Zilberman-Kravits, and N. Meyerstein. The mechanism of the dextran-induced red blood cell aggregation. *European Biophysics Journal*, 36:85–94, 2007.

[91] M. Rampling and G. Martin. Albumin and rouleaux formation. *Clinical Hemorheology*, 5:761–765, 1992.

[92] M.W. Rampling. *Handbook of Hemorheology and Hemodynamics*, chapter Compositional Properties of Blood, pages 34–44. IOS, Amsterdam, 2007.

[93] O. Reynolds. An experimental investigation of the circumstances which determine whether the motion of water shall be direct or sinuous, and of the law of resistance in parallel channels. *Philosophical Transactions of the Royal Society*, 174:935–982, 1883.

[94] A.M. Robertson, A. Sequeira, and M.V. Kameneva. *Hemodynamical Flows: Modelling, Analysis and Simulation*, chapter Hemorheology, pages 63–120. Birkhaeuser Basel, 2008.

[95] L.E. Rodd, J.J. Cooper-White, D.V. Boger, and G.H. McKinley. Role of the elasticity number in the entry flow of dilute polymer solutions in micro-fabricated contraction geometries. *Journal of Non-Newtonian Fluid Mechanics*, 143:170–191, 2007.

[96] L.E. Rodd, T.P. Scott, D.V. Boger, J.J. Cooper-White, and G.H. McKinley. The inertio-elastic planar entry flow of low-viscosity elastic fluids in micro-fabricated geometries. *Journal of Non-Newtonian Fluid Mechanics*, 129:1–22, 2005.

[97] A. Rothert, R. Richter, and I. Rehberg. Transition from symmetric to asymmetric scaling function before drop pinch-off. *Physical Review Letters*, 87:084501, 2001.

[98] W.B. Russel, D.A. Saville, and W.R. Schowalter. *Colloidal dispersions*. Cambridge University Press, Cambridge, 1989.

[99] R. Sattler, C. Wagner, and J. Eggers. Blistering pattern and formation of nanofibers in capillary thinning of polymer solutions. *Physical Review Letters*, 100(16):164502, 2008.

[100] H. Schmid-Schönbein and R. Wells. Rheological properties of human erythrocytes and their influence upon anomalous viscosity of blood. *Physiology Reviews*, 63:147–219, 1971.

[101] H. Schmid-Schönbein, R. Wells, and R. Schildkraut. Microscopy and viscometry of blood flowing under uniform shear rate. *Journal of Applied Physiology*, 26:674–678, 1969.

[102] P. Schümmer and K.H. Tebel. A new elongational rheometer for polymer solutions. *Journal of Non-Newtonian Fluid Mechanics*, 12:331–347, 1983.

[103] C.M. Schroeder, R.E. Teixeira, E.S.G. Shaqfeh, and S. Chu. Characteristic periodic motion of polymers in shear flow. *Physical Review Letters*, 95:018301, 2005.

[104] T.P. Scott. Contraction/expansion flow of dilute elastic solutions in microchannels. Master's thesis, Massachusetts Institute of Technology, 2004.

[105] D.M. Sforza, C.M. Putman, and J.R. Cebral. Hemodynamics of cerebral aneurysms. *Annual Review of Fluid Mechanics*, 41:91–107, 2009.

[106] R. Skalak, P.R. Zarda, K.M. Jan, and S. Chien. Mechanics of rouleau formation. *Biophysical Journal*, 35:771–781, 1981.

[107] A.G. Smart. *physicstoday, Physics update: Blood plasma not so simple after all*, February 2013. `http://www.physicstoday.org/daily_edition/physics_update/blood_plasma_not_so_simple_after_all`.

[108] P.C. Sousa, F.T. Pinho, M.S.N. Oliveira, and M.A. Alves. Extensional flow of blood analog solutions in microfluidic devices. *Biomicrofluidics*, 5(014108):1–19, 2011.

[109] P. Steffen, C. Verdier, and C. Wagner. Quantification of depletion-induced adhesion of red blood cells. *Physical Review Letters*, 110:018102, 2013.

[110] M. Stelter, G. Brenn, A.L. Yarin, and P. Singh. Validation and application of a novel elongational device for polymer solutions. *Journal of Rheology*, 44:595, 2000.

[111] R.I. Tanner. A theory of die-swell. *Journal of Polymer Science, Part A-2: Polymer Physics*, 8:2067–2078, 1970.

[112] R.I. Tanner. *Engineering Rheology*. Oxford Science, 1985.

[113] G.B. Thurston. Viscoelasticity of human blood. *Biophysical Journal*, 12:1205–1217, 1972.

[114] G.B. Thurston. *Advances in Hemodynamics and Hemorheology*, chapter Viscoelastic Properties of Blood and Blood Analogs, pages 1–30. JAI Press Inc., Greenwich, 1996.

[115] G.B. Thurston and N.M. Henderson. *Handbook of Hemorheology and Hemodynamics*, chapter Viscoelasticity of Human Blood, pages 72–90. IOS, Amsterdam, 2007.

[116] G. Tomaiuolo, L. Lanotte, G. Ghigliotti, C. Misbah, and S. Guido. Red blood cell clustering in poiseuille microcapillary flow. *Physics of Fluids*, 24:51903, 2012.

[117] P. Townsend and K. Walters. Expansion flows of non-newtonian liquids. *Chemical Engineering science*, 49:749–763, 1994.

[118] F.T. Trouton. On the coefficient of viscous traction and its relation to that of viscosity. *Proceedings of the Royal Society of London Series A*, 77:426–440, 1906.

[119] B. Vincent. The calculation of depletion layer thickness as a function of bulk polymer concentration. *Colloids and Surfaces*, 50:241–249, 1990.

[120] B. Vincent, J. Edwards, S. Emmett, and A. Jones. Depletion flocculation in dispersions of sterically-stabilised particles ("soft spheres"). *Colloids and Surfaces*, 18:261–281, 1986.

[121] G. Vlastos, D. Lerche, B. Koch, O. Samba, and M. Pohl. The effect of parallel combined steady and oscillatory shear flows on blood and polymer solutions. *Rheologica Acta*, 36:160–172, 1997.

[122] R.E. Wells and E.W. Merrill. Shear rate dependence of the viscosity of whole blood and plasma. *Science*, 133:763–764, 1961.

Acknowledgments

Ich möchte mich ganz herzlich bei Prof. Dr. Christian Wagner bedanken für die Möglichkeit der Promotion in seiner Arbeitsgruppe, die Unterstützung während der gesamten Zeit und nützliche Diskussionen über das spannende Thema Blutrheologie.

Mein großer Dank gilt ebenso allen ehemaligen und aktuellen Mitarbeitern der Arbeitsgruppe Wagner für das einzigartige Arbeitsklima, der Hilfe bei den verschiedensten Problemen und der großen Unterstützung. Ebenso für spannende Kickerduelle, der Erörterung wichtiger Fragen der Menschheitsgeschichte und lustigen Wanderungen bei klirrender Kälte und brütender Hitze. Dasselbe gilt auch für die ehemaligen Mitarbeiter der AG Huber.

Danke an die mechanische Werkstatt für die stets schnelle Durchführung aller notwendigen Arbeiten zum Aufbau der Messapparaturen und der Unterstützung bei deren Planung. Außerdem für eine hervorragende Platzierung unseres gemeinsamen Teams beim Firmenlauf im Sommer 2010. Im besonderen ist hier noch Werkstattleiter Michael Schmidt zu erwähnen, der stets gute Lösungsvorschläge hatte, wenn man einmal nicht mehr genau wusste, was man eigentlich wollte und bei kurzen Kekspausen mit Urlaubsanekdoten für die notwendige Ablenkung gesorgt hat. Ebenfalls ein großes Dankeschön an unsere Sekretärin Elke Huschens und an unsere Chemielaborantin Karin Kretsch für das Übernehmen vieler zeitraubender Kleinigkeiten.

Je remercie Monsieur Chaouqi Misbah pour la possibilité de faire cette thèse en cotutelle avec l'Université de Grenoble. J'aimerais rendre grâce à Gwennou Coupier et Thomas Podgorski pour les discussions à Grenoble et leur aide avec les expériences dans le Laboratoire Interdisciplinaire de Physique. Aussi à toute l'équipe LiPhy pour deux beaux séjours au pied des alpes.

Le temps à Grenoble était vraiment une belle étape de ma thèse et je veux remercier tous les doctorants français et internationaux pour les expériences multiculturelles, particulièrement pendant les trois beaux week-ends en montagne. Merci à Xavier, Othmane, Darja, Aparna, Purvi, Prem, Pierre-Yves, Teodora, Rachel, Caterina, Valentina, Levan, Xabel, Giovanni, Michaël, Vincent, Maëva, Guntars, Flore, Sofia, Luca et Johannes.

Merci beaucoup à Othmane et Flore pour corriger les épreuves dans les parties françaises de cette thèse.

Mille grazie a Luca, mio coabitatore a Grenoble, per tre mesi grandiosi, la cucina italiana alla mamma e una amicizia in lontananza. Anche a Sofia per una nozze bellissima in Toscana e a Filippo per due giorni typici irlandese a Roma.

Vielen Dank an Christof für seine große Hilfe bei allem, um was man ihn auch nur mit einem halben Wort im Nebensatz gebeten hat. Danke an Patrick für eine tolle Zeit während der Promotion und für herrliche Situationen bei einigen Dienstreisen, die sich kein Autor jemals hätte ausdenken können. An Mr. Ruff für Unterstützung in allen Computerangelegenheiten, an Volker für tolle Serien und schöne Skatpartien, an Ines, Daniel und Flo für tolle Mittagspausen, ebenso an Conny, Alex und Leni für genausotolle Mittagspausen, an Max, Mona, Lars, Eric, Yvonne, Wadim, Mußler und Patrick, dafür, dass ich eine grandiose Studienzeit mit euch verbringen durfte.

Danke an meine Handballmannschaft (mein Herz schlägt vier!) für den sportlichen Ausgleich und die tolle Saison inklusive Meisterschaft, an die ganze „Handballfamilie“ für Erfolge, Niederlagen und das wiederkehrende, tollste Wochenende des Jahres, an die talentfreien Montagskicker für grandiosen Zauberfußball, an Ines für viele Reisen und unzählige Essenseinladungen. Für Skiurlaube, gemütliche Fußballabende, Reisen zu nahen und fernen Zielen, lustige Unternehmungen, unterhaltsame, aber auch nachdenklich machende Kinofilme und tolle gemeinsame Stunden, die ich mit euch verbracht habe, ein herzliches Dankeschön an Bini, Conny, Egla, Nadine, René, Marika, Leni, Mo, Pipa, Wege, Mona, Max, Rasse, Christof, Eva+Mark, de Haetz, Michaela, Thomas+Sabine, Lukas, Markus, Jana.

Ein weiteres Mal vielen herzlichen Dank, für das aufmerksame Korrekturlesen dieser Arbeit an Max Ebbinghaus!

Special thanks to Dr. Sheldon Cooper, Barney Stinson, Abed Nadir, Hank Moody, Quentin Tarantino and the "Kansas City Shuffle".

Abschließend bedanke ich mich besonders bei meinen Eltern, die mich immer unterstützt haben und ohne die vieles sicher nicht möglich gewesen wäre. Ein ganz herzliches Dankeschön auch an meine Großeltern, die ebenfalls immer für mich da waren. Ebenso danke ich meiner Schwester für ihre Hilfe bei allen möglichen kleinen und größeren Problemen.